UNIVERSITÀ DEGLI STUDI DI TRIESTE

XXXII CICLO DEL DOTTORATO DI RICERCA IN

BIOMEDICINA MOLECOLARE

PO FRIULI VENEZIA GIULIA - FONDO SOCIALE EUROPEO 2014/2020

Development of a novel Polymer-based delivery system for siRNAs to hepatocellular carcinoma cells

Settore scientifico-disciplinare: BIO/12 Biochimica Clinica e Biologia Molecolare Clinica

DOTTORANDA
FRANCESCA PERRONE

COORDINATORE
PROF. GERMANA MERONI

SUPERVISORE DI TESI
PROF. GABRIELE GRASSI

CO-SUPERVISORE DI TESI
PROF. MAJA ČEMAŽAR

ANNO ACCADEMICO 2018/2019

Index

1 Abstract

For Hepatocellular carcinoma (HCC) there are no effective treatments thus, the individuation of novel therapeutic approaches and molecular targets are urgent. Small interference RNA (siRNAs) are small double stranded RNAs able to induce gene silencing thus, representing an attractive therapeutic strategy. The main impediment in using siRNAs is the fast degradation rate in the biological environment. To protect siRNAs from degradation, we developed a novel delivery system based on the polymer α,β-poly-(N-2-hydroxyethyl)-D,L-aspartamide (PHEA) derivatized with diethylene triamine (DETA) linked via a polyethylene glycol (PEG) to galactose (GAL) molecules (PDPG). The GAL residue has been introduced to target to the asialoglycoprotein receptor (ASGPR), overexpressed in HCC cells.

Using a fluorescently labelled PDPG (PDPG-BodipyTRX) carrying a model siRNA, we demonstrated that the PDPG polymer can specifically deliver the siRNA to HuH7 cells, a cellular model of HCC. Notably, the elimination of the Gal residue from the PDPG (PDP) or the chemical block of ASGPR, resulted in an evident reduction of PDPG targeting effectiveness. These data have been confirmed in HuH7 constitutively expressing the enhanced green fluorescence protein (EGFP) using a functional siRNA against EGFP. Finally, PDPG delivery specificity and effectiveness was proved also *in vivo* in a mouse dorsal skinfold window chamber assay. Together, our data support the remarkable targeting ability of the developed PDPG.

When PDPG was loaded by siRNAs targeting HCC proliferative factors (eEF1A1, eEF1A2 and E2F1), we observed a clear decrease of HuH7 cell vitality and cell number. These phenomena were paralleled by the reduction of targeted mRNAs and relative proteins levels. Interestingly, siRNAs-PDP, lacking the Gal residue was poorly effective in reducing HuH7 vitality and number.

Finally, *in vivo* experiments performed in a subcutaneous xenograft mouse model of HCC, revealed the ability of siRNAs-PDPG to reduce HCC tumour growth compared to controls. Notably, PDPG did not show significant polymer-related toxic effects as evaluated by monitoring animal weight and the levels of markers of organs function.

In conclusion, our study demonstrates the priceless potentials of PDPG as a novel delivery system for siRNA paving the way for innovative anti-HCC treatments.

2 Introduction

2.1 The liver: structure and functions

The liver is one of the principal organs of the human body whose main functions are to metabolize nutrients and excrete waste metabolites. Its weigh is approximately 1,5 kg and it is located in the right upper quadrant of the abdomen, protected by the diaphragm and thoracic cage. The organ is covered by Glisson's capsule and divided into 4 lobes: right, left, caudate and quadrate. The caudate and quadrate lobes are smaller and placed posteriorly, while the left and right lobes are larger and located anteriorly[1]. The liver receives both arterial blood, through the hepatic artery, and venous blood, through the portal vein that collects blood from the intestine and spleen (Fig. 2.1).

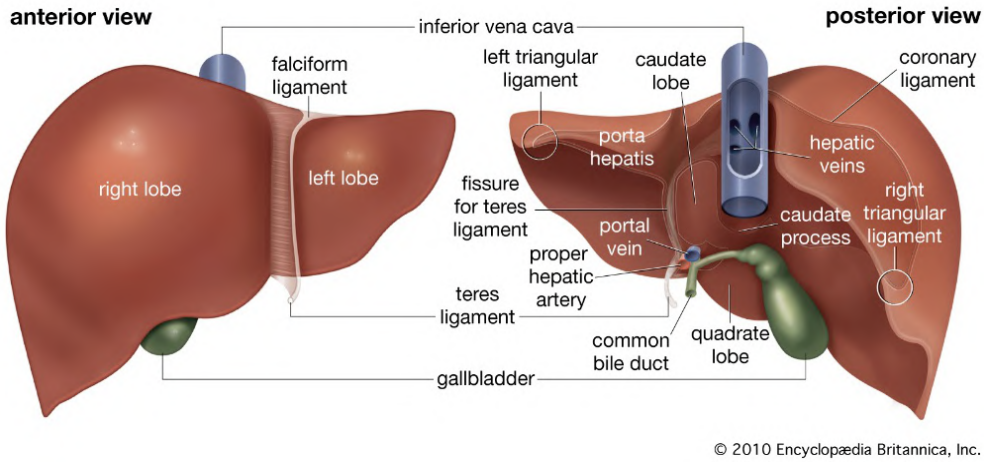

Figure 2.1. Liver anatomic structure[445].

Hepatic lobule is the basic functional unit of the liver, having a hexagonal shape and characterized by repetitive structures along each corners of the lobule. The repetitive structures consist on the portal triad, portal vein, hepatic artery, bile duct, and the centrolobular vein, located in the middle of the hexagonal structure[2]. Hepatocytes constitute the parenchymal cells of the liver and they are placed next to the hepatic sinusoids. The sinusoids are a system of vessels carrying blood from the portal vein to the central hepatic vein of the lobule and they are separated from hepatocytes by the space of Disse[3]. Nutrients are processed and stored by hepatocytes while the blood flows toward the central vein passing through the sinusoids and the space of Disse. At the same time, the circulating blood is purified from worn out blood cells and bacteria[2] (Fig. 2.2).

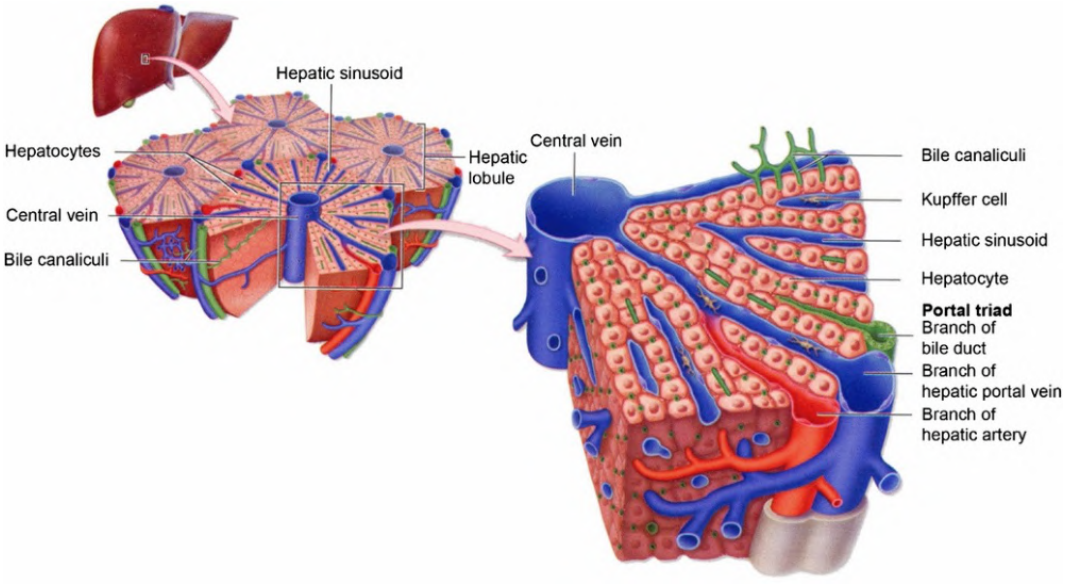

Figure 2.2. Anatomic structure of hepatic lobule[446]

The liver contains many different cell types:

- Hepatocytes: the most abundant representing the 60 % of liver cells. These cells are characterized by the presence of many and large mitochondria, lysosomes, peroxisomes and many organelles like Golgi apparatuses and endoplasmic reticulum[4]. Hepatocytes are mainly involved in the carbohydrate, protein and lipid metabolism, and they are responsible for the production of bile, albumin and coagulation factors. In addition, processes like the detoxification and excretion of drugs occur in these cells[5].
- Sinusoidal endothelial cells: these are endothelial cells that constitute the walls of the hepatic sinusoids; for their discontinuous architecture they represent a permeable barrier. Their main function is to allow the exchange and the uptake of molecules from the blood[6]. Sinusoidal endothelial cells have an endocytosis activity enabling to engulf molecules having small size. Moreover, they also display a role in the immunological response, regarding the clearance of viruses, secreting cytokines and eicosanoids and acting as an antigen presenting cells[7].
- Kupffer cells: most of the Kupffer cells present in the human body are placed in the liver. They are activated in the presence of an injury producing pro-inflammatory cytokines, reactive oxygen species and nitric oxide. Receptors on their cell surface are able to target and bind immunoglobulins covering the cells resulting in the phagocytosis process activation[8]. Kupffer cells play a role in the immunological response removing bacteria

from the sinusoids of the liver and other particles from the portal blood. They are also responsible for the elimination of intestinal bacteria from the blood coming from the gut and pancreas[9].

- Hepatic stellate cells: these cells store lipids and Vitamin A and are located in the space of Disse, between sinusoids and hepatocytes[10]. Hepatic stellate cells main functions are the control of the turnover of extracellular matrix and sinusoid contractility. Under stressful condition, they are activated and transformed, taking part in the inflammatory fibrotic response[11].

Main functions of the liver are to drain intestinal blood and to capture nutrients, metabolize and distribute them to other organs. Drugs and toxic molecules are also metabolized into the liver, where they undergo detoxification. In this way, these molecules can be eliminated by kidneys, preventing excessive accumulation and adverse effects[2]. The liver is also involved in several processes important for the normal physiology of the human body.
In particular, it is responsible for the metabolism of:

- Proteins: plasma proteins like albumins and blood coagulation factors *(*prothrombin, fibrinogen, and clotting factors*)* are synthesizes in the liver[12].
- Sugars: sugars from the diet are processed by the liver. Hepatocytes can store sugars as glycogen molecules and release them into the bloodstream when necessary[13].
- Fats (lipids): examples are triglycerides and cholesterol. Lipids are metabolized, transformed and partly eliminated from the liver[14].
- Vitamins: The liver synthesizes vitamins like vitamin B, vitamin K and the lipo-soluble vitamins (A-D-E)[2].
- Minerals: The liver stores the iron and the copper. The iron is present as ferritin, an iron-protein complex; the iron can be then released into the bloodstream (conjugated with transferrin) for red blood cell production[15].
- Hormones: the liver metabolizes hormones produced by the different glands of the organism[16].
- Other compounds: The liver synthesizes several non-essential amino acids and serum enzymes including aspartate aminotransferase, alanine aminotransferase, lactate dehydrogenase and alkaline phosphatase[17].

The liver is the organ where the bile is produced. The bile is a fluid, whose main function is to allow the absorption of lipids and A,D,E,K vitamins from food by small intestine. It is also important for the elimination of the bilirubin, a substance produced by the catabolism of heme[18].

Alterations in the function of the liver may decrease the ability of the organ to capture, transform and eliminate bilirubin and therefore, increasing its concentration in the blood. This can cause the typical yellowish coloration of eyes and skin (jaundice), characteristic of many hepatic diseases[19].

The liver can store a large volume of blood because of its extensive vascular network. It can also release blood to maintain systemic circulatory volume in the event of hemorrhage. During some stages of the embryogenesis and fetal development, the liver represents the main hematopoietic organ. Indeed, here there are hematopoietic stem cells that can produce all leukocytes cell types[20]. In addition, the liver contains Kupffer cells and NK cells, which play an important role in the immune response[2].

The liver is the only organ in the human body having regenerative properties, activated when the organ is damaged chronically. Sometimes, when the regenerative process occurs very frequently, it can cause abnormal growth of the liver destroying its normal anatomy and circulation, giving rise to the pathological conditions, such as cirrhosis[21].

The main harmful factors that can cause hepatic damages are infectious agents (viruses, bacteria, parasites), toxic substances (drugs, alcohol, chemicals) or disorders of other organs (heart disease, metabolic diseases, tumours). The exposure of the liver to harmful agents leads to the production of inflammatory cytokines and the activation of resident macrophages triggering an inflammatory response. Inflammation of the liver, especially if it becomes chronic, may lead to a dysregulation of the normal physiology of the organ[22]. In this scenario, matrix deposition occurs, resulting in the imbalance between fibrogenesis and fibrosis processes. The matrix deposition lead to scar formation made up of the abnormal accumulation of extracellular matrix with a vascular reorganization, leading to the liver fibrosis. Liver fibrosis can culminate in liver cirrhosis, which can bring to liver failure[23].

2.2 Hepatocellular carcinoma

Cancer develops when normal cells do not respond appropriately to signals that regulates the normal cell proliferation and they start to divide in an uncontrolled manner invading normal tissues and organs. The loss of the growth control is due to mutations that accumulate in the cells over time resulting in a deregulation of several cellular pathways[24].

The primary liver cancer originates in the liver and the most common is the Hepatocellular Carcinoma (HCC). The HCC is the sixth most common cancer in the world, and it is the third leading cause of all cancer-related deaths, accounting around 80–90% of all primary liver cancers. Males are more prone to develop the HCC than females and the pathology appears around 50-60 years of age[25]. The HCC is more common in Asian countries including China, Mongolia, Southeast Asia, Sub-Saharan Western and Eastern Africa. Its prevalence in developed countries of the world is lower, except for Japan, Italy, and France. The diffusion of HCC is increasing significantly in the USA in the last decades, probably due to the higher incidence of alcoholic liver diseases, Hepatitis C virus (HCV) and Hepatitis B virus (HBV) infections (Fig. 2.3)[26].

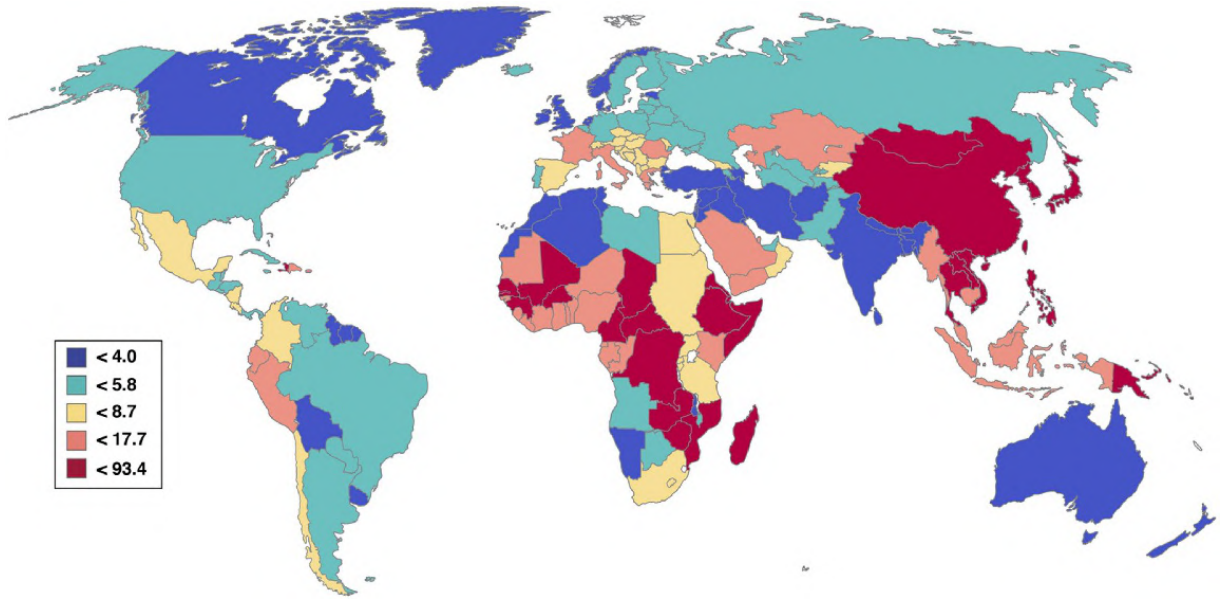

Figure 2.3. Distribution of HCC incidence in the world. The rates are reported per 100,000 persons[447].

Liver cancer occurs mostly in people who already have chronic liver diseases, like cirrhosis or viral Hepatitis[27]. HCC is often asymptomatic and the latency period from hepatic damage to tumour development is very long. Available treatments include liver resection or transplantation,

effective if the diagnosis is made in the very early stages of the disease[28]. Unfortunately, in most of the cases, HCC is diagnosed in the advanced stages when available treatments are often poorly effective. In this case, Radiation, Targeted therapy and Chemotherapy treatments provide only a palliative care for patients, even if they can somehow prolong patients' life span of few months. Systemic chemotherapy has limited effectiveness too, due to the chemoresistance that is very frequent in HCC patients[29].

Chronic liver disease and cirrhosis are the main risk factors for the development of HCC, while virus infections (Hepatitis B and C virus) and toxic agents (alcohol and aflatoxin) most often sustain chronic liver inflammation. Minor risk factors are represented by metabolic disease (diabetes and non-alcoholic fatty liver disease, hemochromatosis) and immune- related disease (primary biliary cirrhosis and autoimmune hepatitis)[25].

2.3 Risk factors for HCC development

2.3.1 Hepatitis B Virus infection

Hepatitis B Virus (HBV) is a human pathogen causing chronic infections affecting mainly the liver, which can lead to cirrhosis and primary liver cancer. It was estimated that 54% of all liver cancers are caused by HBV infection[30].

Chronic HBV infection increases the risk for HCC development of 15–20-fold with a mortality rate of approximately 30%–50% among all cases[26]. HBV is widespread in the world especially in the Western Pacific and African regions. The Eastern Mediterranean, South–East Asian and European regions have fairly high prevalence of infected people, while the North and South American regions have the lowest number of individuals affected by HBV[31]. It was estimated that 25% of people infected by HBV will die for cirrhosis or HCC, and according to the WHO data, the mortality is increasing per year[30]. HBV infection can be prevented by vaccination, effective against all of HBV genotypes, giving an immunological memory for about 20 years[32].
The virus infection occurs through exposure to blood or bodily infected fluids, sexual contact, blood transfusions and perinatal and early infant transmission (vertical transmission from mother to child (MTCT))[33,34].

The Hepatitis B virus is a circular partially double-stranded DNA belonging to the *Hepadnaviridae* family. It exists in ten different genotypes, named with letters from A to J, and they are widespread in different geographical areas with different outcomes[35].
Virions are spherical and composed by two shells[36,37]:
-an envelope, constituting the outer part of the virus and made by host lipid and surface proteins;

-an icosahedral capsid, constituting the inner part of the virus, composed by proteins and containing the genomic DNA[38].

The genome is 3.2 kilobase (kb) pairs in length, characterized by having gaps in both strands and with 4 partially overlapping open reading frames[39]:

- *S (surface) ORF*: encoding the surface proteins HBsAg[36].
- *C (core) ORF*: encoding the core antigen HBcAg, that forms the nucleocapsid, the e antigen (HBeAG), a marker for the active viral replication, and an upstream region for the S (pre-S) and C (pre-C) genes[39].
- *X (X gene) ORF*: encoding the transcriptional transactivator X protein[40].
- *P (polymerase) ORF*: encoding the viral polymerase[41].

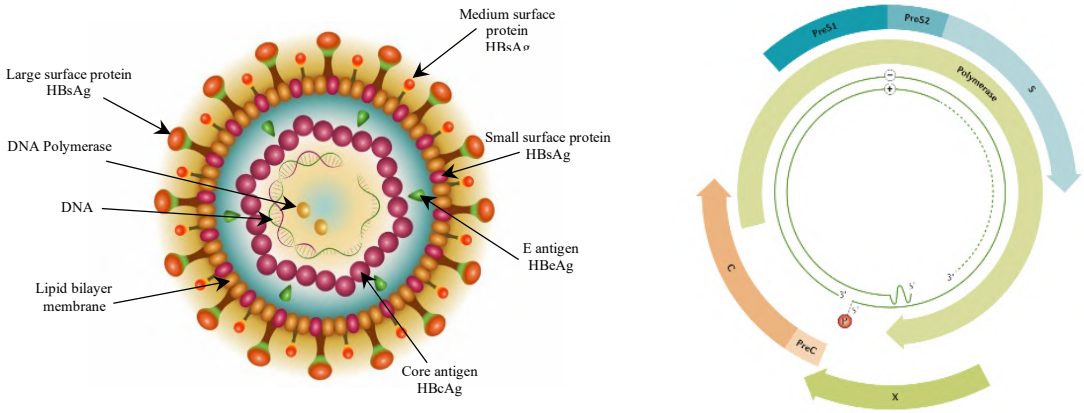

Figure 2.4. Hepatitis B virus structure and genome (adapted from[48,448]).

2.3.1.1 Viral life cycle

The Hepatitis B virus has an incubation period of approximately 2-4 weeks in healthy adults and decades in newborns[42]. Following this period, the disease becomes symptomatic and the HBeAg can be detected in the serum. The duration of the stage is approximately 3-4 weeks for patients with acute infection and 10 years or more for patients with chronic infection, before cirrhosis or HCC developed[43]. Then the viral replication is no longer measurable in the serum because more likely the viral genome is integrated in the host's hepatocyte genome[44] and the infection becomes chronic[45].

The infection of HBV is a multistep process starting with the binding of a highly conformational determinant region of the HBsAg glycoprotein to heparan sulfate proteoglycans present on the host hepatocytes cell surface. This is a low-affinity binding reaction and it is still a

reversible process[46]. After that, the HBV interacts with the hepatic bile acid transporter sodium taurocholate co-transporting polypeptide (NTCP)[47] which shows a high affinity for the large HBsAg (L) protein, leading to the internalization of the virus. Once inside the cell, the partially double-stranded viral DNA is transported into the nucleus by chaperons where the viral polymerase makes the DNA a fully double stranded DNA. Afterwards, the dsDNA is transformed into covalently closed circular DNA (cccDNA) by host cellular enzymes[48]. The cccDNA, associated with histone H3, histone H4 and non-histone proteins derived from host cell, forms the so called minichromosome, which utilizes the host cell transcriptional machinery to produce all viral RNAs[49]. Two species of transcripts are produced: the pregenomic RNA (pgRNA), which works as the template for reverse transcription of the viral genome, and the precore RNAs, used to produce viral proteins. Virions are assembled from these viral transcripts and they can be released by the cell or return to the nucleus to produce more copies of the virus[48,36]. Double-stranded linear HBV genomes enclosed in some nucleocapsids can integrate into the host cell genome leading to the development of liver diseases, including the HCC[50].

2.3.1.2 Hepatocellular carcinoma and HBV

HBV is linked to the HCC in approximatively 50% of the cases. The mechanism responsible for the development of hepatocarcinogenesis is still unclear, but the hepatitis B virus can promote HCC development in two different ways[51].

In the direct way the viral genome integrates into the host genome randomly, or in critical positions like in retinoic acid receptor alpha and human cyclin A gene regions[52,51]. The viral genome integration can cause deletion, insertions or translocations, inversions, duplications leading to genome instability or the overexpression of factors involved in cell cycle proliferation with a consequence of HCC development. It has been seen that the deregulation of the Ras-Raf-MAP kinase pathway, often found implicated in HCC development, is associated with the HBx gene expression[53]. In addition, HBx is a transactivator factor, able to interact with different transcription factors such as CREB (cyclic adenosine monophosphate [cAMP]–response element-binding protein), TP53 and ATF-2 (activating transcription factor 2), interfering with their normal cellular activities[54,55].

In the indirect way, chronic infection of HBV causes liver inflammation, with the activation of fibrogenic processes and fibrosis and cirrhosis formation, which may culminate in liver disease or in HCC[36]. The produced pro-inflammatory factors can trigger hepatocytes proliferation with the replacement of the infected hepatocytes. The cell turnover is very high during chronic hepatitis B

causing a higher rate of hepatocytes proliferation with accumulation of mutations, leading to genomic instability, uncontrolled cell proliferation and consequently HCC development[55].

Interferon therapy and inhibitors of reverse transcriptase can control the virus proliferation, but they do not eliminate the virus. Up to day, vaccination is the best way to prevent HBV infection[48].

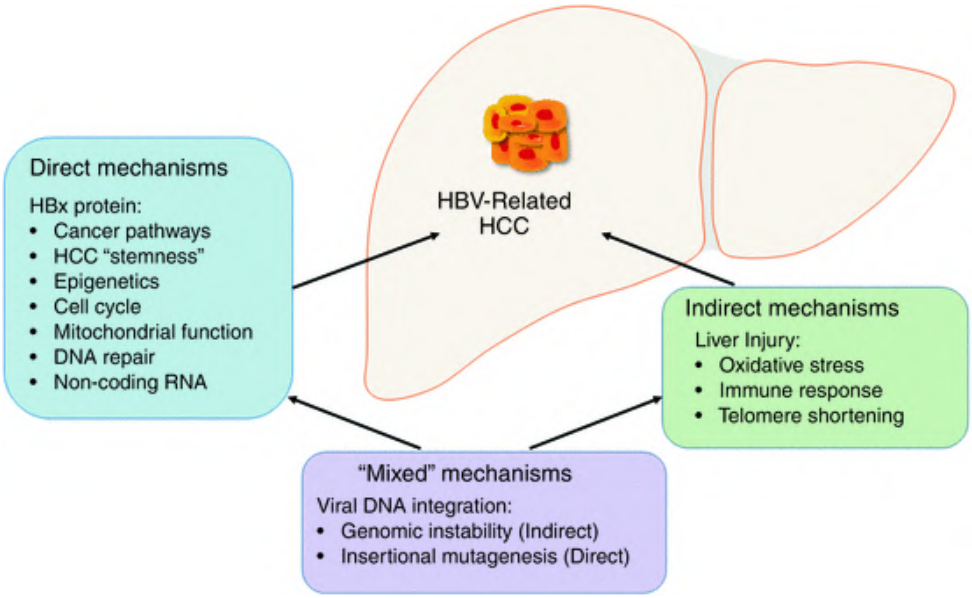

Figure 2.5. Representation of mechanisms involved in HBV-related HCC development[449].

2.3.2 Hepatitis C Virus infection

The Hepatitis C virus belongs to the *Flaviviridae* family and it is responsible for the development of diseases affecting the liver, like the hepatitis C, and liver cancer, like HCC in humans[56].

The HCV is widely spread in the world, especially in North Europe, North Africa and Egypt. Countries like United Kingdom and Scandinavia show a lower incidence, while in Italy, Spain, China and Japan the incidence is increasing. An estimation of around 117.5 million adult people is affected by HCV, of which 27% have cirrhosis and 25% developed HCC[57]. The main contagious routs are through the blood and by the use of infected stringers. The infection can be transmitted by sexual contact with the infected partner or by infected medical equipment during medical operations. Maternal-foetal transmission of HCV is rare, except in the case in which the mother shows high levels of HCV RNA in the blood. However, there are a large number of HCV infection cases in which the rout of contagious cannot be identified[58].

HCV is often asymptomatic and its diagnosis during the acute phase is very rare, although the development of antiviral drugs has improved the HCV treatment[59]. It has been seen that people affected by acute HCV infection showed a good response to the interferon (IFN) therapy, recommended for the treatment of acute and chronic HCV infection. The diagnosis is usually made when the disease is in the chronic stage, and interferon, alone or in combination with ribavirin, was the most effective treatment used in the past years[60].

As of today, the most applied HCV therapy is the recombinant interferons IFN alfa-2b (Intron-A) and IFN alfa-2a (Roferon-A). Since the beginning of 2001, the IFN was modify adding the propylene glycol (PEG) conferring to the classic IFN more stability, better absorption, slower rate of clearance. The PEG-IFN was approved by FDA and it is available for the treatment of chronic HCV. Nowadays, PEG-IFN combined with Ribavirin (RBV) is the standard therapy for HCV infection treatment[61]. The combined treatment sofosbuvir/velpatasvir/voxilaprevir (SOF/VEL/VOX), known as Vosevi®, was recently approved by the FDA (July 2017) for the treatment of patients with acute HCV and without cirrhosis or with compensated cirrhosis[62]. Vosevi® inhibits three proteins essential for virus replication and infection: NS5B RNA-dependent RNA polymerase (sofosbuvir); NS5A protein (velpatasvir) and NS3/4A protease[63].

2.3.2.1 Viral life cycle

Studying the Hepatitis C virus is very difficult because of the impossibility to grow the virus in cell culture. Data collected by different *in vitro* and *in vivo* experiments allowed to have a general overview of the virus cell cycle[64].

The Hepatitis C virus exists in different genotypes divided in seven type and around 80 subtypes, based on nucleotides variation due to the high replication rate of the virus and the poor proofreading activity of the RNA-dependent RNA polymerase[65,66].

The Hepatitis C virus is constituted by a lipid membrane envelope and an icosahedral core of basic protein forming the viral nucleocapsid. The nucleocapsid wraps a positive-sense single-stranded RNA genome encoding for a large polyprotein of 3010 amino acids. The core of the virus is made by the first 192 amino acids of the polyproteins and it is able to interact with many cellular proteins causing a deregulation of different pathways in the cell, like lipid metabolism, apoptosis process and gene transcription[67]. The virus uses the cellular machineries to process the polyprotein into smaller and active viral proteins: core-envelope proteins (E1 and E2), p7 and nonstructural proteins (NS2, NS3, NS4A, NS4B, NS5A, NS5B) (Fig. 6). NS3 serine-like protease and the NS5B RNA-dependent RNA polymerase (RdRp) are the most important proteins used by the virus for its maturation and replication[66].

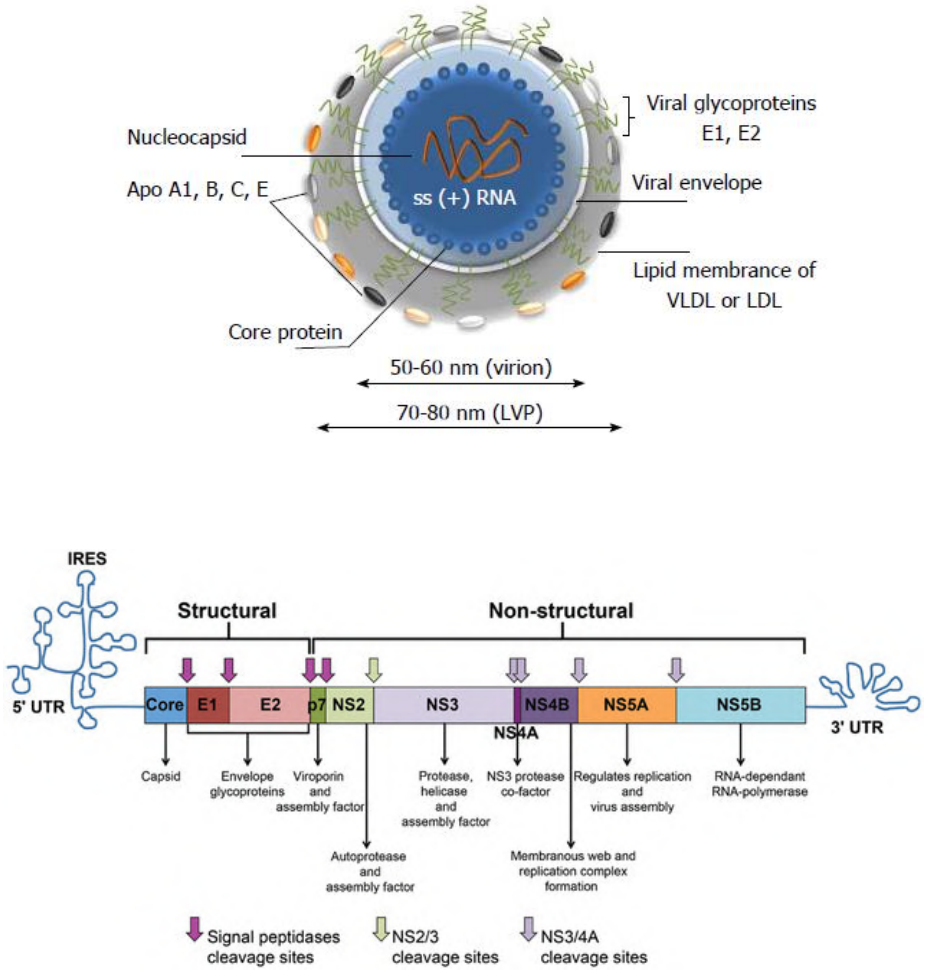

Figure 2.6. Hepatitis C virus structure and genome[69,450].

The virus can enter into the host cell through different surface molecules like CD81, mannose-binding lectins (DC-SIGN and L-SIGN), glycosaminoglycans and member of the claudin family (CLDN1, 6 and 9) proteins[68]. After the attachment, the virus interacts with SR-BI and CD81; in particular, E2 protein binds the external loop of CD81 with high affinity. Then the virus is internalized and the nucleocapsid released into the cytoplasm. Here, the positive strand RNA virus is used as mRNA to translate the polyprotein into the endoplasmic reticulum[69]. A negative strand RNA is synthetized by the NS5B RNA-dependent RNA polymerase in order to be used as a template for the synthesis of the positive strand RNA virus genome. The encapsidation of the virus could take place in the endoplasmic reticulum, while the envelope coating of the nuceluocapsid could happen in the Golgi apparatus[70].

2.3.2.2 HCV and Hepatocellular carcinoma

The mechanism of HCC development induced by HCV infection is not fully understood yet, since there are not effective *in vitro* model systems to study HCV biology. HCV virus cannot integrate into the host genome, so it causes HCC development indirectly[71].

Many data allowed to make some hypothesis on how the HCV infection can cause HCC in patients. It has been shown that HCV infection induces a chronic inflammatory state with formation of fibrosis and cirrhotic tissue, creating an optimal environment for HCC development. Progressive liver fibrosis lead to the formation of neoplastic clones with genetic and epigenetic alterations and consequently to carcinogenic tissue formation[72]. The risk of HCC development could be correlate with the severity of liver fibrosis, especially in patients affected by chronic HCV infection[73].

HCV infects not only hepatocytes but also other liver cells like monocytes and stellate cells. Damaged hepatocytes release fibrotic factors, inflammatory molecules and cell death signals, while hepatic stellate cells promote the fibrotic process through cell proliferation and matrix degradation. Profibrogenic mediators like TGF-β are induced by HCV core and nonstructural proteins. The virus can also induce the production of TGF-β1 by the formation of oxygen species (ROS) and p38 MAPK, JNK, ERK, NF-kB pathways activation[74]. Pathways that are very important in the cell proliferation and apoptosis evasion are activated by NS5A virus protein. Examples are PI3K/AKT, β-catenin/WNT pathways and inhibition of caspase-3[75]. In addition, NS5A inhibits TGF-β signaling and consequently, Smad proteins cannot translocate in the nucleus of the cells to activate the transcription of the tumour suppressor CDKN1A[76]. The continuous proliferation of hepatocytes to replace damaged cells causes the telomere shortening leading to a senescence state of the cell in normal condition, activating ATM, TP53, and CDKN1A, which are factors preventing the carcinogenesis[77]. In the presence of HCV virus, core proteins can induce the downregulation of CDKN2A expression via DNA methylation leading to senescence escape in the hepatocytes. These hepatocytes present shorter telomers and mutations in telomerase reverse-transcriptase promoter with favouring HCC development[78].

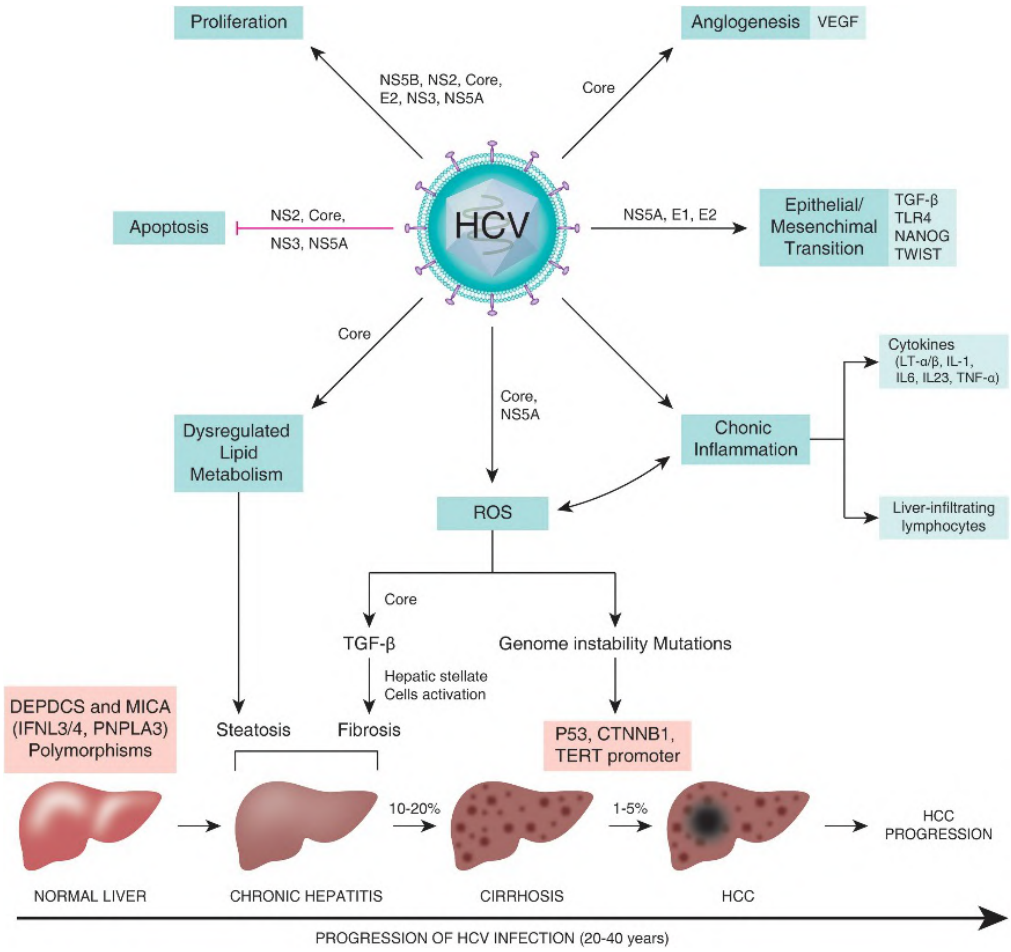

Figure 2.7. Mechanisms involved in the HCV-related HCC development[451].

2.3.3 Diabetes and obesity

Diabetes is a group of metabolic disorders characterized by the increase of glucose level in the blood[79]. There are three types of diabetes:

-type 1: pancreas does not produce insulin due to the autoimmune response activation, which destroys pancreatic cells;

-type 2: referred also as "insulin resistance". In this case, target cells are resistant to a various degree to insulin action, i.e. glucose internalization into the cell;

-Gestational diabetes: it occurs during pregnancy[80].

Diabetes, in particular the type 2 diabetes mellitus (DM), is associated to the risk of the development of different type of cancers including HCC, even if it is difficult to explain how they are correlated each other[81]. Diabetes is also linked to the HCV infection, where the virus infects the pancreatic cells decreasing the insulin production and causing a disfunction of β-cells. In addition, the HCV virus activates T lymphocyte-mediated immune response with the production of tumour necrosis factor-α (TNF-α) and interleukin-6 (IL-6), causing the development of the

insulin resistance and the increase of glucose levels in the blood. This condition can lead to the onset of the type 2 diabetes mellitus simultaneously with an imbalance in the adipokine level and the liver fibrosis formation caused by HCV which can culminate in HCC[82].

On the other end, it has been seen that diabetes can arise in the end stage of liver diseases, where an increasing glucose levels and intolerance were observed. Diabetes is also a risk factor for the onset of the non-alcoholic liver disease (NAFLD) and for the non-alcoholic steatohepatitis (NASH), other risk factors for HCC development[83,84].

Epidemiologic studies from Europe, Asia, and North America reveled that diabetes mellitus is an independent risk factor for HCC. Indeed, hyperinsulinemia causes the increase of insulin-like growth factor 1 (IGF-1), which promotes the proliferation of hepatocytes, and the secretion of matrix proteins and some factors involved in hepatic fibrosis by hepatic stellate cells. In addition, it causes hepatic fibrosis formation and hepatocellular injury decreasing mitochondrial β-oxidation of fatty acids[85]. The contemporary presence of diabetes mellitus and chronic liver inflammation can promote the development of HCC[86].

Obesity is another risk factor for HCC, which is also associated with liver cirrhosis and liver fibrosis progression. It has been seen that obesity is linked also to DM, where carcinogenesis can be promoted by the secretion of proinflammatory cytokines produced by visceral adipose tissue[85]. Recent analysis showed that obese people and overweight people have 90% and 17% higher risk to develop HCC respectively, compared to people with normal weight[87]. Moreover, other studies showed that obesity is correlated to HCC because of the secretion of some adipokines and vascular endothelial growth factor (VEGF) by visceral adipose tissue, which are involved in angiogenesis dysregulation and other clinical symptoms[88].

2.3.4 Diet and toxins

Alcohol abuse is very common in western countries and, together with other HCC risk factors like DM, HBV and HCV infections, can have a synergistic effect in the development of HCC[89]. The consumption of alcohol can cause the oxidative stress promoting DNA damages and cirrhosis, factors that can lead to HCC. Moreover, alcohol is metabolized to acetaldehyde, a compound able to damage the hepatocytes DNA, causing DNA alterations[90]. Some studies evidenced that there is a direct effect of elevated alcohol consume in inducing HCC through hepatic inflammation with progression to liver fibrosis or cirrhosis. Kikuchi M *et al.* (2015)

performed a study in which 1,478 alcoholic liver cirrhosis patients showed to have also diabetes mellitus with high risk to develop HCC[91].

One of the main functions of the liver is to store the iron, but an overload of this metal contributes to hepatocarcinogenesis. This condition is frequent in hereditary hemochromatosis cases or as a consequence of chronic inflammation, observed mainly in patients with high alcohol consume[92]. In these patients the HCC risk can be reduced treating them with chelating agents and repeated phlebotomy[93]. In other cases, an iron overload is due to the high amount of ingested iron, a condition very frequent in some regions of the world such as Sub-Saharan Africa, affecting about 15% of black rural Africans. These people consume an elevated home-made beer saved in drums or pots, which contain a high amount of iron[94].

Several studies showed that coffee consumption appears to have a positive effect on the prevention of liver diseases, including HCC. Different hypotheses tried to explain why coffee can prevent the HCC. One of them supposes that the consume of the coffee decreases the levels of gamma-glutamyltransferase (GGT) in the serum, an enzyme found associated with a lower probability to develop HCC[95].

Many studies tried to demonstrate if there are connections between diet and the risk of HCC. For instance, there is a trial from Italy in which dietary habits of 185 patients affected by HCC and 142 healthy patients were examined. It has been observed that patients consuming more calories were affected by HCC and they were more likely to be infected by virus like HCV and HBV[96]. In addition, the high consume of iron and thiamine increase the risk of HCC of 3-fold and 2-fold respectively. On the contrary, people who consumed carotene and linoleic acid have a reduced risk of developing HCC[87]. It seems that red meat and saturated fat consumption are linked with chronic liver disease and HCC risk, while green vegetable consumption decreases the risk of the hepatic cancer[97]. Indeed, studies on European and Japanese population showed that the incidence of HCC appears to be lower in people eating high amounts of green vegetable[98]. Moreover, the Mediterranean diet is associated with a lower risk for HCC, as observed in a study on people from Greece and Italy, suggesting that the consume of white meat and fish can decrease the risk of HCC development[99].

The results from different studies are disputable making difficult to recommend the consumption of specific food that could decrease the risk of developing HCC.

Aflatoxin B1 (AFB1) is a mycotoxin produced by the fungus Aspergillus which grows in grains, soil, decaying vegetation, hay and in food stored under warm and damp conditions[100]. The consumption of food contaminated by AFB1 represents a frequent risk factor of HCC development. AFB1 is metabolized into AFB1-exo-8,9-epoxide in the organism, which is

responsible for DNA damages and mutations in some genes such as the p53 tumour suppressor gene. Indeed, p53 mutation in frequently found mutated in 50% of HCC tumours especially in southern African people[101]. In addition, Aflatoxin exposition can induce mutation in CTNNB1 gene, encoding for β-Catenin. This protein accumulates in the cell leading to a deregulation in WNT-signaling pathway, found altered in HCC[102].

2.3.5 Non-alcoholic Fatty Liver Disease (NAFLD)

Non-alcoholic Fatty Liver Disease (NAFLD) includes different liver conditions characterized by an abnormal accumulation of fat in the liver cells unrelated to alcohol consumption[103]. Weight loss, dietary and exercises are considered able to contrast NAFLD[104]. NAFLD is widespread in the developed countries, affecting about 25-26% of Europeans and 25% of Americans. The peak of the disease is in the 5th and 6th decades of life and female are more affected (65% - 83% of cases) than males[105]. NAFLD is classifies as an idiopathic case for HCC and recent studies suggest that it is related also with cryptogenic cirrhosis, observed in 5-30% of patients affected by advanced stage of liver disease[106].

There are different conditions of NAFLD, ranging from the non-alcoholic fatty liver (NAFL), which usually does not cause liver damage, to the non-alcoholic steatohepatitis (NASH), which instead can cause liver inflammation and consequently liver damages[107]. Early stage of NAFLD does not usually cause problems, but when the level of the fat in the liver becomes very elevated, serious health problems and liver failure can occur. NASH is the more serious stage of NAFLD and it can evolve in fibrosis and/or in cirrhosis, causing a permanent liver damage and liver failure which lead to the cancer development[108].

Numerous cases showed that NASH, together with Diabetes Mellitus are responsible for HCC development[109]. Fat in the liver cannot disturb the normal liver function in the presence of NAFL, but in the case in which the liver undergoes to insults, the NAFL condition can evolve into non-alcoholic steatohepatitis (NASH), where inflammation and sometimes fibrosis coexists with steatosis[110].

2.4 Hemochromatosis

Iron, a very important metal for the normal function of human cells, is absorbed by the intestine and accumulated mainly in hepatocytes. The condition in which the iron exceeds 5g in the total body is defined as "iron overload", resulting in a variety of illnesses. The liver is the organ mostly affected by iron overload, leading to hereditary hemochromatosis (HH) and African dietary iron overload[94].

HH is an autosomal recessive inherited disorder (also referred as "Primary hemochromatosis") characterized by the progressive accumulation of the iron in different organs and in particular in the liver. This pathology presents mutations in different genes like the *HFE* gene, as observed in 70-95% of patients affected by HH. Mutations in *HFE* cause the impaired expression of the human hemochromatosis protein (HFE) on the cell membrane of hepatocytes thus destabilizing their sensitivity to the iron[111]. Consequently, the transcription and release of hepcidin is compromised, with a low secretion of hepcidin and iron overload. Hepcidin plays an important role in the control of iron absorption and in the systemic metabolism of the iron. Rare forms of HH are caused by missense mutations in other genes involved in hepcidin transcription, regulation of its release and biological activity[94].

HH exists also in another form called "Secondary hemochromatosis", which can be developed from different conditions like anemia, liver disease or blood transfusions and where genes mutations have not been found[112].

The loss of hepatocytes sensitivity to the iron concentration lead to the metal accumulation with the denaturation of ferritin subunits and ionic iron accumulation in the hepatocyte cytoplasm. Iron is a metal able to produce reactive oxygen intermediates causing oxidative tissue damages, protein modifications, lipid peroxidation, DNA instability with hepatocyte damage and dysfunction. This condition is favorable for the development of fibrosis and cirrhosis which can culminate in the HCC, already observed in 45% of patients affected by HH[113].

2.5 Hepatocarcinogenesis

2.5.1 Pre-cancerous lesions in HCC

HCC development is a multi-step process requiring very long time. It usually arises when the liver is already damaged by hereditary diseases or liver damage, but it has been reported that the tumour develops without previous organ injuries in some cases (15%-20% of HCC)[114]. Macroscopically nodular injuries with abnormal morphology precede and accompany often HCC arising in cirrhotic patients, showing sometimes malignant features[115].

Typical morphological lesions during the initial steps of hepatocarcinogenesis are dysplastic lesions, distinguishable in dysplastic foci and dysplastic nodules. All of them are referred as pre-neoplastic lesions and they have been found throughout the liver[116].

Dysplastic foci are composed by a group (cluster) of dysplastic hepatocytes with a large or small cell type. They can be distinguished in dysplastic foci showing small cell changes (SCC) or in dysplastic foci with large cell changes (LCC)[114]. In the first case, cells show a low amount of cytoplasm, the nucleus is polymorphic and is larger than normal hepatocytes with an increased nuclear/cytoplasmic ratio. They are also characterized by the high proliferation rate that can be a predisposition for HCC development[117]. The second type of dysplastic foci (LCC) are cluster of hepatocytes with bigger nucleus, high amount of cytoplasm, normal nucleus/cytoplasm ratio, prominent nucleoli and nuclear pleomorphism. Moreover, they have abnormal DNA and aberrant chromosomes which can cause cell changes leading to HCC development[118]. Both SCC and LCD, represent high risk factors of HCC development, especially in patients affected by cirrhosis[119]. However, it has been observed that only a few SCD foci evolve into HCC, probably due to their high proliferation rate and resistance to the apoptosis. Instead, LCD foci were mainly observed in patients where cirrhosis and HCC are both present and HCC development is probably due to the aberrant DNA characterizing LCD foci[120].

Dysplastic nodules are bigger than dysplastic foci, with size more than 1 mm. They can be distinguished in high-grade and low-grade lesions. Both dysplastic lesions are mostly found in cirrhotic patients and they could represent pre-cancerous lesions for HCC[121]. High-grade dysplastic nodules have irregular nucleus located in the cell periphery, high nuclear/cytoplasmatic ratio, basophilic cytoplasm, rare mitoses and can occasionally present arteries formation[122]. Low-grade dysplastic nodules have a normal nuclear/cytoplasmic ratio, no mitosis and present few abnormalities[123]. Dysplastic nodules can be composed by many cells, but less than 10 cells per nodule. Cirrhotic patients usually have liver containing dysplastic nodules, but a few cases in which they were present in liver without cirrhosis were reported[124].

2.5.2 Genetic alterations in HCC

It is well known that cancer development is a multistep process. Chromosomal instability and in general genomic alterations accumulate slowly in the early stage of the tumour and increase in the late stage of its development. Indeed, cancer cells are characterized by an aberrant number of chromosomes, like aneuploidy, or/and chromosomes defects, like deletions, translocations and amplifications[125]. These abnormalities are very frequent in HCC and several studies demonstrated that they are placed in specific chromosome regions. For example, episodes of gain of function in chromosomes 1q, 5p, 6p, 7q, 8q, 17q and 20q and loss of function in chromosomes 1p, 4q, 6q, 8p, 9p, 13q, 14q, 16p-q, 17p, 21p-q and 22q due to chromosomal instability were often observed. Genes having a tumour suppressor function or oncogenes like *c-myc*, *cyclin D* and *PTEN* are placed in these chromosomes and they were found associated to HCC arising[126,127].

Mutations in the 1q chromosome is one of the most frequent chromosomal abnormality detected in HCC. In particular, the amplification of the chromosome 1 was found especially in the II-IV grade of HCC and in HCV-associated HCC. Genes like neurotrophic tyrosine kinase receptor type 1 (*NTRK1*), tropomyosin alpha-3 chain (*TPM3*), B-cell CLL/lymphoma 9 protein (*BCL9*) and aryl hydrocarbon receptor nuclear translocator (*ARNT*), which are involved in cancer, are encoded in the regions. These findings indicate that amplifications in chromosome regions containing these gene cause their overexpression, thus, playing an important role in hepatocarcinogenesis[125].

Amplifications in 8q chromosome are also very frequent in HCC. In particular, 8q24.21-24.22 region, where oncogenes like myelocytomatosis viral oncogene (MYC) and human melanoma-derived leucine zipper extra-nuclear factor (*MLZE*) are placed, was observed frequently amplified[125]. The amplification of *c-myc* oncogene was found in early stages of hepatocarcinogenesis and it seems that this gene is very important for HCC progression[128].

8q21.13, 8q22.3, and 8q24.3 regions were also found amplified in HCC. Here, genes involved in cancer development and progression, i.e. hairy/enhancer-of-split related with YRPW motif protein 1 (HEY1), are encoded[129]. Loss of the short arm of the chromosome 8 with the deletion of 8p21-22 region is very frequent in HCC. DLC-1 gene, which is found to be down-regulated in HCC, is located in this region. Moreover, it has been observed that its normal expression can decrease the tumour growth and activate apoptosis[130].

The amplification of the 7q21.3 region was supposed to be involved in the progression or development of HCC. Oncogenes in this region, like the cytoplasmic dynein 1 intermediate chain 1 (DYNC1I1), paternal express gene 10 (PEG10) and Epsilon-sarcoglycan (SGCE) genes, could be involved in HCC[131,132].

Loss of heterozygosity (LHO) occurs when one of the two alleles is lost at one or more loci with the absence of a functional tumour suppressor gene[133]. The LHO was observed in several chromosomes like 4q, 6q and 16q. In particular, LOH on chromosome 8 is very common in HCC, especially in high-grade dysplastic nodules. Many tumour suppressor genes, often deleted in liver cancer 1 (*DLC1*), elongator complex protein 3 (*ELP3*) and coiled-coil-domain containing protein 25 (*CCDC25*) are located in the chromosome 8[125].

Deletions in the 16q chromosome are very frequent in HCC, especially in the 16q22 region, where two tumour suppressor genes, CDH1 and TAT, probably involved in HCC are present. In particular, mutation of CDH1 result in uncontrolled cell proliferation induction with metastasis formation[134,135].

Genes important for the regulation of cell cycle or involved in cell proliferations are often found to be mutated in HCC. Examples of these genes are: *TDP53* gene, located on 17p13.1 chromosome, telomerase reverse transcriptase (*TERT*) and catenin beta 1 (*CTNNB1*)[126].

The balance between oncogenes and tumour suppressor genes is very important for the normal homeostasis of cells. The oncogenes promote cell proliferation, inhibit differentiation and apoptosis. Instead, tumour suppressor genes promote apoptosis and repress the transcription of genes involved in the cell cycle progression[136]. When some tumour suppressor genes are inactivated or oncogenes are overexpressed due to mutations, cells start to proliferate out of control. In addition, apoptosis is often repressed, thus contributing to the accumulation of genome mutations causing tumour development[137].

Many tumour suppressor genes, like *TP53, Rb, CDK1NA* and *pTEN* can be inactivated in HCC, losing the cell cycle regulators with cancer development. In particular, in the case of the HCC, it has been observed that the Hepatitis b virus X (HBx) gene, when it is integrated in the host genome cell, can be activated and act as a proto-oncogene, interacting with cellular signaling pathways like RAS/RAF/MAPK, MEKK1/JNK and PI3K/AKT/mTOR. Moreover, it can be also involved in transcriptional regulations, cell cycle progress, DNA repair and cell death[138].

2.5.3 Aberrant molecular signaling pathways in HCC

Tumour cells are characterized by altered pathways, which cause an uncontrolled proliferation rate, apoptosis escape and morphology changes. Many pathways involved in angiogenesis process, cell cycle regulation and cell proliferation have been found deregulated in HCC, playing an important role in cancer development.

An example is the VEGF factor, implicated in VEGF-mediated angiogenesis, which has been found overexpressed in HCC patients[139]. The tumour needs blood vessels to growth and thus tumour angiogenesis is triggered via the activation of endothelial cells, an increased vessel permeability and extracellular matrix reorganization. All these alterations, concurrently with the overexpression of pro-angiogenetic factors, like Ang-2 and VEGF, culminate in the formation of new vessels in the HCC tumour region[140]. One of the functions of VEGF is to stimulate hepatocytes or cancer cells through VEGF receptors increasing cell proliferation rate. Moreover, hypoxia, a typical condition in the growing tumour, can release a large amount of the hypoxia inducible factors (HIFs) that targets VEGF, which in turn stimulates the proliferation and migration of the endothelial cells with the formation of tumour blood vessels[141].

In the normal liver, hepatocytes are in the quiescence phase G0 of the cell cycle. In some cases, for example after surgery or when cells are subjected to injuries, they can start to proliferate in order to replace damaged hepatocytes or repair wounds[142]. Progression in the cell cycle is regulated by cyclins and their respective cyclin-dependent kinases (Cdk). Upon mitogenic factors or injuries, cyclin D is synthetized and complexed to Cdk4 or Cdk6, promoting the G1 to S phase progression[143]. Cyclin D was found mutated and overexpressed in HCC playing an important role in tumour cell proliferation and in HCC development. Moreover, its overexpression correlates with advanced tumour and stage progression[144].

Proteins involved in the cell cycle progression are also the E2F protein family. In particular, the activator E2F proteins E2F1, E2F2 and E2F3 were found up-regulated in HCC[145,146]. Moreover, it has been seen that the retinoblastoma protein (pRb) present different mutations in HCC. The alteration of the pRb pathway lead to the evasion of growth suppressors promoting cell division[142].

Another molecular signaling pathway that play an important role in the pathogenesis of HCC is the Wnt/β-catenin signaling pathway. It is involved in tissue homeostasis, cell proliferation, cell polarity and cell fate during embryonic development[125]. The pathway is activated when an extracellular ligand of Wnt binds the receptor on the cell membrane triggering a cascade of event that culminates in the destruction of β-catenin. This results in β-catenin translocation into the nucleus where it binds to many transcription factors involved in several cellular processes like cell cycle regulation, cell proliferation, migration and metastasis[147]. β-catenin is present in low levels in normal hepatocytes due to the presence of the β-catenin destruction complex (APC, axin, and GSK-3). The deregulation of this pathway can be caused by mutations in the exon 3, encoding for β-catenin gene (*CTNNB1*) leading to a constitutive activation of the Wnt/β-catenin signaling pathway, strongly associated with the initial step of the HCC

formation[148]. Another way in which Wnt/β-catenin signaling pathway might be altered depends on mutations and loss-of-function in the negative regulator of β-catenin genes, *AXIN1/2* and *APC*[149]. The accumulation of β-catenin in the cytoplasm and its translocation in the nucleus, causes the deregulation of different processes like proliferation, apoptosis, and cell motility. Indeed, β-catenin mutation was found in around 20–40% of all cases of HCC[150]; AXIN1 mutation in 3–16% and AXIN2 mutation in 3% of HCC. Moreover, it has been seen that patients with HCV-related HCC showed an high frequency of *CTNNB1* gene mutations compared to HCC patients affected by HBV and non-viral HCC tumours[151].

Transforming growth factor beta (TGF-β) family is involved in several cellular processes like cell differentiation, cell growth, embryonic development, apoptosis and extracellular matrix (ECM) production[152]. The pathway is activated when one of ligands, TGF-β1, TGF-β2 or TGF-β3, binds to the TGF-β receptor 2. This interaction activates a cascade of events in the cell that culminates in the activation of different transcription factors[153]. TGF-β family shows a pleiotropic effect in cancer, acting as a tumour suppressor gene or an oncogene. This usually depends on the stage of tumour, but in general, its deregulation causes the loss of cell polarity, the increase of cell migration and the activation of the epithelial-mesenchymal transition (EMT)[152]. TGF-β superfamily genes have been found mutated in various cancers including HCC. Mutations in genes involved in TGF-β signaling cascade, like Smad4 and TGF-β receptors have been observed[154 155].

Other pathways frequently found deregulated in HCC are Ras/Raf/MAPK, PI3K/AKT/mTOR and Hedgehog.

Ras/Raf/MAPK is involved in cell growth, survival and cell differentiation. It was found overexpressed in HCC and its overexpression correlates with an advanced stage of HCC. The up-regulation of this pathway can be also caused by hepatitis viral proteins, such as hepatitis C core proteins and HBx protein[156].

PI3/AKT/mTOR signaling pathway is involved in cell growth, cell division and programmed cell death. It has been observed that this pathway is activated in 30-50% of HCC[157]. In the normal liver tissue, the tumour suppressor phosphatase PTEN negatively regulates the activation of this pathway. Alterations in PTEN expression and activity cause the constitutive activation of the PI3K/AKT/mTOR pathway resulting in an higher cell proliferation rate with tumour development[158].

The Hedgehog signaling pathway is very important for normal embryonic development, in the adult development, in cell differentiation, cell proliferation and tissue polarity[159]. It is abnormally activated in the carcinogenesis process inducing the transcription of Gli family transcription factors, which cause the uncontrolled cell proliferation and differentiation. It has been

seen that the Hedgehog signaling pathway deregulation is due to the overexpression of Hedgehog ligands Sonic hedgehog, Smo, Ptch and Gli1, which, in turn, regulate *c-myc* gene expression[160].

2.5.4 Epigenetic alterations in HCC

Epigenetic is related to any process in which genes are altered without changes in the genome sequence and, contrary to genetic mutations, these alterations are not permanent. The regulation of epigenetic process is very important for cell differentiation and during mammalian development[161]. Indeed, its deregulation causes several diseases in humans and it represents one of the main causes for tumour development. Processes involved in epigenetics are: histone (de)acetylation, DNA methylation and RNA associated silencing[162]. DNA methylation is the most frequent epigenetic process in which a methyl group is added to the position 5 of the cytosine ring in the CpG region and the reaction is catalyzed by the enzyme DNA methyltransferase (DNMT)[163]. There are two different DNMT enzymes: DNMT1, which is active during DNA replication to maintain the methylation on cytosines from the parental strand, and DNMT3, which is involved in de novo methylation, typical in the embryonic development[161]. Promoter regions of genes are rich in CpG dinucleotides and they can be hypomethylated or hypermethylated. When the CpG-rich promoter region is demethylated, the genome sequence is accessible to the polymerase and transcription factors. On the contrary, when they are methylated, gene silencing occurs. Hypomethylation is usually associated to genomic instability, instead, hypermethylation to chromatin structure alterations. Moreover, aberrant methylation usually occurs during the initial phase of HCC development and it increases proportionally during its development[164].

Methylation plays an important role in cancer development, where genes involved in DNA repair, cell cycle control and apoptosis are usually hypermethylated. It is not fully understood the mechanisms involved in aberrant DNA methylation, but recent studies indicated that genes like DNMTs, the ten-eleven translocation (TET) family of proteins, isocitrate dehydrogenase 1 and 2 (IDH1 and IDH2) are responsible of this alteration. Many genes involved in epigenetic mechanisms have been found deregulated in HCC. Promoters of the following genes *P15*, *P16*, *Ras association domain family 1 isoform A* (*RASSF1A*), and *Retinoblastoma 1* are hypermethylated and thus, the respective genes are not expressed in HCC[165,166,167]. Abnormal methylations in gene promoter were also found for the following genes in HCC: *WNK2, EMILIN2, TRIM58, GRASP, TM6SF1, HIST1H4F*, and *TLX3*[168]. *E-cadherin* gene promoter is frequently methylated in HCC cells, indeed, Lim S.O. *et al.* (2008) demonstrated that the methylation of the *E-cadherin* promoter occurs by histone deacetylase 1 (HDAC1) and DNA methyltransferase 1

(DNMT1). The enzymes are activated through PI3K-Akt pathway which, in turn, is activated by Snail, expressed after reactive oxygen species (ROS) production[169]. In another work, Okamoto Y. *et al*. (2014) showed that in mice with humanized liver, the Hepatitis B virus (HBV) or Hepatitis C virus (HCV) infection could induce alterations in DNA methylation[170]. Epigenetic alterations have been found also in patients affected by NAFLD[171]. Gao W. *et al.* (2008) demonstrated that gene promoters of *miR-219*, *MMP-14*, *RASSF1A*, *TBX4*, *GNA14*, *CDKN2A*, and *CCNA* are hypermethylated in HCC. In their work they restore the expression of these genes using the 5-aza-deoxycytosine, an DNMTs inhibitor[172].

Many tumour suppressor genes present hypermethylated CpG islands in their promoter in HCC. Examples of these genes are *SOC-1,* involved in JAK/STAT signaling pathway and found suppressed in around 60% of HCC patients, and *APC*, hypermethylated in 53% of HCC patients[173].

DNMT1, DNMT3A and DNMT3B enzymes are overexpressed in HCC patients. Genes like *CDKN2A, CDKN2B, CDH1*, and *Rb1*, which are normally unmethylated, were found hypermethylated by DNMT3A and DNMT3B[173].

The structure of chromatin is regulated by histones modifications, methylation and acetylation, catalyzed by several enzymes such as HMT, HAT, and HDAC. Acetylation and deacetylation of histones are processes that determine the expression or silencing of genes. Alterations in the expression of these enzymes lead to aberrant histones modifications and consequently, epigenetic alterations[174]. Many findings showed that several histone modifications are associated with HCC, altering the cellular processes. For example, the overexpression of Enhancer of Zeste homolog 2 (EZH2), a histone-lysine N-methyltransferase enzyme, which adds a methyl group to histone H3 at lysine 27, has been detected in HCC[175]. Magerl C. *et al*. (2010) observed the low expression of the demethylation of histone H3 at lysine 4 (H3K4diMe) in HCC[176]; instead, another research group noted that Patt1, a GNAT family acetyltransferase, showed low levels in HCC compared to the normal liver cells in which the expression of the enzyme is high[177]. The inactivation of the MLL1, an enzyme responsible for H3KYMe, due to somatic mutations, has been revealed in around 1-6% of HCC[178]. SETDB1, a histone methyltransferase for H3K9, was found upregulated in HCC. Its overexpression, due to the lower expression of miR-29 and mutations in the chromosome 1q21, correlates with progression and cancer metastasis[179].

Histone deacetylases (HDACs) are enzymes involved in genes regulation removing acetyl groups from DNA histones and making the DNA more compact with a consequence of gene silencing. Overexpression of HDACs is correlated with poor prognosis in many tumours including HCC[180]. In particular, HDAC3 was found overexpressed in the advance stage of HCC. It was noted

that cancer development could be caused by the inactivation of HDAC3, NCOR and SMRT, which cause the increase of the acetylation of histones in S cell cycle phase. In conclusion, HDACs can be considered as tumour suppressor genes and used as target for cancer therapy[181].

Therapy resistance and poor prognosis are associated to DNA methylation, especially in solid tumours. Hence, demethylating drugs like nucleoside and non-nucleoside DNMT inhibitors represent a good therapy. Examples of these drugs are 5-azacytidine (azacitidine, AZA) and its derivates, 5-20-deoxycytidine (decitabine, DAC), zebularine, guadecitabine, hydralazine, procaine and MG98[182]. Nevertheless, the use of demethylating drugs does not allow the demethylation of specific target genes but involves all of the DNA. After all, low concentration of demethylating drugs showed the best results in clinical trials with limited toxicity[182].

Long noncoding RNAs (lncRNAs) are RNA molecules that are not translated into proteins, but principally involved in the regulation of many cellular processes like cell cycle. They are usually more than 200 nucleotides long and regulate gene expression either through binding to RNA polymerase II directly or binding co-regulators of genes transcription[183]. They are also involved in the epigenetic processes like histone methylation and chromatin structures. Examples of lncRNAs associated to HCC development are HULC, TUC338, HEIH, MVIH, H19, and MEG3[184]. Several experiments showed that lncRNAs play an important role in processes like apoptosis, cell migration and metastasis promoting the progression of HCC. These RNAs can act as oncogenes, promoting invasion and metastasis of HCC cells through the increase of the motility of the cells and their invasion characteristics. Examples of these lncRNAs are: LINC00052, ZEB1-AS1 and LINC01225[185]. It has been observed that many lncRNAs are down-regulated in HCC, acting as tumour suppressor, and others, like *FTX*, are up-regulated[184]. HOTTIP and HOXAIR lncRNAs are overexpressed in HCC causing tumour progression and metastasis[186]. Instead, HOXA-AS2, XIST, CCHE1, AFAP1-AS1 and HOST2 lncRNAs expression increase in HCC promoting cell proliferation[185]. On the other hand, several lncRNAs, such as AK058003 and lncRNA-p21, act as tumour suppressor genes preventing HCC tumour progression[187,188].

2.6 HCC treatments

The treatment of HCC is very difficult and the type of therapy to be applied depends on many factors like the stage of the tumour and patient's age. There are several HCC classification systems, but the Barcelona Clinic Liver Cancer (BCLC) classification is the most used. The BCLC staging classification takes in consideration the stage of the tumour (size and position), liver function status, patient's performance status (PS) and cancer-related symptoms[189]. BCLC classifies patients in five different stages: BCLC 0, BCLC A, BCLC B, BCLC C and BCLC D.

BCLC 0 and BCLC A indicate the early stage of tumour. In particular, BCLC 0 refers to patients with one tumour with size around 2 cm or less and no symptoms are present[190]. BCLC A stage comprises patients with one to up three tumours measuring <3 cm without showing any symptoms. In both cases the tumour is present only in the liver without invasion or extrahepatic diffusion and the organ is well functioning. The recommended treatments for patients in BCLC 0 or BCLC A stage are liver transplantation or hepatic resection[191]. When these treatments are not suitable for patients, radiofrequency ablation (RFA) is the alternative therapeutic choice. Recent data showed that RFA is as effective, in terms of patients' survival, as hepatic resection for the treatment of small HCC lesions[192]. Many patients with cirrhotic liver do not satisfy the BCLC A criteria and they cannot be subjected to hepatic resection. In this case, they are treated using RFA or percutaneous ethanol injection (PEI)[193]. Indeed, liver transplantation is recommended only when there are up to three tumours less than 3 cm or a single tumour with less 5 cm in size[194].

BCLC B stage refers to the intermediate-stage of the disease including patients presenting heterogenous characteristics for tumour extension, etiology of the disease and liver function[195]. They may present a single large nodule, considered inoperable, or more than three nodules larger in size of 3 cm, without vascular invasion or distant metastases. Liver function is well-preserved or moderately impaired. The trans-arterial chemoembolization (TACE) is the recommended treatment for these patients[192].

People in the advanced stage of the disease and physical impairment are included in BCLC C group. They show cancer-related symptoms and the tumour grow invading surrounding vessels and spreading in extrahepatic tissues[196]. Systemic treatments are recommended for patients in this stage. Indeed, *Sorafenib*, a multikinase inhibitor, is considered the standard treatment for patients at this stage[197].

The BCLC D stage includes patients in the final stage of the disease showing cancer symptoms and impaired physical status. They present a huge tumour with metastasis and the liver

function is not preserved. They are not good candidates for liver transplantation and the systemic treatments give them only a palliative care[192].

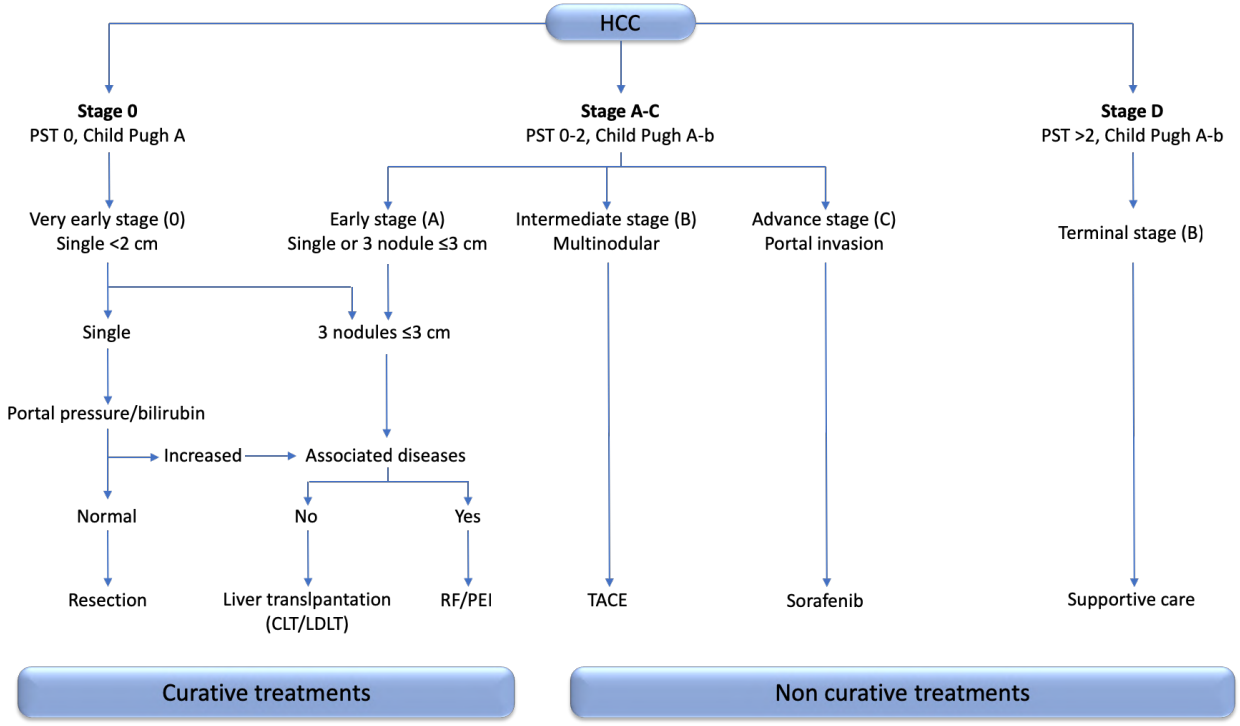

Figure 2.8. Scheme of BCLC classification and HCC treatments.

HCC resection is performed in non-cirrhotic liver and in patients in the very early stage of the disease. Individuals with a single asymptomatic nodule and without damages to the liver are the best candidates for HCC resection with 70% of survival at 5 years[193].

Liver transplantation is the best curative treatment for cirrhotic patients, where tumour and preneoplastic lesions are removed. It is applied in patients with a single nodule measuring less than 5 cm or up to 3 nodules less than 3 cm, and no vascular and extrahepatic spread are observed. The survival rates is more than 70% at 5 years and recurrence less than 15%[29].

Percutaneous ablation is performed in patients in the BCLC stage 0 and A with unresectable tumour with survival rate of 40 –50% for 5 years[196]. The technique consists in using chemicals agents, like acetic acid and alcohol to destroy neoplastic cells, radiofrequency to alter the temperature in the tumour area, cryoablation or laser[198].

Transarterial embolization (TAE) is a palliative treatment for patients in the intermediate stage of the disease. In this approach, tumour necrosis is caused by the block of hepatic artery following the insertion of an embolus, usually made of gelatin mixed with lipiodol, into the blood vessel. In the case of TACE, embolus includes chemical agents that attract tumour cells in order to destroy them[199]. TACE is a standard therapy for HCC patients with asymptomatic multinodules,

not-impaired liver function, and where vascular invasion or extrahepatic diffusion are not present. In this case the survival rate could be 40– 50% for 5-year[200].

Another approach to treat HCC is the immunotherapy, in which cancer cells are recognized by the immune system and killed. Immunotherapy is no toxic and induces anti-cancer activity for long term. Immunomodulators and vaccines are used to activate the immune system against HCC cells; instead, adoptive immunotherapy is based on active immune cells delivery to kill tumour cells[201]. The most used are antibodies targeting the PD-1, a protein expressed on cell surface and involved in the regulation of the immune system response. Examples are *Nivolumab*, *Pembrolizumab* and *Camrelizumab*[202].

Unfortunately, when HCC is in the advanced stage, only systemic chemotherapy can be applied even in the case in which the prognosis is very negative. There are different chemotherapeutic agents able to target specific molecules involved in pathways altered in HCC[203].

Currently, *Sorafenib* represents the first line systemic chemotherapy approved by the FDA for the systemic treatment for HCC. It is an oral multi-kinase inhibitor which targets kinases expressed on cell surface or inside the cell, involved in tumour progression[204]. VEGF receptor (VEGFR-) 1, VEGFR-2, VEGFR-3, platelet-derived growth factor receptor (PDGFR-) β, RET, c-KIT and FMS-like tyrosine kinase-3 are inhibited by *Sorafenib*, reducing the angiogenesis process and cell proliferation. This drug inhibits molecules like extracellular kinases (Raf-1) and intracellular serine/threonine kinases (B-Raf), involved in Ras/MAPK pathway, which are overexpressed in many cancers including HCC[205]. *Sorafenib* treatment has some effects for patients in advance stages of HCC even if the tumour has macrovascular invasion and extrahepatic spread, but patients do not have impaired liver function. It is also used for patients in the early stage with asymptomatic HCC but unresectable tumour[206]. The efficacy of *Sorafenib* was tested enrolling patients with advanced HCC and without previously systemic chemotherapy treatment in two trials named as SHARP and Sorafenib Asia-Pacific (AP)[207,208]. In these studies, patients were divided randomly in two groups; one group of patients received 400 mg of Sorafenib twice daily and the other group received the placebo. The treatment has been stopped when death or progression of the disease had occurred in the case of Sorafenib AP trial, or when patients had shown symptoms and progression of the disease in the case of SHARP trial. Patients treated with *Sorafenib* showed a significantly prolonged overall survival (OS) in both trials, compared to placebo-patients-treatment. In particular, in SHARP trial, OS was 10.7 months vs 7.9 months ($P < 0.001$) and for Sorafenib AP was 6.5 months Vs 4.2 months ($P < 0.05$). Nevertheless, a complete response to the treatment was not observed in any patient[207,209]. To improve the efficacy of systemic therapy, *Sorafenib* is also used in combination with other systemic chemotherapeutic

molecules. Combination of *Sorafenib* with octreotide and oxaliplatin, cisplatin and gemcitabine, doxorubicin, tegafur/uracil and AVE 1642 reported survival advantages compared to *Sorafenib* alone treatment[210]. *Sorafenib* appears to have good results in patients treated with TACE, which causes a hypoxic environment due to the block of the vascular arterial blood suppling the tumour. In this condition, VEGF is activated and produced, stimulating the neovascularization of the tumour. *Sorafenib*, administrated during TACE treatment, inhibits VEGF production and thus, tumour vascularization and tumour growth[211]. Nevertheless, many patients developed drug resistance to *Sorafenib,* and the mechanism of this phenomenon is not still completely understood. Hypothesis for this condition could be related to changes in tumour microenvironment, epithelial-mesenchymal transitions and alterations in cellular pathways in tumour cells[212].

Sunitinib (Sutent; Pfizer, Inc., New York, N.Y., USA) is an oral multitargeted tyrosine kinases inhibitor already approved by the FDA for renal cell carcinoma and imatinib-resistant gastrointestinal stromal tumour treatments[213]. It has antiproliferative and antiangiogenic activity targeting VEGFR-1/VEGFR-2/ VEGFR-3 and PDGFR- alfa/PDGFR-beta receptors involved in the hepatocarcinogenesis. It showed an antitumour effect in phase II HCC trials where patients had HCC in advanced stage[214].

Linifanib (ABT-869) is another multitarget-kinases inhibitor targeting VEGFR and PDGFR, but it is not able to target cytosolic tyrosine kinases and serine/threonine kinases. Its efficacy in advanced HCC treatment was demonstrated in a phase II clinical trial[215]. In an open-label phase III trial, the efficacy of *Linifanib* was compared versus *Sorafenib* in patients who did not receive systemic therapy previously and with HCC in advanced stage. However, *Linifanib* showed moderately superior efficacy compared to *Sorafenib,* but safety tests favor *Sorafenib* to *Linifanib*[216].

Brivanib is an oral and selective inhibitor of the fibroblast growth factor receptor (FGFR) and vascular endothelial growth factor receptor (VEGFR). It demonstrated antiproliferative and antiangiogenic effects in different tumour cell lines, including HCC cell lines[204]. Moreover, in a phase II study *Brivanib* has been indicated as a second-line therapy in patients with advanced stage of HCC where prior antiangiogenic therapies failed[217].

There are other drugs tested for the treatment of HCC; for example, *Tivantinib* (ARQ 197)*,* an oral selective inhibitor of the mesenchymal-epithelial transition factor (MET) receptor, found dysregulated in HCC. The use of *Tivantinib* in tumour biopsy samples reduced the activity of MET and the expression of downstream signaling pathways[218]. It also showed good results in a phase 2 study, where patients with advanced HCC and cirrhosis were treated with *Tivantinib*[219].

Everolimus is an inhibitor of the mammalian target of rapamycin (mTOR). In a phase III trial, it didn't show an increase of survival in patients where treatment with Sorafenib failed[220].

Regorafenib and *Nivolumab* are both approved by the FDA as a second-line treatment for HCC. *Nivolumab* is a human immunoglobulin G4 anti-PD-1 monoclonal antibody, already approved for several tumours and approved by the FDA in September 2017[221]. *Regorafenib* is an oral Sorafenib-derived drug, inhibitor of VEGFR1-3, PDGFR, FGFR, TIE2, Ret, c-kit, wild type or V600-mutated B-RAF. *Regorafenib* showed to increase the overall survival of patients compared to the placebo-patients-treatments (10.6 mo vs 7.8 mo; HR = 0.63, 95%CI: 0.50-0.79, $P < 0.0001$) in the RESORCE trial, a phase III randomized, double-blind trial[222].

Currently, other molecules are under evaluation as possible candidates for HCC systemic therapy. These molecules could act against factors that play an important role in angiogenesis process, like VEGF or against other pathways deregulated in HCC, like MET[223].

Epigenetic alterations are very frequent in HCC, since it is well known that many genes involved in cell cycle regulation are silenced by cytidine methylation. Thus, therapeutic molecules that can restore the aberrant methylation may be used for HCC treatment. 5-azacytidine (Vidaza; 5-aza-CR) and 5-aza-2′-deoxycytidine (Decitabine; 5-aza-CdR) are the most famous demethylating agent, already approved by the FDA for the myelodysplastic syndrome and acute and chronic myeloid leukemia treatment[224]. They are cytidine analogs and thus are incorporated into newly synthesized DNA. Azacytosine-guanine dinucleotides are DNMTs substrates, which usually adds a methyl group to the cytosine, resulting in a covalent bond forming a complex that blocks the DNA synthesis. Therefore, the complex is excited and degraded with the following repair of the DNA and its synthesis continues in the absence of DNMTs[225]. This process results in hypo methylation of newly synthesized DNA and consequently, the expression of some silenced genes can be restored. High doses of demethylating drugs result in a cytotoxic effect for the cell; however, at lower doses, they have a demethylating effect[226]. Recently, the effect of 5-aza was tested also in solid tumours including HCC. Venturelli S. *et al.*(2010), showed that 5-azacytidine (Vidaza) was able to induce apoptosis in several HCC cell lines and to make them more sensible to TRAIL-induced apoptosis death [227].

2.7 Small interference RNAs (siRNAs)

Small interference RNAs (siRNAs) are double-stranded RNAs produced from the cleavage of a long dsRNA, most often derived from extracellular sources. siRNAs production in the cell is a biological response to endogenous and exogenous pathogenic double stranded RNAs in order to eliminate them. Moreover, it is also believed that siRNAs are involved in the silencing of potentially harmful genome segments, like transposons, which can cause destabilization of the genome[228]. The term "RNA interference" was first coined by Fire *et al.* in 1998, when they observed the silencing of specific genes after the introduction of dsRNA into the nematode worm *Caenorhabditis elegans* cells[229]. Later, this mechanism was also described in plants and in mammalian cells, making this technology applicable for the study of the role of several genes[230].

Once in the cell, long dsRNAs are processed in the cytoplasm by a specific ribonuclease (RNase) III-like enzyme called Dicer, into smaller dsRNA molecules known as siRNAs, usually not longer than 21-23 nucleotides. Dicer enzyme is composed by different domains, which are, from the N- to C-terminus: helicase domain (DExD/H, TRBP-BD and HELICc), DUF283 domain, PAZ (Piwi/Argonaut/Zwille) domains, RNase IIIa and IIIb domains and dsRNA-binding domain (RBD)[231]. The DExD/H C-terminal binds the double-stranded RNA, instead the DUF283 domain binds the single-stranded nucleic acid[232]. The catalytic core of Dicer, made by RNase IIIa and IIIb domains, cuts one of the two strands of the dsRNA every ~20 base pairs (bp)[233]. The generated small dsRNAs are composed by two strands named sense (or passenger) and antisense (or guide) strands, characterized by the 3' nucleotide overhangs and terminal phosphate groups at the 5' on each strand[234]. The 3′ overhang is recognized by the PAZ domain, responsible also for the recognition of the phosphorylated 5′ end of small RNAs[235]. Then, the siRNA interacts with the RNA-induced silencing complex (RISC), composed by many ribonucleoproteins, including the endonuclease Argonaute 2 (AGO2). AGO2 shares with Dicer the PAZ domain, which recognizes and binds the 3' terminus of the siRNA, while the 5' terminus is bound by the Mid domain of the AGO2[236]. AGO2 cleaves the passenger strand, whereas, the guide strand remains associated with the RISC and it guides the RISC complex to its mRNA target for its cleavage by AGO2 component. The guide strand binds the mRNA target in a fully complementary region, resulting in the mRNA degradation, thus, in specific gene silencing[237]. siRNAs have always been used to study the gene functions and the specific gene silencing effect makes them useful for target identification and validation in drug discovery and development[238].

Cancers are often characterized by the upregulation of gene expression that lead to uncontrolled cell growth. siRNAs can downregulate the expression of these genes inducing the

degradation of their mRNAs and in turn, reducing the respective protein levels. This mechanism makes siRNAs promising candidates for innovative therapies in cancer treatment and more in general for different human diseases. Moreover, as siRNA can be chemically synthesised, they can be potentially used to specifically target any mRNA causing disease[239,240].

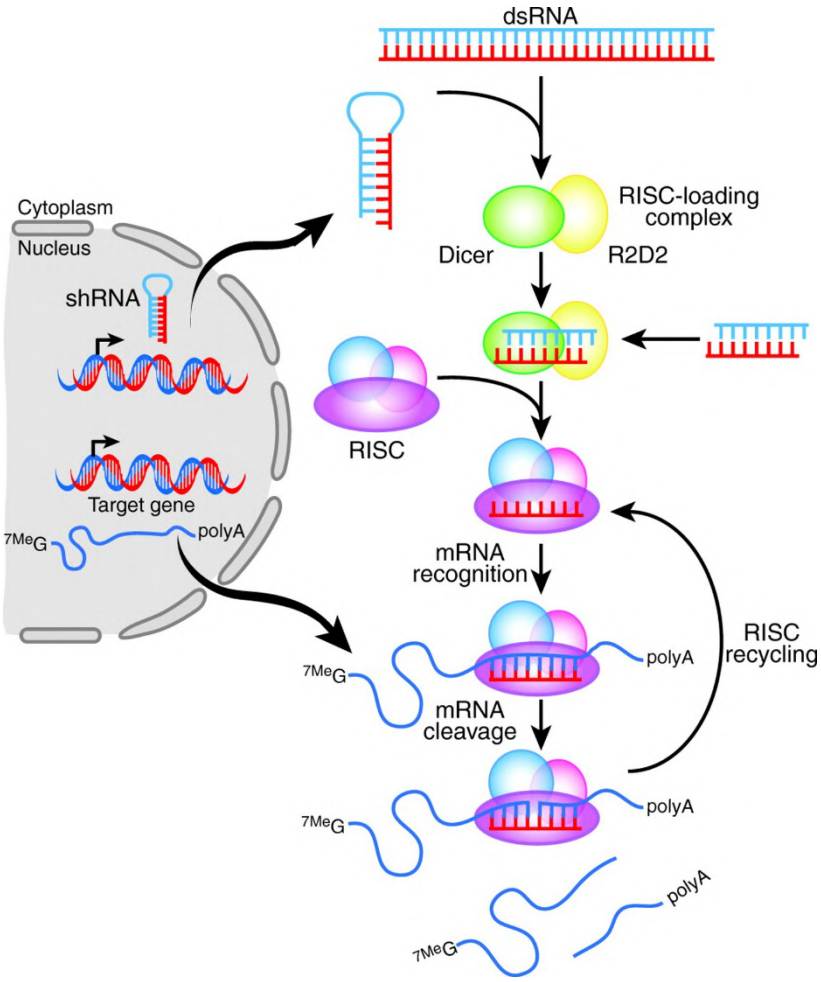

Figure 2.9. RNA interference mechanism[234].

2.8 Delivery systems

siRNAs are promising therapeutic molecules in biomedicine field for the treatment of several diseases including cancer. However, clinical applications of siRNAs are still difficult for a number of reasons. Constituted by RNA, siRNAs are characterized by a negative electric charge and have poor stability in the biological environment[241]. Thus, siRNAs need to be embedded into specific carriers to get protection and to efficiently reach the target cells. It should be considered that for a systemic administration, siRNAs encounter a number of obstacles that can dramatically reduce the possibility to get to the target cancer cells. Once in the blood stream (Figure 2.10), siRNA can be: 1) degraded by blood nucleases; 2) eliminated by the phagocytic system, 3) cleared from blood via kidney filtration and/or sequestered by the liver[242] and to activate the innate immunity[243].

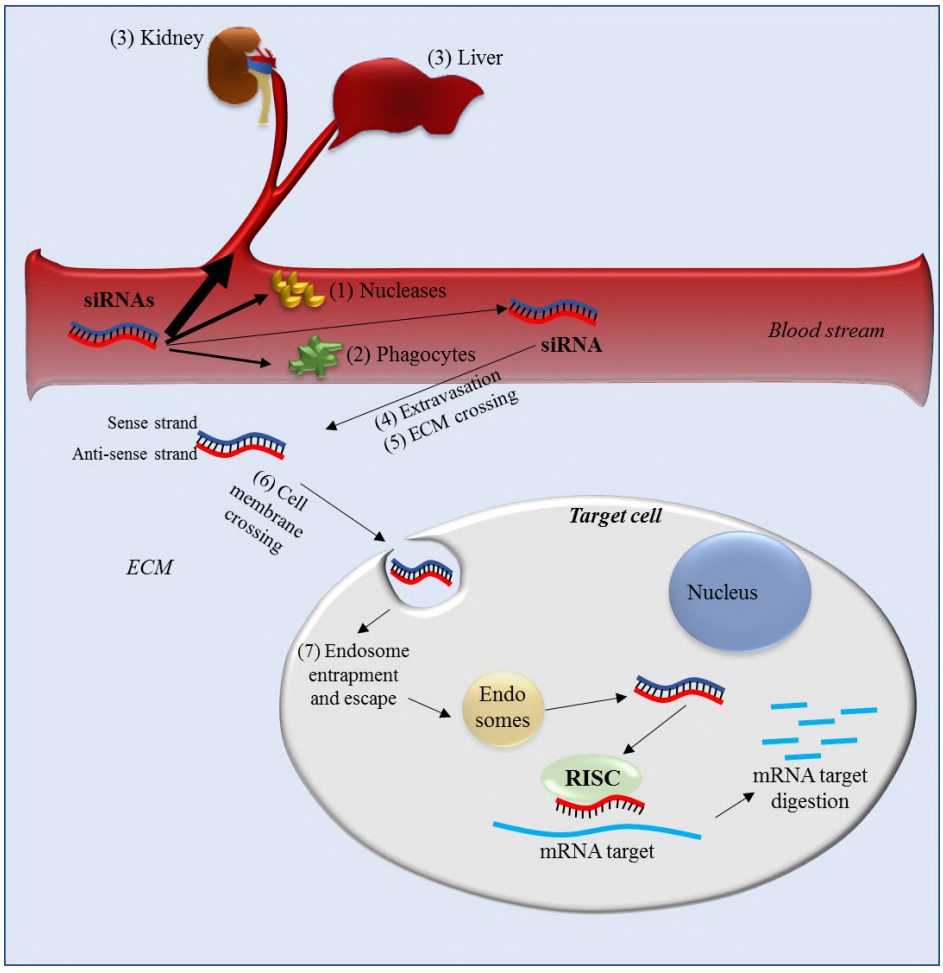

Figure 2.10. Obstacles for systemic siRNAs delivery on the biological environment.

Once the siRNAs reach the target tissue, additional obstacles remain, like crossing the vessel wall (extravasation -4), the migration through the extracellular matrix (ECM -5) and then crossing the cellular membrane (6) (Figure 2.10). This last step is particularly inefficient for naked siRNA as their global negative charge, derived from the phosphate groups of their backbone, induces the repulsion of siRNA from the negative charged molecules present on the outer side of the cell membrane. Moreover, the hydrophilic nature of siRNA substantially prevents the crossing through the hydrophobic inner layer of the cell membrane. Only a reduced amount of siRNA can be internalized via endocytosis. Finally, once into the target cell, siRNAs can be entrapped into endosomes (7), an event that can further reduce the amount of siRNA that can reach the target[241].

For the above considerations, siRNAs need to be encapsulated in nanoparticles, which protect them from the biological environment ensuring their stability and facilitating cell-membrane cross. In this way, they can reach the cytoplasm where siRNAs suppress the specific target gene expression.

There are several systems to enhance and optimize the efficiency of siRNA delivery *in vitro* and *in vivo*, including chemical modifications[244,245] of siRNAs structure and/or the complexation of siRNAs with viral or non-viral vectors[246]. The modification of nucleotide phosphate group (by phoshorothioate modification or boranophosphate modification) or the sugar group are examples of chemical alterations. The drawback of this strategy is the possible reduction of siRNAs activity *in vivo*[237]. Viral vectors are characterized by the highly efficient gene transfer, but are more likely to cause undesired immune system reactions, mutational insertions and oncogenicity risks[246]. Instead, non-viral vectors present advantages such as lower cytotoxicity and immunogenicity. Among non-viral vectors, liposomes, cationic polymers, micelle-based carriers, nanodiamons and dentrimers have been evaluated as good siRNA carriers[246].

2.8.1 Lipidic nanoparticles

Nowadays, lipid-base nanoparticles (LNP) are the most used delivery systems in biomedical field to deliver drugs and nucleic acids[247]. They showed good results both *in vivo* and *in vitro* experiments, since liposomes morphology mimic cellular membranes and they can easily deliver molecules inside cells. Liposomes, lipoplexes, lipidoid and exosomes are some examples of lipidic nanoparticles[248].

Liposomes are spherical self-closed vesicles, deriving from synthetic or natural phospholipids, largely used for their biodegradability and low immunogenicity reactions[249,250]. They can accumulate in the tumour site, where siRNAs are released inside the cells to target the

specific gene[251]. These nanoparticles can be positively, neutral o negatively charged, based on the nature of lipids forming the particles. Among these, cationic liposomes are the most used because of their ability to escape from the endosomal membrane facilitating siRNA delivery into cytoplasm. On the other hand, they show a low "fusogenicity" and can activate the complement system causing their rapid clearance by macrophages[252]. Neutral liposomes show a relatively long blood circulation, a highly efficient tumour infiltration, less toxicity than cationic liposomes and did not active the complement system response. Problems in their application are the less efficiency in the interaction between neutral liposomes and target cells, due to their neutral charge, and their hard synthesis process[253]. Anionic liposomes show a lower stability and circulation time than positive and neutral charged liposomes and they active the complement system immune response[254]. Moreover, negative charges make siRNAs hard to be encapsulated, due to the repulsion force and they are not efficiently absorbed from the target cells, because of the repulsion with anionic membrane cell[255].

Stable nucleic acid lipid particles (SNALPs) are lipid nanocarriers with the surface charge nearly neutral and constituted by a lipid bilayer of an ionisable cationic lipid, DLinDMA or DLin-KC2-DMA, to facilitate siRNA internalization, a conjugated poly-ethylene glycol (PEG) for complex stabilization, and a neutral lipid like DSPC or cholesterol that permit endosomal escape[246]. siRNAs are placed in the inner membrane of liposomes by electrostatic interactions. Appropriate modifications in SNALPs, for example in the type and ratio of the different components, can prolong the nanocomplex circulation time without complement system activation and other undesirable responses[249].

Solid-lipid nanoparticles (SLN) are novel carriers developed in the last years, derived from nanoemulsions where the oil is replaced by solid lipids dispersed in water or aqueous surfactant solution[256]. They are usually made by partial glycerides (Imwitor), steroids (cholesterol), triglycerides (tri-stearin), waxes (cetyl palmitate) and fatty acids (stearic acid, palmitic acid)[257]. However, they present some disadvantages such as low molecules loading capacity and a possible expulsion of the incorporated molecules during nanocarrier storage[257]. To decrease their cytotoxicity and minimize immune responses, SLN can be made by physiological lipids, like the natural protein-free LDL, or derived from the natural high-density lipoproteins (HDL), which mimic the biological complexes[258,259].

To overcome some obstacles in siRNA delivery and to prolong circulation time, liposomes have been modified adding biocompatible polymers, like the polyethylene glycol (PEG), which increases the siRNA stability for both *in vivo* and *in vitro* applications[249]. Nanoparticles can be also modified by the conjugation of neutral lipids such as cholesterol (Chol) or 1,2-dioleoyl-sn-

glycerol-3-phosphoethanolamine (DOPE), to stabilize the lipid-based siRNA delivery nanocarriers for *in vivo* and *in vitro* applications. The complex is taken more easily from the cells and have a longer circulation time. Cholesterol is also used to anchor molecules like DNA or polyethylene glycol (PEG) to the lipid particles[260].

2.8.2 Inorganic nanoparticles

Recently inorganic nano-vectors, like nanogold particles, calcium phosphate, mesoporous silica nanoparticles, have been exploited for nucleic acids delivery. In particular, calcium based ceramic nanoparticles, like calcium phosphate (CaP) and calcium carbonate (CaCO3), have been widely used for their biocompatibility and biodegradability, due also to their natural presence in the human body[261].

Mesoporous silica nanoparticles (MSN) are solid complex of silica with surface areas constituted by porous with a variable volume and in which small molecules can be introduced[262]. These nanoparticles are usually complexed with poly(2-dimethylaminoethyl methacrylate) (PDMAEMA) or polyethyleneimine (PEI) allowing the endosomal escape through the proton-sponge effect; or with polyethylene glycol (PEG) to decrease their cytotoxicity[263]. The major advantages of MSNP are the variable porous size (from 2 to 200 nm) that permits to incorporate a large variety of loads, and the possibility to modify chemically the porous surfaces using hydrophobic, basic or acid residues[263]. Despite MSNPs present many advantages, their drawbacks are the quick clearance by excretory system and immune system activation[264].

Another example of inorganic nanoparticles is the membrane/core nanoparticles (MCNPs), which are composed by a lipid bilayer as the shell and one or more inorganic nanoparticles as the core. The core can be constituted by calcium phosphate (CaP) or silica (SiO2) nanoparticles. The surface of these inorganic nanoparticles is porous, in which siRNAs are loaded[253].

2.8.3 Micelles

Micelles are a composition of amphiphilic copolymers that are self-assembled to form structures characterized by hydrophobic residues as core and hydrophilic residues as shell. The latter residues make micelles soluble in aqueous environment; instead, hydrophobic residues interact each other to form nanoaggregates[265]. Micelles are usually made of cationic polymers, allowing electrostatic interactions with siRNAs for their encapsulation. Examples of cationic polymers are poly(ethylene glycol) (PEG) and poly(propylene sulphide), which self-assemble in aqueous solution to form micelles [266]. Lee SY *et al.* (2016) proposed a multifunctional micellar

delivery system using cationic PDMA-block-poly(ε-caprolactone) (PDMA-b-PCL) complexed with the polyethylene glycol (PEG). These micelles are tested as carriers for a siRNA whose target was the human vascular endothelial growth factor (VEGF). This delivery system reached tumour regions, showing an efficient silencing of the target in the cancer cells[267].

2.8.4 Microbubbles and nanobubbles

Microbubbles and nanobubbles represent a novel approach for cationic polymers and liposomes responding to external stimuli (ultrasounds). They are composed of a core filled by a gas and a shell constituted of polymers, proteins or phospholipids. First synthetized microbubbles contained air as gas, able to pass through pulmonary capillaries, but characterized by the instability and poor solubility. Subsequently, they were filled with sulphur hexafluoride or perfluorocarbons gas, ensuring a longer circulation time of the nanoparticles[268].

Nanobubbles are usually composed of a core filled of a fluorinated gas, such as perfluorocarbons or sulphur hexafluoride[269]. Molecules can be associated with nano-spheres directly, or by a covalent linkage to the polymer, or by electrostatic interactions[270]. Molecules delivered by nanobubbles are released in a desiderated site emitting specific ultrasounds, which cause their disruption when they reach the target area. Moreover, these perturbations induce bubbles collapse that emit waves producing a temporary membrane permeabilization of the surrounding cells. These phenomena, called “sonoporation”, create transient holes through which molecules contained in the nanobubbles enter the cell[271]. Applying the correct ultrasound energy, the effect of nanobubbles can be controlled improving the deposition of molecules in a localized tissue[272]. Nanobubbles can be modified adding cationic polymers, like PEG or PEI, on the shell to enhance their circulation time, to facilitate endosomal escape and to bind more efficiently negative-charged molecules[273].

2.8.5 Superparamagnetic iron-oxide nanoparticles (SPIONs)

Superparamagnetic iron-oxide nanoparticles (SPIONs) are another type of nanoparticles recently applied in the biomedical field due to their biocompatibility and biodegradability properties. They are composed of magnetite (Fe_3O_4) that is converted in maghemite (γ-Fe_2O_3) by oxygen exposure[274]. Iron-oxide nanoparticles are known to be “supermagnetic” and in the presence of an external magnetic field, they become magnetized[275]. Using magnetic field, SPIONs can be guided to the target tissue, reducing molecules wastage and avoiding side effects[276]. These nanoparticles can be coat by organic or inorganic molecules and drugs or siRNAs are loaded on

the surface or within the nanoparticles by electrostatic interactions or hydrophilic/hydrophobic interactions[277]. SPIONs surface can contain peptides, receptors or ligand for binding to specific targets. The surface can contain branched polyethylenimine (bPEI) showing a lower toxicity and a higher uptake from the cell. Moreover, PEI can easily interact with negatively charged molecules such as siRNA or DNA, holding them in the particle[278].

2.8.6 Polymers

Polymers are solid and biodegradable nanoparticles widely used as carriers for siRNAs. They can be synthetized from natural or synthetic molecules. Examples of natural polymers are chitosan (CH), poly(lactic acid-co-glycolic acid) and atelocollagen; while PEI, PLL, PEG, dimethylaminoethyl methacrylate and cyclodextrin-based polycations (CDP), are examples of synthetic polymers[279,244].

PEIs, composed by repeat units of amine, is the most used cationic polymers, although it is more toxic than natural polymers. Because it is positively charged, it binds negative-charged molecules easily. It is often used to cover liposomes reducing particles size and increasing their circulatory time[280]. In order to decrease its cytotoxicity, PEI is subjected to chemical modifications, including adding hydrophilic and hydrophobic motives or cell/tissue-specific ligands[281]. PEI with high molecular weight is high cytotoxic and it is not easily degraded by cells. On the other hand, experiments employing PEI for gene delivery showed good results and high transfection efficiency because of its "proton sponge effect", which protect encapsulated molecules from endosomal degradation[282].

Polyethylene glycol (PEG) is a polymer of ethylene oxide monomers considered non-toxic and safe. It is also usually used to cover polymeric nanoparticles or to conjugate covalently a reactive functional group on the nanoparticles surface, to overcome problems like low transfection and delivery efficiency[283]. The PEG addition is widely used to modify liposomes in order to decrease their toxicity, to stabilize the nanocomplexes and for the specific attachment of the liposome to target ligands, but it does not promote a specific targeting[284]. PEG polymer is widely used because of its solubility in aqueous environment and organic solvents. Polymers constituted by polysaccharides are recently applied for molecules delivery because of their less toxicity, biocompatibility and biodegradability[285].

Chitosan derives from chitin and belongs to the natural polymers. It has a carbohydrate backbone characterized by two types of repeating residues, 2-amino-2-deoxy-glucose (glucosamine) and 2-N-acetyl-2-deoxy-glucose (N-glucosamine), linked by (1-4)-β-glycosidic linkage. Chitosan are positively charged and molecules like DNA and siRNAs can be incorporated

by electrostatic interactions[286]. Disadvantages in these nanoparticles application are low transfection efficiency and low solubility, overcome adding PEI, PEG or Poly(amidoamine) (PAMAM) dendrimers. In order to increase chitosan physicochemical and biological properties, different modifications, like the variation in the degree of the deacetylation and molecular weights, can be made. Different chitosan derivatives have been synthetized by alteration of hydroxyl or amine functional groups, improving their properties[287]. Zhong J. *et al.* (2015) realized modified chitosan polymers, MixNCH, in order to increase siRNA stability in biological environment. They used these complexes to deliver Midkine siRNA (MK-siRNA) in HepG2 cells. Midkine is a heparin-biding growth cytokine that has been found over-expressed in some tumours, like in the HCC. They observed that hepatocellular cells transfected with MK-siRNA decreased their proliferation[288].

Cyclodextrins (CDs) are cyclic oligosaccharides, characterized by 6, 7 or 8 glucose units, derived by enzymatic degradation of the starch. These nanocarriers have a truncated cone shape with an internal hydrophobic structure, able to interact with various hydrophobic molecules, and an hydrophilic structure in the outside, making the cyclodextrins soluble in water[289]. The most used form of cyclodentrins is β-cyclodextrins, which presents amphiphilic and cationic modifications. It has been shown to have good results both *in vivo* and *in vitro* siRNA delivery[290]. Fitzgerald K.A. *et al.* (2016) synthetized β-cyclodextrins modified with different Adamantane derivates, making polymers positively charged. Adamantane is a highly hydrophobic molecule that can bind to the β-cyclodextrins efficiently. A siRNA against PLK1 gene has been incorporated into β-cyclodextrins-Adamantane complexes. Different prostate cancer cells lines, DU145, VCaP and PC3 cells, have been transfected with siRNA–nanocarrier complexes, showing a remarkable knockdown of the PLK1 gene in prostate cancer cells *in vitro*[291].

Many polymers can be conjugated with stearic acid (SA), which is a hydrophobic chain, to create micellar structures. For example, chitosans are not able to self-assemble to form micelles, so they can be conjugated with SA. Moreover, polymers modified with SA can include a specific target-ligand in order to deliver efficiently the encapsulated molecules and to enhance the specific targeting[292]. Poly-[(N-2-hydroxyethyl)-aspartamide] (PHEA) is one of the most used polymers, ideal to incorporate hydrophobic small-molecules. It is neutral charged and characterized by a polypeptide backbone. This polymer is high water soluble, nontoxic, biodegradable, biocompatible and nonantigenic[293]. PHEA modified with poly(ethylene glycol) (PEG) or/and hydrophobic micro/macromolecular groups has widely used as a delivery system[294]. On the other hand, PHEA-based polymers have some drawbacks regarding difficulties in the preparation process limiting their applications[295].

2.9 The targeting of HCC

Conventional chemotherapeutic agents give often a low response rate and severe side-effects. They can be toxic and damage also proliferating normal liver cells. Moreover, chemo-resistance is very frequent in HCC [296]. The effective delivery of specific molecules to the liver using an appropriate delivery system able to target only the hepatocytes can overcome some of these problems. In general, biological targets are molecules that are overexpressed in the tumour cells or molecules involved in anti-proliferative or pro-apoptotic processes[297]. The choice of optimal target(s) and/or the appropriate delivery systems is not simple, since many overexpressed molecules in HCC are also expressed in normal hepatocytes. Delivery systems equipped with specific molecules/moieties able to recognize specific antigens on HCC cells seem to be the best approach. This strategy could restrict the delivery of molecules to cancer cells, avoiding targeting also normal hepatocytes[298,299,300].

Several HCC targeting molecules have been selected as good candidates for cancer therapy. The problem is that many of them are also expressed on normal hepatocytes, limiting their effective use for HCC treatment.

Glypican-3(GPC3) belongs to membrane-bound heparan sulfate proteoglycans and it is abnormal expressed in HCC, but not in normal liver. It is considered as a specific marker for HCC, although it is expressed also in other tumours like liposarcoma and squamous cell carcinoma of the lung[301].

Transferrin receptor (TfR) is a transmembrane glycoprotein involved in the uptake of transferrin, low expressed on normal hepatocytes. In particular, a new member of TfR family, TfR-2, has been identified as strictly expressed on hepatocytes and enterocytes of the small intestine. It can be considered a specific ligand to target tumour hepatocytes, since it was found overexpressed in HCC cells and on proliferating cells[298].

AF-20 antigen is a homodimeric glycoprotein specifically expressed on HCC cell lines and in particular in HuH7 cells. It is not detectable in normal liver cells and it is recognized by the monoclonal antibody AF-20, making this molecule a good candidate for specific delivery approach for HCC[302].

Other receptors overexpressed on HCC cells surface are retinoic acid receptor, epidermal growth factor receptor, somatostatin receptor and folate receptor. The presence of these receptors is not limited to the liver, but they are also expressed in normal liver cells and in other organs. For this reason, they cannot be considered as specific targeting molecules to be delivered specifically in HCC cells[298].

2.10 Asialoglycoprotein receptor (ASGPR)

The Asialoglycoprotein receptor (ASGPR), also known as 'The Ashwell–Morell Receptor', is a glycoprotein expressed on the hepatic cell surface, specifically in the basolateral part of liver cells and in the sinusoidal membranes[303]. Its expression is not limited to hepatocytes, but also human testes, human intestinal epithelial cells, human sperm, peripheral blood monocytes and peritoneal macrophages express the receptor. Nevertheless, ASGPR expression is much less in other cells than on hepatocytes, and together with the easily accessibility to the receptor from the vascular compartment, represent good characteristics which make the receptor as a promising target for HCC. Moreover, the specific targeting of ASGPR could allow a higher concentration of a drug in the liver with minimum off-target effects[304].

ASGPR is characterized by high rate of the uptake of different molecules showing a high efficacy. The receptor interacts with of pro-thrombotic components, serum immunoglobulin-A and cellular fibronectin. However, the most important role of ASGPR is the clearance of desialylated glycoproteins exposing non-reducing D-galactose (Gal) or N-acetylgalactosamine (GalNAc) as end groups[305]. The receptor binds, internalizes and degrades these extracellular proteins, but it cannot distinguish between Galactose and D-glucose configurations[304].

Human ASGPR is constituted by two homologous polypeptide subunits with different molecular weight, 50 kDa and 46 kDa. Subunits are called HL-1 (from Hepatic Lectin, or ASGPR1) and HL-2 (or ASGPR2) and they are in a 2-5:1 stoichiometry ratio, with HL-1 as the major present subunit[303]. Each polypeptide is a C-type II transmembrane proteins constituted by a short N-terminal localized in the cytoplasm, an intermediate region and a calcium (Ca^{+2}) dependent carbohydrate recognition domains (CRDs). CDRs are localized outside the cell membrane, they have three binding sites for Ca^{2+}, two of which show high affinity, and one has low affinity for Ca^{2+}. This ion is essential for the interactions between ligands and the receptor[306].

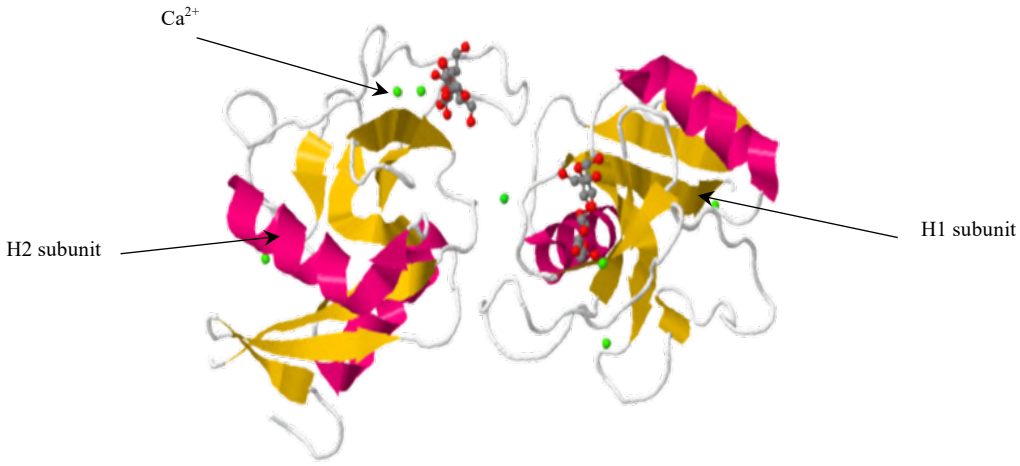

Figure 2.11. Asyaloglicoprotein receptor structure.

The active site for ligands binding is formed by the following amino acids: aspartic acid 241, aspartic acid 265, asparagine 264, glutamic acid 252, glutamine 239 and tryptophan 243. All of them belong to H1 subunit of the receptor[304].

When the receptor binds the ligand, internalization via clathrin enabled receptor-mediated endocytosis occurs. Receptor and ligand are coated by clathrin pits and internalized very fast with a half-life of approximately 3 min. Once the internalization is completed, clathrin coat is shed off by heat shock proteins and reused for another internalization process. The uncoated vesicles fuse with other vesicles forming the early endosomal vesicles and following the late endosomes which fuse with pre-lysosomal vesicles making mature lysosomes[307]. These particles have 5.4 acid pH and contain lysosome enzymes. This environment causes the release of ligand from ASGPR due to the lower affinity of Ca^{2+} to the receptor caused by the low pH of lysosomes. Then, the ligand is degraded into lysosomes; instead, the ASGPR is released and reused up to 200 times through a recycling endosome process with a turnover time of 20 min. ASGPR on the membrane is replaced during the recycling and the de-acylated ASGPR is re-acylated in order to be replaced on the membrane surface. Half-life studies indicated that the receptor is present on the cell membrane for about 20 h[304].

The natural ligands of ASGPR are multiple molecules of galactose and galactosamines consisting of asialofetuin (AF), asialotransferrin, asialoorosomucoid (ASOR) and asialoceruloplasmin[308]. In particular, molecules complexed with many Gal residues showed a stronger binding with the receptor. It has been seen that the ASGPR has higher affinity for ligands presenting from tri- to tetra antennary Gal structures than mono-antennary Gal ligands. However,

it has been observed that the binding affinity to ligands does not increase in a relevant way adding more than three Galactose residues. Monosaccharides exhibited a lower dissociation constant in the interaction with CRD compared to oligosaccharides and tri-antennary ligands[309].

The ASOR glycoprotein has five branched chain of carbohydrates and the AF has tri-antennary carbohydrate units. Both of them are widely studied as delivery systems for proteins and genes[310,311]. Other ASGPR natural ligand are Lactoferrin and Arabinogalactan (AG). Lactoferrin is a glycoprotein able to bind the iron of the transferrin family and it has a very high affinity to ASGPR. Ca^{2+} is also important for Lactoferrin binding ligands but in contrast to other natural ligands, it is internalized through a galactose-independent mechanism. Arabinogalactan (AG) is a carbohydrate ligand and a glucose-based polymer extensively used for studying ASGPR as a targeting receptor[304].

Synthetic ligands with Gal- or GalNAc motives showing high affinity for ASGPR have been synthetized in order to target the receptor specifically. Jayaprakash K. Nair *et al.* (2014) synthetized a delivery system composed by a synthetic trivalent N-acetylgalactosamine ligand conjugated covalently to a modified siRNA against the ApoB100 gene, in order to target the liver parenchyma. The synthetic ASGPR ligand showed high specificity and affinity for the receptor resulting in a specific silencing of ApoB100 mRNA following the hepatocyte-specific uptake of the siRNA-polymer into isolated primary mouse hepatocytes[312]. Efrat Korin *et al.* (2017) developed N-acetylgalactosamine (GalNAc) nanoparticles (GalNAc-NPs) conjugated to a siRNA against STAT3. They observed that after intravenous injection of the GalNAc-NP in BALB/c mice, the nanoparticles localized in the liver. Moreover, cellular uptake of GalNAc-NPs studies in HepG2 cell line showed that nanoparticles uptake occurred in about 50% of cells, instead nanoparticles without GalNAc did not enter into HepG2 cells. These results demonstrated that the GalNAc-NPs uptake occur via ASGPR. In addition, the silencing of STAT3 following GalNAc-NPs delivering a siRNA against STAT3 demonstrated the efficacy of the delivery system[313].

Ca^{2+} is very important for the correct function of the receptor and receptor binding with ligands occurs only in the presence of the ion. The importance of its role has been investigated in several studies in which it was demonstrated that the depletion of Ca^{+2} by chelator agents decreased ligand-receptor interaction. For example, the binding of hepatitis C virus to ASGPR was reduced using the ethylene glycol bis(β-aminoethyl ether) N,N,N′,N′,-tetraacetic acid (EGTA), a chelator agent[314].

The intracellular signaling could be blocked by ions that bind to cytoplasmic tail of ASGPR. McAbee D.D. and Jiang X. demonstrated that using two different ions, Copper and zinc (0–220 μM), alone or in combination, the ASGPR was reversibly blocked in isolated rat

hepatocytes up to 93–99% and the cells surface had 50% less receptor. Similar results were obtained using iron instead of copper and zinc[315]. The receptor can be also blocked adding an excess of the natural ligand, like galactose, or increasing the pH of endosomes during the internalization process by alkalinizing chemicals, or with the depletion of adenosine triphosphate[316].

ASGPR has been found in well differentiated HCC cell lines. Grassi G. *et al.* (2017) showed that the expression of ASGPR increased with the differentiation grade of HCC cell lines proportionally[317]. HuH7 cell line, characterized by an intermediate differentiation level, present high density of receptor expression, as demonstrated by mRNA expression levels of the receptor compared to IHH (immortalized non tumour human hepatocytes) cell lines[317]. The human HCC cell line HepG2, characterized by a high differentiation level, shows a density of 76,000 of the receptor, while the HuH7 and HuH6, a medium-differentiated hepatocyte-derived carcinoma cell line, express a density of ~3000 ASGPR/hepatocyte[318]. Immunofluorescence analysis in liver tissues demonstrated that ASGPR was expressed irregularly and without a precise localization in Tre-Met transgenic mouse model, while it is normally present in the basolateral membrane of the normal hepatic cells[303]. Similar results were obtained by an immunoistochemical study, where the ASGPR was found more expressed in well differentiated HCC cells and localized on the plasma membrane[319].

2.11 The eukaryotic elongation factor 1 A (eEF1A)

The synthesis of protein is divided into four steps: initiation, elongation, termination and ribosome recycling. The translation starts when ribosomes are recruited by translation initiation factors to the mRNA, culminating in the formation of the 80S ribosome with the P-site occupied by the initiator tRNA, attached at the start codon. The elongation process consists of the polypeptide chain formation and elongation. The correct aa-tRNA, placed in the A-site of the ribosome, binds the mRNA codon following the peptide bond formation. Then, the ribosome translocates to the next codon of the mRNA to continue the process. The translation process ends when ribosome reaches the termination codon and the 80S ribosome dissociates into 60S and 40S subunits to be reused in the next translation initiation process[320,321].

The eukaryotic elongation factor 1 A (eEF1A) is the main factor involved in the elongation step of the protein. It consists of three domains (I, II and III), which are associated with different eEF1A functions. The Domain I is responsible for the GTP binding, and, together with domain II, binds the GEF-eEF1Bα complex for nucleotide exchange. Domain III mediates the binding with actin and, together with domain II constitutes the aa-tRNA binding site[322]. eEF1A is a GTP-depending protein and it binds the aa-tRNA during the elongation process. Then the aa-tRNA is transported to the site A of the ribosome where a conformational change in the ribosome conformation due to the recognition of the correct codon causes the GTP hydrolysis[323]. This event determinates the transition from eEF1A-GTP to eEF1A-GDP with the dissociation of the aatRNA to eEF1A-GDP. Then, the peptide bond formation between the aa-tRNA in the A-site and the aa-tRNA in the P-site occurs. eEF1A-GDP is recycled into eEF1A1-GTP in order to bind a novel aa-tRNA, by the eukaryotic elongation factor eEF1B, a guanine nucleotide exchange factor (GEF), which converts the GDP in GTP[324]. It seems that eEF1A is involved also in the nuclear export of mammalian proteins poly(A)-binding protein (PABP1) and van Hippel-Lindau (VHL) tumour suppressor[325].

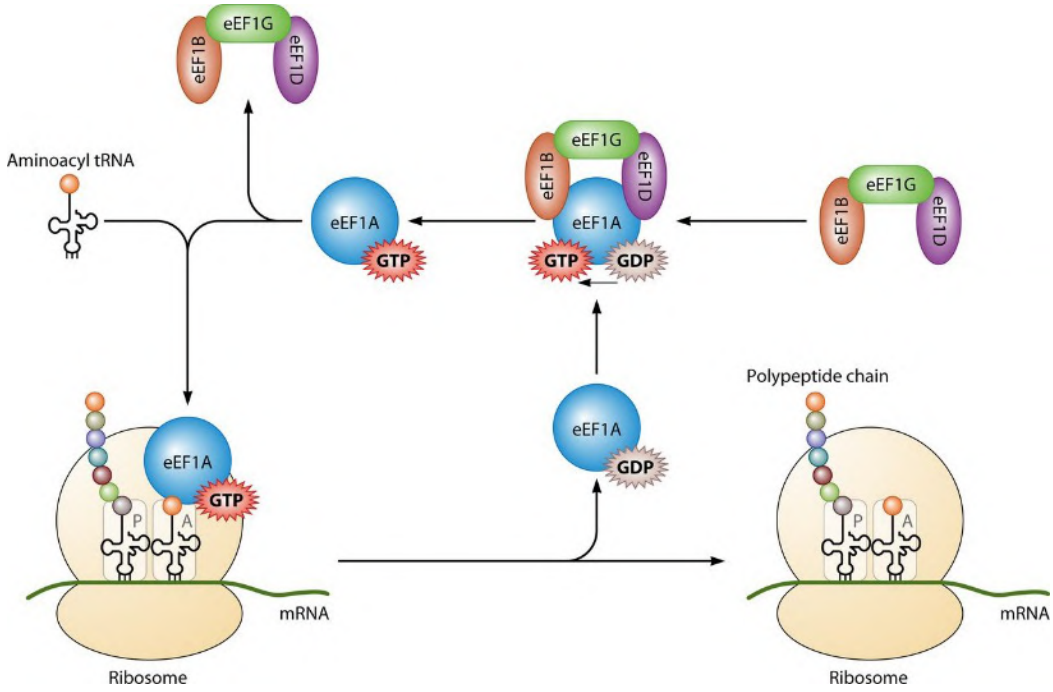

Figure 2.12. The role of the eEF1A in the protein synthesis[452].

The eEF1A is one of the most abundant protein, representing about 1-2% of the total proteins present in the cell. It exists into two isoforms named eEF1A1 and eEF1A2, which genes are encoded into different chromosomes, chromosome 6q14.1 for *EEF1A1* gene and chromosome 20q13.3 for *EEF1A2* gene[326]. The isoforms share 78% of coding sequence and 92% of protein homology, having the same molecule weight of 50.1 kDa[327]. Both of them display the same function regarding the protein translation process; indeed, they are involved in the elongation step of the protein synthesis, recognized as the "canonical function". Nevertheless, they have different affinity for eEF1B guanine exchange factor. eEF1A1 shows a 7-fold higher dissociation rate for GDP compared to the eEF1A2. This is probably due to eEF1A1 biophysical properties which make it less resistant to urea denaturation, more hydrophobic and with the ability to more easily self-associate compared to the isoform 2[328]. The two isoforms differ for their distribution among tissues: eEF1A1 is expressed in almost all tissues, instead, eEF1A2 is present only in the brain, heart, and skeletal muscle tissues[329].

eEF1A is characterized by the abundance of post-translational modifications (PTMs). Different phosphorylation patter has been observed in the two isoforms, which may explain their involvement in distinct processes. An example is the phosphorylation made by BRAF, which phosphorylates Ser21 and Thr88 in eEF1A1 and only Ser21 in eEF1A2[330]. Lin KW *et al.* (2010) observed the phosphorylation at Ser300 on eEF1A1 mediated by TGF-β receptor, which has serine/threonine kinase activity. This phosphorylation prevents the binding of the aa-tRNA to

eEF1A1 reducing cell growth and protein synthesis both *in vitro* and *in vivo*[331]. Thus, Ser300 phosphorylation by TGF-β can be a novel mechanism responsible for the regulation of the cellular protein synthesis demand. Moreover, eEF1A1 has Tyr29 and Tyr141 phosphorylated through Zap-70 kinase signaling, and Tyr85 and Tyr86 phosphorylated by the mesenchymal-epithelial transition factor (c-MET)[332]. In addition, eEF1A2 interacts with $p16^{INK4A}$, an antiproliferative protein, showing a reduction in its expression and activity causing a lower cell proliferation rate and protein synthesis in tumour cells[333]. Recently, it has been demonstrated that miR-663 and miR-744 downregulated eEF1A2 expression causing a decrease in cell proliferation in human cancer cells[334].

eEF1A proteins are also regulated by other mechanisms like methylation and acetylation. The acetylation modifications occur by histone deacetylase class I and II, which reduces proteins activity. It has been reported that eEF1A has the N- and C-terminal ends both methylated[335]. In particular, Jakobsson M. E. *et al.* (2018) observed the lysin methylations on eEF1A by lysine methyltransferases (KMTs). They showed that eEF1A-KMT3 KO cells lacking Lys-165 methylation on eEF1A had altered translation of specific genes compared to wild-type cells. These results indicated that lysine methylation has an important role in protein synthesis modulation, and it might mediate the interaction between eEF1A and aminoacyl-tRNA or ribosome during protein synthesis process. Moreover, there is the possibility that lysin methylation could be involved also in non-canonical functions of eEF1A1[336].

1.11.1 Non-canonical functions of eEF1A1/eEF1A2

Both isoforms are also involved in other functions named "non-canonical functions". eEF1A1 plays a role in the cytoskeleton organization due to its ability to bind F-actin and in the cell cycle progression due to its interaction with microtubules. The interaction with these structures occurs on the same binding site and it is still unclear how these interactions are regulated. Recent data showed that another function of eEF1A1 is to recognize the damaged proteins and degrade them through the proteasome[324]. Moreover, eEF1A1 showed a proapoptotic function, even if in some cases it showed an antiapoptotic effect[323]. In contrast, eEF1A2 has been always shown an antiapoptotic effects. It interacts with the peroxiredoxin-1 (Prx-1) protein, which reduces reactive oxygen species, protecting cells from apoptosis induced by oxidative stress. The antiapoptotic effect is due to the downregulation of caspase 3 and caspase 8 with parallel activation of Akt to promote cell survival[337]. It has been shown that eEF1A1 is expressed in myoblast during embryonic development, but then replaced by eEF1A2 two weeks after birth. This change is probably due to the fact that eEF1A1 displays a pro-apoptotic role, while eEF1A2 displays an anti-

apoptotic role[338]. Thus, probably most of tissues express eEF1A1 during the development but then it is replaced by eEF1A2 in tissues where its apoptotic role could be deleterious. eEF1A2 is also involved in filopodia formation, membrane structures used by cell for migration thus, important for cancer metastasis. Overexpression of eEF1A2 upregulates cytosolic and membrane levels of phosphatidylinositolo-4,5-biphosphate [PI(4,5)P2], which activates actin nucleation, important for filopodia formation[339].

eEF1A1 and eEF1A2 play an important role also during viral infection. For example, the human immunodeficiency virus (HIV) proteins like Nef and Tat can interact with eEF1A during early stages of virus replication and viral proteins translation[337].

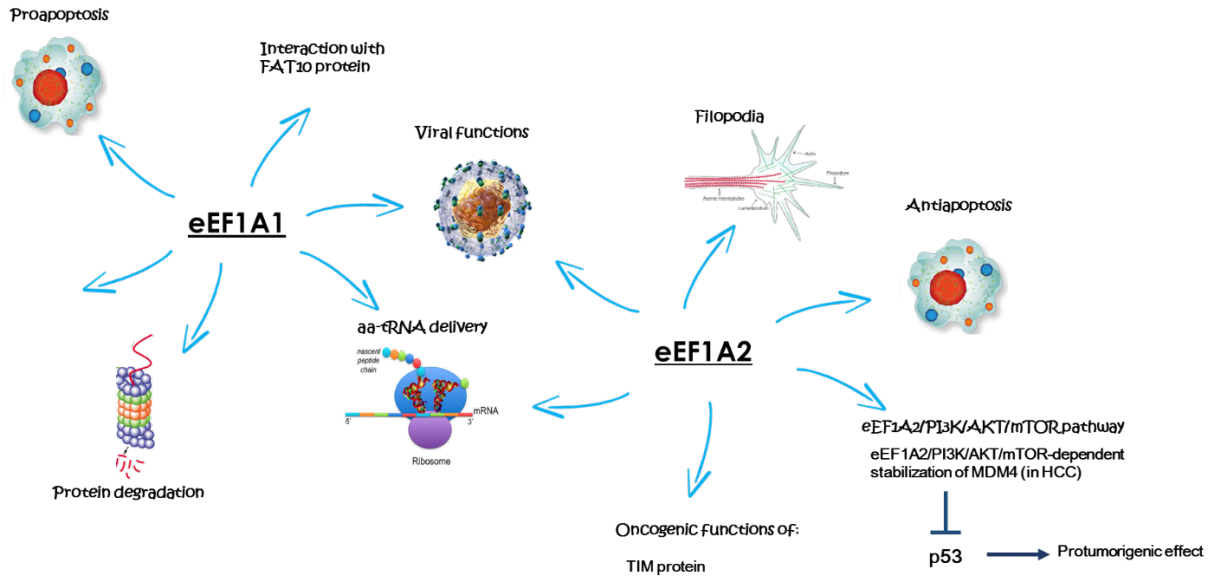

Figure 2.13. Schematic representation of eEF1A1 and eEF1A2 non-canonical functions.

1.11.2 The role of eEF1A isoforms in HCC

Both eEF1A proteins play a role in human tumours, mainly due to the dis-regulation of their non-canonical functions as described for many human cancers including HCC[340]. Normal hepatocytes do not express eEF1A2, but in human HCC cell lines, eEF1A2 is expressed and this overexpression correlates with cancer cell growth and differentiation phenotype[341,342]. eEF1A1, which is normally expressed in normal hepatocytes, was found overexpressed in HCC. It has been suggested that the overexpression of eEF1A is not always due to the multiplication of gene loci and/or epigenetic modifications, but also to the post-transcriptional modifications[343,342].

Recently, it has been shown that eEF1A2 takes part in the eEF1A2/PI3K/AKT/mTOR-dependent stabilization of MDM4 (Mouse Double Minute homolog 4). MDM4 was found upregulated in HCC due to its stabilization through the direct phosphorylation by AKT or through

the protection from the proteasome degradation by ubiquitin-specific protease 2a, which deubiquitinate MDM4. MDM4 binds to the N-terminal transactivation domain of p53, repressing its transcriptional activity. Recent studies of human HCC showed that eEF1A2 is upregulated in concomitant with MDM4 and it is responsible for Akt and mTOR signaling activation, which in turn stabilize MDM4 protein. The inhibition of MDM4 degradation results in the inactivation of the anti-oncogene p53 thus, resulting in a pro-tumourigenic effect in HCC. Notably, the activation of the EEF1A2/PI3K/AKT/mTOR/MDM4 axis significantly influences the survival probability of HCC patients[344]. eEF1A2 has been also implicated in the oncogenic function of the mammalian timeless (TIM) protein in HCC. TIM protein is important in the regulation of the mammalian circadian rhythm, DNA damage response and replication. Elgohary N. *et al.* (2015) showed that TIM, found overexpressed in different HCC cell lines, directly interact with eEF1A2 activating the protumourigenic EEF1A2/AKT/MDM4 pathway[345].A recent study showed that eEF1A2 interacts with interferon-induced, double-stranded RNA-activated protein kinase (PKR, EIF2AK2), which is important for cancer cells survival in HeLa cells[346].

With regard to eEF1A1, its overexpression relates with HCC cell growth and differentiation phenotype. It seems to mediate the tumourigenic functions of the human HLA-F adjacent transcript 10 (FAT10) protein in HCC. FAT10 is a ubiquitin-like protein involved in apoptosis, cell cycle regulation and cancer development. It was found upregulated in many cancers including HCC[347]. Yu X. *et al.* (2012) demonstrated the direct interaction between FAT10 and eEF1A1 in Hep3B cell line and they assumed that eEF1A1 may be regulated by FAT10 in HCC[348]. In addition, Blanch A. *et al.* (2013) observed that p53 and p73 are inhibited by the overexpression of eEF1A1, which also induced a chemoresistance blocking the chemotherapy-induced apoptosis[349]. Huang J. *et al*. (2017) observed that eEF1A1 is involved in the promotion of HCC proliferation regulating cyclin D1 expression, a cyclin responsible for the G1/S phase transition. They demonstrated that eEF1A1 overexpression increased the total STAT1 expression in the cell, which interacts with cyclin D1 promoter. This interaction increases the transcriptional activity of cyclin D1 promoting HCC cell proliferation[350]. These findings underline a novel mechanism in which eEF1A1 is involved in promoting proliferation in HCC cells.

Finally, the contemporary targeting of eEF1A1 and eEF1A2 by means of an aptameric DNA molecule resulted in the profound impairment of the viability of cultured HCC cell lines, further witnessing the involvement of eEF1A1 and eEF1A2 in HCC[351].

Grassi G. *et al.* (2007) observed that the expression of eEF1A1 is inversely correlated to cell differentiation in HCC cell lines. In particular, they observed that the eEF1A1 mRNA levels were 28-folds, 24-folds and 177-folds higher in HepG2, HuH7 and JHH6 respectively, compared

to the normal liver cells; while eEF1A2 mRNA levels were significantly high only in JHH6 (205-folds). Indeed, HepG2 and HuH7 showed an increment of eEF1A2 mRNA levels of 1,5-folds and 2,9-folds respectively, compared to the normal liver cells. HCC cells where eEF1A1 was overexpressed were characterized by the evasion of cell cycle arrest, having the ability to proliferate under non optimal growth conditions. They speculated that the high level of eEF1A proteins may be explained by the higher protein synthesis demand from the cell to sustain the proliferation rate and cytoskeleton organization, important for cell migration[342].

2.12 E2F1 transcription factor

The various pathways involved in the initial step of the cell cycle process and its progression have been defined over the past several years. Many factors are responsible for the progression of cells from the quiescent phase (G0 phase) to G1 and S phases of the cell cycle. Activation of cyclin-dependent kinases (CDKs), cyclins and the phosphorylation of different proteins are the principal events[352].

E2Fs are a family of transcription factors that regulates the progression of the cell from G1 to the S phase of the cell cycle. The mammalian E2Fs family includes nine distinct gene products encoded by eight chromosomal loci. Based on *in vitro* studies, they are classified into activators (E2F1, E2F2 and E2F3a) and repressors (E2F3b, E2F4, E2F5, E2F6, E2F7 and E2F8)[353]. E2Fs activator promote the transcription of genes, which are active during the late G1/S phase by binding to their promoters. Instead, E2Fs repressor prevent the transcription of the target genes for the progression of the cell to the early G1 phase and they are also important in the cell cycle regulation[354]. The main E2Fs activators target genes promote the transcription of proteins like cyclin E and cyclin A. Several other genes activated by E2F proteins encode for proteins involved in DNA synthesis like the thymidine kinase (TK), DNA polymerase (pol) and dihydrofolate reductase (DHFR). E2F also binds promoter regions of some cellular proto-oncogenes, including PRAD1/Bcl1 (cyclin D1), N-myc, B-myb, c-myc, c-myb, erb-B and the epidermal growth factor receptor[355].

pRB (retinoblastoma protein), p130 and p170 are pocket proteins required for the cell cycle regulation during the late G1 and S phases. These proteins bind E2F proteins inhibiting their transcriptional activity, playing an important function as transcriptional regulators in the cell cycle process[353].

Among E2F family members, the E2F1 is the most studied. E2F1 is mainly involved in the cell cycle regulation, but it has been seen that it is involved in other cellular processes like differentiation, metabolism, cell migration, proliferation and cell reprogramming[356]. E2F1 protein is composed by 437 amino-acids and it is characterized by having a transactivation domain (TD) through which it binds target gene promoters, a conserved-DNA binding domain (DBD) and a dimerization domain. TD domain contains a short amino-acid sequence responsible for the interaction with the pocket protein pRB, which prevents the E2F1 transcriptional activity[357]. The dimerization domain allows the binding of the E2F1 with a member of the dimerization partner family (DP1-DP3). In particular, the bind between E2F1 and DP-1 allows DNA binding promoting the transcription of target genes[358]. E2F1 also has a signal for nuclear localization and a cyclin A

binding site. The binding site for cyclin A is important for E2F1/DP1 phosphorylation by cyclin A/cdk2 (cyclin dependent kinase 2). This event results in the disruption of the E2F1/ DP1 complex with consequent loss of the bond with the DNA. This situation occurs during the late S phase of the cell cycle when levels of cyclin A are high and the transcriptional activity of E2F1/DP1 is no longer necessary[357].

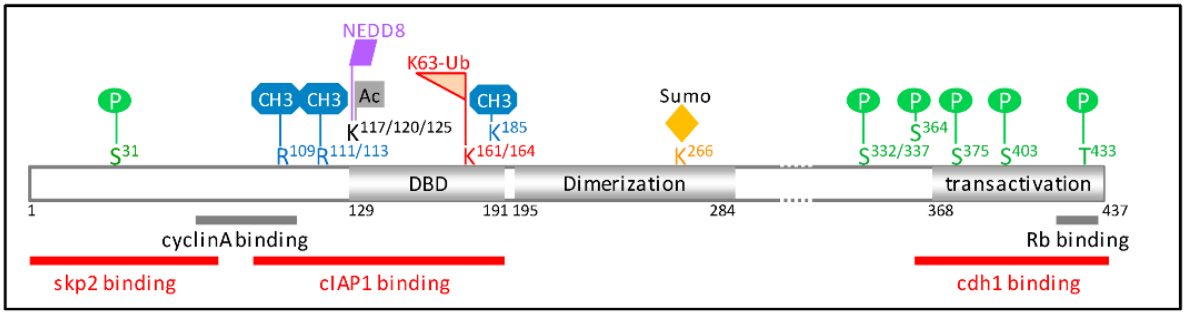

Figure 2.14. Structure of E2F1 protein[356].

Cells in the quiescent G0 phase are characterized by the expression of the repressors E2F4 and E2F5, which are associated with p130 and p107. They bind promoter regions thus preventing the transcription of genes promoting the entry into the G1 phase. During G0 phase the transcriptional activity of the complex E2F1/DP1 is inhibited by binding to the tumour suppressor pRb. In the presence of the mitogenic signals, cyclin D is produced and binds to cdk4-6 (cyclin dependent kinase) kinase inducing the G1 phase entry[356]. Pocket proteins are phosphorylated by cyclin-CDKs expressed in G1 phase resulting in the release of the E2F4 and E2F5 in the cytoplasm, freeing the regions of DNA previously occupied. The cyclinD/cdk4-6 complex phosphorylates pRb protein inducing the release of the E2F1/DP1 complex which is free to go into nucleus to bind the promoter regions of the target genes[359]. In particular, the complex induces the transcription of the cyclin E, which binds cdk2. Cyclin E/cdk2 complex hyperphosphorylates pRB with completely dissociation of the E2F1 from pRb. This event increases the levels of free E2F1/DP1, promoting cell growth by the activation of the transcription of several genes implicated in S phase of the cell cycle like cyclin A and DNA replication genes[353].

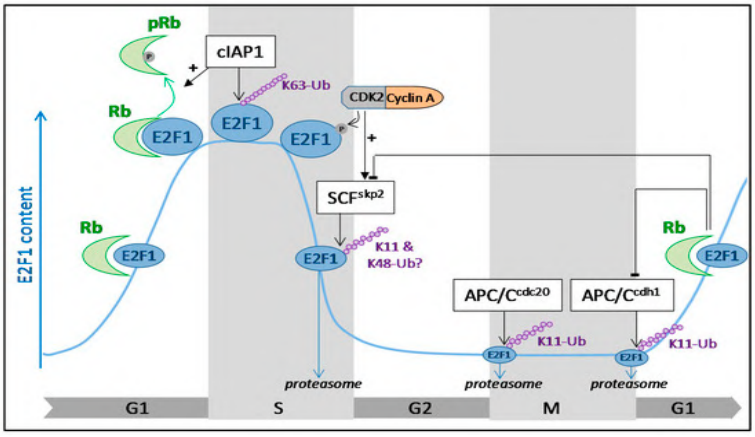

Figure 2.15. The role of the E2F1 in the cell cycle[356].

During late S phase, cyclin A/cdk2 phosphorylates DP1 with loss of binding to E2F1 that is not able anymore to bind the promotor regions. E2F1 is then degraded and transcriptionally repressed by E2F7/8[360]. E2F7 and E2F8 proteins accumulate during the G1/S phase and bind DNA promoter regions inducing the transcription of genes responsible for the repression of the cell cycle[361,362].

It is well known now that the disruption or the deregulation of one or more of components taking part of this pathway can lead to the cell cycle regulation out of control causing transformation and cancer development. For example, mutations in pRB protein can cause the loss of the regulation of E2F1 transcriptional activity which is free to go into nucleus and actives the transcription of genes in the absence of a proliferation stimulation signal[363].

Despite of the regulation of the cell cycle is the main role of the E2F1, it can promote other cellular processes like apoptosis and DNA repair. In normal cells, the events switching E2F1 from cell cycle promotion to apoptosis is well regulated. On the contrary, in the tumour cells, the presence of defective E2F1 downstream targets like p53 can induce the pro-apoptotic function of E2F1[146].

2.12.1 The role of the E2F1 in the hepatocellular carcinoma

E2F1 is found overexpressed in many tumours including the HCC[364]. Its overexpression can cause cancer promotion through the deregulation of the cell cycle process inducing uncontrolled cell proliferation. For this reason, E2F1 could be a potential target to inhibit or decrease cancer cell proliferation and its development[365,146]. Farra R. *et al.* (2011) observed that the silencing of the E2F1 by siRNAs in three different HCC cell lines (JHH6, HuH7 and HepG2) resulted in the reduction of the cell growth in several *in vitro* tests (cell cycle analysis, cell counting and vitality). In particular, they demonstrated that the depletion of E2F1 by siRNAs caused the block of cell proliferation in G1 phase, since the transcription factor regulates the G1/S phase transition[366].

One mechanism that could be involved in the promotion of HCC mediated by E2F1 is the upregulation of SKP2 (S-phase kinase-associated protein 2). This protein is involved in different steps of the cell cycle progression, including G1/S transition, S phase progression, and S/G2 transition. Its overexpression has been detected in HCC where E2F1 is responsible for the upregulation of the SKP2 expression promoting the progression of the cell cycle[367].

Recent studies have shown that E2F1 can promote cell proliferation through micro-interfering RNA (miRNA) pathways. miR-429 is an example of link between E2F1 and HCC development. This miRNA is upregulated in HCC and one of its targets is the Rb binding protein 4 (RBBP4) that form a complex with pRb1, constituting the pRb1/RBBP4-associated histone deacetylase complex. RBBP4 targeting results in the inhibition of interaction between pRb and E2F1, thus, E2F1 is free to go to the nucleus inducing the transcription of pro-proliferative genes which promote HCC[368].

Wang S. N. *et al.* (2016) observed that the intestine-specific homeobox (*ISX*) gene plays an important role in the cell proliferation and in HCC development. *ISX* activates the transcription of E2F1 and binds directly the E2F promotor regions showing an oncogenic activity. *ISX* expression phosphorylates the serine in 332 position of E2F1, determining E2F1 translocation into the nucleus where it binds to DP-1 forming the E2F1–DP-1 complex. Moreover, they observed that *ISX* and *E2F1* co-expression promoted cell proliferation and apoptosis escape *via* pRB and p53 pathways. In addition, the depletion of ISX and E2F1 by siRNAs resulted in cell proliferation reduction in hepatoma cells *in vitro* and malignant transformation *in vivo*[369].

Wang B. *et al.* (2015) observed that E2F1 protein is stabilized by the deubiquitylase POH1, which binds and deubiquitylates E2F1. In particular, they demonstrated that the conditional knockout of Poh1 alleles in primary mouse liver cells resulted in the reduction of the expression of E2F1, suggesting the contribution of the POH1–E2F1 regulation in HCC development[370].

Histone-lysine N-methyltransferase SET7/9 is a protein lysine involved in the methylation of the histone H3K4 and several non-histone proteins. Many human cancers showed that SET7/9 is deregulated. Mullin L. B. *et al.* (2013) observed that SET7/9 and E2F1 were upregulated in 68 samples of HCC tissues compared to the healthy liver samples. They demonstrated that SET7/9 and E2F1 interact each other and that HCC cells treated with 5' deoxy 5' methylthioadenosine (MTA), an inhibitor of proteins methylation, had lower levels of SET7/9 and E2F1 proteins, which resulted in a reduction of migration, invasion and cell proliferation. Moreover, reduction of E2F1 downstream targets like cyclin E, cyclin A2 and CDK2 were also downregulated following MTA treatment and SET7/9 downregulation[371].

2.13 Animal models in HCC

The application of animal models in the research had increased since the beginning of the twentieth century in order to demonstrate what already observed in *in vitro* tests. Animal models can be applied for different purposes and the choice of the right model depends on the purpose of the research[372].

Tumour induction and growth in animal models directly into the liver represent the best way to study the biological mechanisms involved in the hepato-carcinogenesis process and the crosstalk between the local environment and liver tumour. Instead, injection of HCC tumour cells in a different place than liver is the best choice for the evaluation of the efficacy of novel therapies or drugs for HCC treatment[373].

An "ideal" animal model of HCC should reproduce the human HCC for basic and translational studies. Model animals which spontaneously develop the diseases can give a more accurate information regarding cell differentiation, cell growth and cell metabolism[374]. Currently, several animal models can be applied for HCC studies, but the mouse model is the most used for its short life span, size, ease in introducing mutations in the genome, easy to breed and for its similarity to human liver histology and lesions[375]. Animal models widely used for HCC studies include chemically-induced animal models, genetically-engineered mouse (GEM) models and engrafted models and humanized mice.

In *chemically-induced animal models* the tumour is induced exposing animals to chemical compounds like Diethylnitrosamine (DEN), Carbon tetrachloride (CCl4) and Thioacetamide (TAA) for a short or long period. In this case, HCC development is triggered by a direct DNA damage inducing preneoplastic lesions formation following chemical agents exposure[374]. Diethylnitrosamine (DEN) induces DNA damaging by the promotion of the oxidative stress and the alkylation of DNA[375]. Carbon tetrachloride (CCl4) is a potent hepatotoxin that acts increasing the oxidative stress in hepatocytes and causing inflammation through the activation of pro-inflammatory cytokines and chemokines resulting in liver inflammation and necrosis[376]. Thioacetamide (TAA) is a chemical molecule used to promote liver fibrosis in rodents. The molecular mechanisms responsible for tumour formation is not completely understood yet, but probably tumour development is caused through oxidation processes[377].

Genetically-engineered mouse (GEM) models result from the inactivation of tumour suppressor genes or activation of oncogenes which promote tumour development. For HCC studies mice with single gene mutations and multiple gene mutations or expressing specific fragments of HBV and HCV genomes have been used[378]. Examples of these animal models are mice in which

MYC oncogene and/or E2F1 are overexpressed resulting in HCC development in 9-12 months[373]. Transgenic mouse models have been generated by Kim C.M. *et al.* (1991), whose generate mice in which HBx gene was placed directly into the germline of mice. These mice showed altered hepatocytes and adenomas formation followed by HCC development[379]. Transgenic mice with Glycine N-methyltransferase (GNMT) knockout (Gnmt-/-) were also generated. These animals developed HCC, chronic hepatitis and fatty liver spontaneously and they were used to individuate cancer biomarkers[380]. It should be reminded that human and mouse HCC genetic profiles are quite different.

Engrafted models represent the most used method to reproduce HCC and consist in the injection of tumour cells in mice either subcutaneously or into the liver. This method allows to easily test new therapeutic molecules or treatment strategies obtaining reproducible data[373]. Based on the place of injection, animal models can be distinguished in orthotopic model, where cancer cells are placed within the tissue of origin, and heterotopic model, where cells are placed in a different tissue than the origin[378]. In the heterotopic model tumour, cells are usually injected subcutaneously, allowing to study the biology of tumour and to monitor the response to the novel therapy. Orthotopic model can reproduce the tumour environment, the organ tropism and metastasis formation more accurately than heterotopic model[373]. Injected cells can be human or murine cancer cells distinguishing the models in syngeneic (or allograft) and xenograft model. In the first case tumour cells are engrafted back into the same inbred strain, i.e. mouse tumour cells injected in mice; in the second case the injecting tumour cells are from a different organism, i.e. human tumour cells injected in mice[381]. Syngeneic models have intact immune system, so that they can be used for immunotherapy studies. Nevertheless, the immune response derives from the mouse and it could be difficult to translate the results back to humans. Xenograft models allow to use human cells for studies, making this model more representative of human cancer mutations, since cells carry the same genetic material of human cells[382]. A limitation of this model is that the contribution of the immune system cannot be evaluated as the animals need to have compromised immune system to allow human cell grafting[383]. Obviously, these animals cannot be employed for immunotherapy studies, since they do not reproduce a full immune response[384].

Immunocompromised mice frequently used include:

-Severe combined immune deficiency (SCID) mice, which lack mature T and B cells[385];

-Nude mice, characterized by the absence of thymus resulting in a loss of T cells[386];

-Non-obese-diabetic–severe combined immunodeficient mice (NOD–SCID), which lack innate immunity with deficient natural killer (NK) cells and impaired B and T cells[387];

-NSG (NOD/SCID-IL2g-/−) strain mice, characterized by IL-2 receptor mutation, absence of T and B cells, NK cells, macrophages, natural killer T cells (NKT)[388].

The disadvantages in using engrafted models is that the model does not fully reproduce the condition in human patients; on the contrary, "humanized" models can.

Humanized mouse models are modified mice expressing human immune cells, mimicking in a better manner the human tumour background (situation, landscape, condition)[373]. Humanized mice can be obtained by different approaches. One of them consists in injecting human peripheral blood leukocytes, mostly used to study human T cell function. In the second approach, human haematopoietic stem cells (HSCs) and precursor cells isolated from fetal cord blood or fetal liver are engrafted in the marrow of irradiated immunocompromised mice in order to allow the development of a functional "human" immune system[389]. The drawback is that there are sex-related differences; indeed female mice support less efficiently human HCC development than male mice, probably due to the fact that female mice have an inferior HSC repopulation than male mice[390]. Recently, mice having humanized liver and hematopoiesis have been generated[391]. In another approach, thymus and human fetal liver are transplanted under the kidney capsule and autologous fetal liver HSCs are injected [392].

Human HCC originates by the combination of chemical insults, viral infections, genetic predisposition and/or life-style behavior, thus the implication of a single approach to reproduce human HCC using animal models is not sufficient. Thus, animal models in which different approaches are used to provoke HCC development, can provide more realistic information about the effectiveness of a novel treatment.

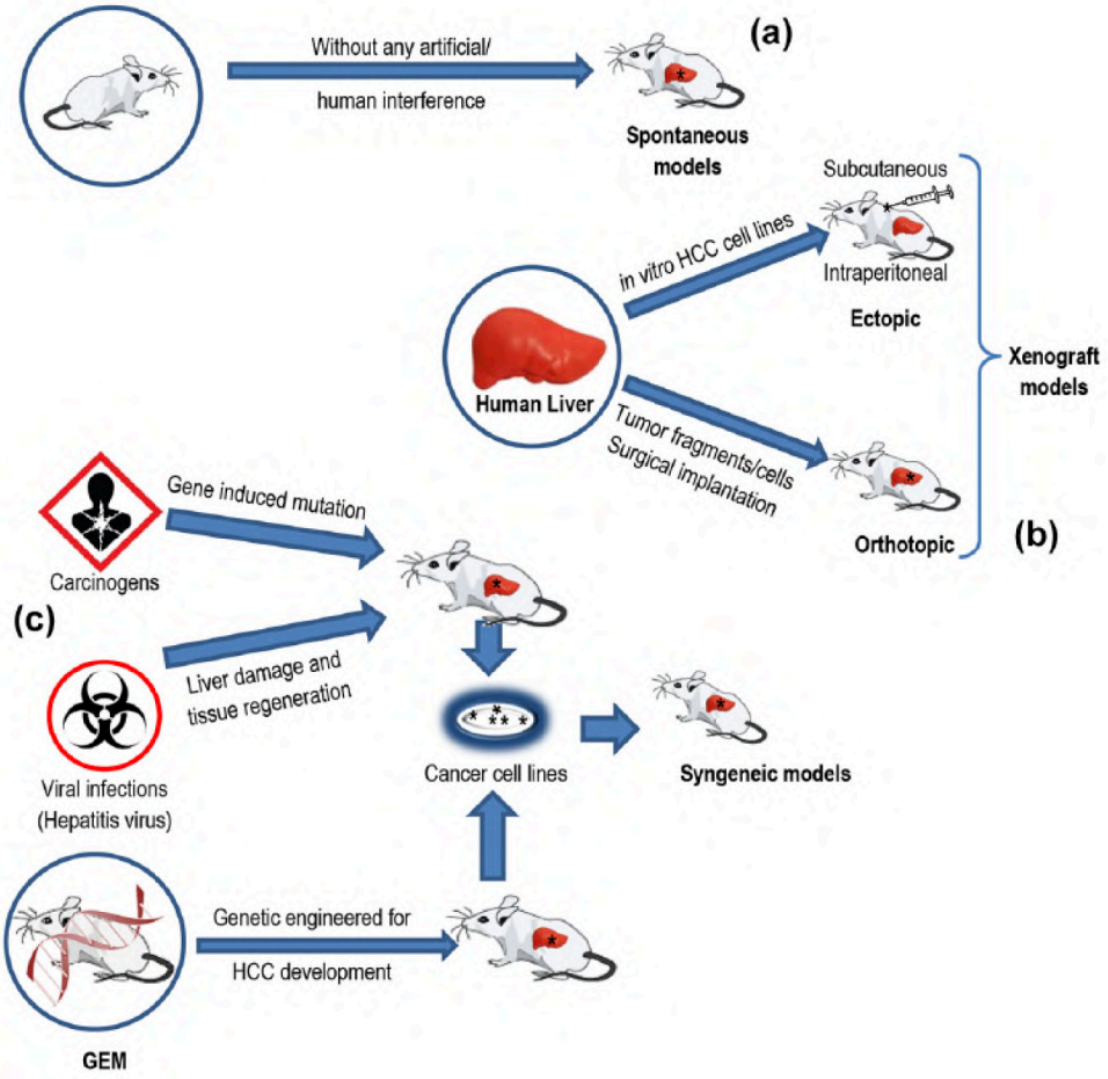

Figure 2.16. Mouse models of HCC: a) spontaneous, b) xenograft and c) chemically-induced animal models and GEM[374].

3 Aims of the thesis

Since for Hepatocellular Carcinoma (HCC) there are no effective treatments, the individuation of novel therapeutic targets and approaches are necessary.

Small interference RNA (siRNAs) are small double stranded RNAs able to induce gene silencing. They represent an innovative therapeutic strategy for cancer treatment as they can decrease the expression of upregulated oncogenes. The main impediment in using siRNAs is the fast degradation rate in the biological environment and their difficulties to cross the hydrophobic cell membrane. To protect siRNAs from degradation, we developed a novel delivery system based on the polymer α,β-poly-(N-2-hydroxyethyl)-D,L-aspartamide-(PHEA) derivatized with diethylene triamine (DETA) linked via a polyethylene glycol (PEG) to galactose (GAL) molecules (PDPG). In particular, PDPG is characterized by the presence of Galactose residues, which confer the ability to target cells expressing the Asialoglycoprotein receptor (ASGPR). This receptor is mainly expressed on hepatocytes and overexpressed in HCC cells. PDPG was designed to deliver siRNAs able to down regulate the expression of oncogenes (eEF1A1, eEF1A2 and E2F1), to hepatic cancer cells.

The main aim of the thesis was to evaluate the ability of the PDPG to target ASGPR-expressing cells and to release siRNAs both *in vitro* and *in vivo*. As target genes, we have chosen eEF1A1, eEF1A2 and E2F1, overexpressed in HCC and known to contribute to tumour development.

In this work, I explored the consequences of the silencing of the above oncogenes using specific siRNAs delivered by the PDPG in order to down-regulate their expression and to observe the consequences of the silencing both *in vitro* and *in vivo*.

The effective uptake of PDPG was proven in cellular (HuH7 cells, using a fluorescently labelled PDPG for confocal microscopy) and animal models of HCC (SCID mice for window chamber experiment). The phenotypic effects of siRNA+PDPG were tested by MTT and cell count in HuH7 (HCC cells overexpressing ASGPR). The molecular effects of siRNAs+PDPG were verified at the protein and mRNA levels. In parallel, control experiments were performed using the polymer lacking GAL motifs (PDP) to demonstrate the specificity of PDPG. Finally, *in vivo* experiments were performed in a subcutaneous xenograft mouse model of HCC (SCID), comparing the effect of siRNAs+PDPG vs control groups (siGL2+PDPG, PDPG and NaCl).

4 Materials and methods

4.1 Cell cultures

The cell line used in the project was the human HCC derived cell line HuH7, which shows a medium hepatic differentiation grade based on the albumin and ferritin levels[342]. This cell line was chosen for the feasible grafting into SCID mice for *in vivo* experiments. HuH7 cells were cultured in Dulbecco's modified Eagle's medium (DMEM) (Euroclone) containing 10% FBS, 100 U/ml penicillin, 100 ug/mL streptomycin and 2 mM L-glutamine (Euroclone).

For the lentivirus production, the 293T (ATCC® CRL-3216™) cell line was used. This cell line derives from the human embryonic kidney 293 cells and it is widely used for retroviral production, gene expression and protein production[393,394]. The cell line was cultured in Dulbecco's modified Eagle's medium (DMEM) (Euroclone) containing 10% FBS, 100 U/ml penicillin, 100 ug/mL streptomycin and 2 mM L-glutamine (Euroclone).

4.2 siRNA *in vitro* transfection and copolymers preparation

siRNAs sequences (Eurofins Genomics) were designed in order to target specifically and with fully complementarity the following mRNA targets: eEF1A1, eEF1A2 and E2F1. A siRNA against the Firefly Luciferase mRNA (siGL2), which cannot bind to any mRNA present in human cells, was used as control siRNA. Moreover, for uptake studies, siEGFP (Dharmacon™, P-002048-01-20 GFP Duplex I) was used. Particular care was put in choosing siRNAs against eEF1A1 and eEF1A2 in order to discriminate the mRNA of the two protein isoforms[395]. All siRNAs sequences are listed in the Table 4.1 and were already described elsewhere[396,397].

As an HCC specific siRNA delivery system for *in vitro* and *in vivo* tests, a functionalized copolymer to direct siRNAs towards the HCC cells has been synthetized in collaboration with Prof Cavallaro's laboratory (Dipartimento di Scienze e Tecnologie Biologiche, Chimiche, Farmaceutiche (STEBICEF), Lab of Biocompatible Polymers, University of Palermo). The copolymer is constituted by a repeat units of a,b-poly-(N-2-hydroxyethyl)-D,L-aspartamide (PHEA), diethylene triamine (DETA) and polyethylene glycol (PEG), equipped with galactose (GAL) molecules at the end of the chain, obtaining PHEA-DETA-PEG-GAL (or named PDPG) copolymer. Briefly, the copolymer was synthetized by subsequent derivatization of PHEA with diethylene triamine (DETA), and with a galactosylated PEG derivative containing galactose (GAL) molecules[317]. Galactose moieties are ligands of the Asialoglycoprotein receptor (ASGPR), a glycoprotein considered a valuable surface biomarker to target HCC cells. It has been shown that

this copolymer is able to target only the ASGPR expressing cells and it biocompatible[317]. In addition, a copolymer lacking galactose moieties (PHEA-DETA-PEG or named PDP) has also been used in the experiments to further prove the specificity of the delivery system.

Copolymer powders were weighted each time before experiments and resuspended in RNAase free water in order to obtain a final concentration of 1 mg/ml. Then they were sterilized under UV light for 15 min before their administration. Copolymers synthesized at different times were used during the experiments.

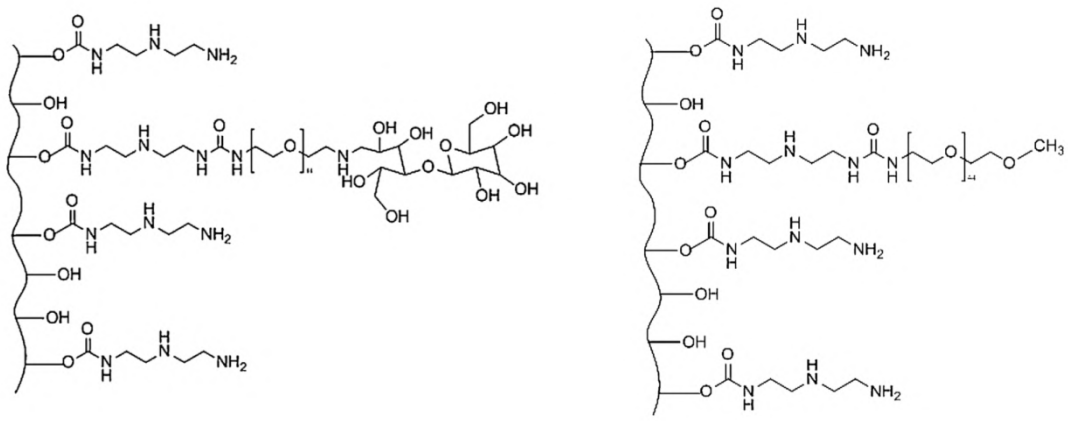

Figure 4.1. Chemical structure of PHEA-DETA-PEG-GAL and PHEA-DETA-PEG copolymers[317].

For the transfection protocol, HuH7 cells were seeded at the density of 3.8×10^3 cells/cm^2 in 6 well plate in 3 ml of DMEM complete medium. The day after, cell transfection was performed either using the Lipofectamine 2000 (1 mg/ml, Invitrogen) or the copolymer PDPG, in order to compare the two different delivery systems. Moreover, the PDP copolymer was used in comparison to PDPG to demonstrate the specificity of the interaction between PDPG and the galactose receptor ASGPR. Lipofectamine 2000 is a commercial cationic liposome able to interact with negatively charged nucleic acid molecules, allowing their uptake into the cell by overcoming the electrostatic repulsion of cell membrane. PDPG is a non-commercial copolymer positively charged and able to interact with siRNAs by electrostatic forces. The used weight ratio of siRNA:transfectant was 1:1 (weight/weight) for both Lipofectamine 2000 and PDPG/PDP. Specifically, 2.55 µg of Lipofectamine 2000 or PDPG or PDP were mixed in 125 µl of serum-free medium Optimem (Invitrogen) for 15 minutes at RT. At the same time, 220 nM of siRNAs were incubated in 125 µl of Optimem medium for 15 minutes at RT. Then, the siRNA+Optimem solution were mixed with the Lipofectamine/PDPG/PDP+Optimem solution for 20 minutes at RT to allow liposome/copolymer-siRNAs complexes formation. After that, 550 µl of Optimem

medium were added to the mixture, to reach the final concentration of copolymer/ Lipofectamine 2000 and siRNAs of 220 nM. Cells seeded in 6 wells plates were washed with PBS (NaCl 137 mM, KCl 2.7 mM, Na_2HPO_4 8.1 mM, KH_2PO_4 1.47 mM, pH 7,4) and then incubated with the mix containing liposome/copolymer-siRNAs for 4h at 37 °C. After the incubation, the transfection mix was removed, cells were washed with PBS and 3 ml of specific complete medium were added to the cells (Figure 4.2).

In all experiments cell collection for analysis was usually done three days after transfection.

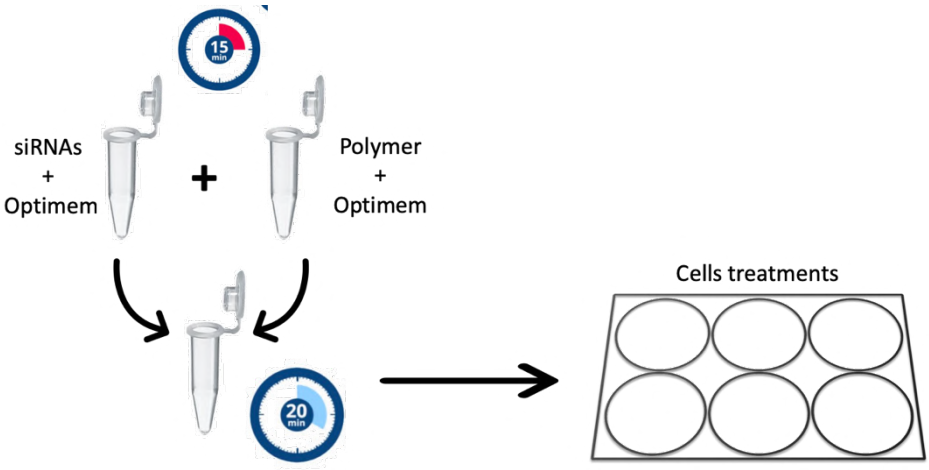

Figure 4.2. Scheme of the siRNAs-PDPG/PDP or siRNA-Lipofectemine 2000 protocol transfection.

Table 4.1. List of siRNAs sequences used in the experiments

siRNAs	Sense	Antisense
sieEF1A1	5'-AUGCGGUGGCAUCGACAAA-3'	5'-UUUGUCGAUGCCACCGCAU-3'
sieEF1A2	5'-GUCGGCUUCAAUGUGAAGA-3'	5'-UCUUCACAUUGAAGCCGAC-3'
siE2F1	5'-GAGGAGUUCAUCAGCCUUU-3'	5'-AAAGGCUGAUGAACUCCUC-3'
siGL2	5'-CGUACGCGGAAUACUUCGA-3'	5'-UCGAAGUAUUCCGCGUACG-3'
sieGFP	5'-AGACUUCAGGGUCAGCUUGC-3'	5'-GCAAGCUGACCCUGAAGUCU-3'

4.3 *In vitro* uptake studies

Uptake studies were performed in order to demonstrate that the copolymer is able to enter the cell. For this purpose, copolymers PDPG and PDP conjugated with a fluorophore, BodipyTRX (Ex/Em=588/616 nm), were synthetized in Prof. Cavallaro's lab.

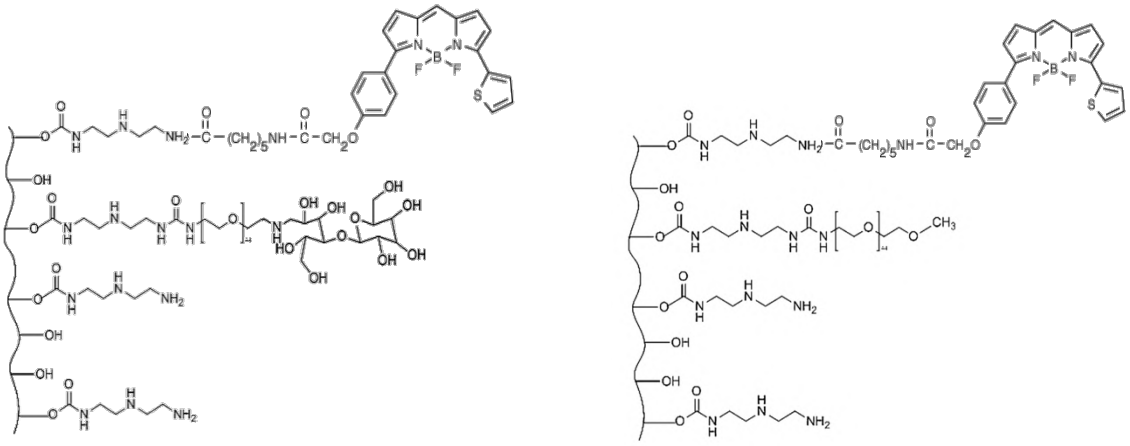

Figure 3.3. PDPG and PDP copolymers conjugated with BodipyTRX fluorophore

HuH7 cells were seeded on slides placed in each well of 6-wells plates at density of 7.4×10^3 cells/cm^2. The day after, cells were transfected with copolymers (PDPG or PDP) delivering siGL2 or 5'fluorescein (FITC) labelled siGL2. For this experiment, the final concentration of siRNAs, and consequently also copolymers concentration, was 880 nM (siRNAs-copolymers ratio 1:1) in order to facilitate the visualization of the copolymers for imaging. Two and twenty-four hours after transfection, cells were fixed in 4% paraformaldehyde (Sigma-Aldrich) for 20 minutes at RT, washed twice with PBS and stained with DAPI (1:2500 in 1X PBS; n-9564; Sigma-Aldrich) for 5 minutes at RT. Then, slides were mounted using Moviol Mounted solution (Mowiol® 4-88, Fluka) and images were acquired using Carl Zeiss Laser Scanning Confocal Microscopy LSM800 Zeiss Airyscan equipped with a 63×, NA=1.3 objective.

An experiment in which the interaction between the ASGPR and copolymers is prevented was performed in order to demonstrate that the polymer is able to enter the cells through the receptor. It was already shown that calcium ions (Ca^{2+}) are very important for ligands-receptor interaction; indeed, in the absence of Ca^{2+}, the receptor is not able to bind its ligands[398]. The experiment was carried out comparing images from HuH7 treated and untreated with EGTA, a chelating agent with high affinity for Ca^{2+}. HuH7 cells were seeded on slides in 6-wells plates at the density of 7.4×10^3 cells/cm^2 and the day after 5 mM of EGTA were added to the cells for 10 minutes. After that, the transfection mix containing PDPG or PDP marked by BodipyTRX and siGL2 was added in each well and cells were incubated for 4h at 37°C. After removing the transfection mix, 3 ml of DMEM complete medium were added in each well and after 2h, cells were fixed in 4% paraformaldehyde for 20 minutes at RT, washed twice with PBS and stained

with DAPI for 5 minutes at RT. Then, slides were mounted using Moviol Mounted solution and images were acquired using Carl Zeiss Laser Scanning Confocal Microscopy LSM800 Zeiss Airyscan equipped with a 63x, NA=1.3 objective.

In order to demonstrate that the copolymer PDPG is able to deliver and release siRNAs inside the cell, HuH7 were transfected with PDPG carrying siRNA (siGL2) marked with FITC. Lipofectamine 2000 was also introduced in the experiment as a positive control, due to its high transfection efficiency.

HuH7 cells were seeded at the density of 7.4×10^3 cells/cm^2 in 6 wells plates in 3 ml of DMEM complete medium. The day after, cells transfection was performed as already described and, after 4h, cells were washed twice with PBS and 500µl of a lysis solution containing 1% of Triton-X-100 (Sigma-Aldrich) and 2% of SDS were added in each well. A complete cell lysis was obtained after 30 min incubation on ice in dark. Then, the lysates were collected from each well and centrifuged for 15 min at 14000 rpm at 4°C. After that, 100 µl of cell lysate from each sample were put in a 96-wells plate and the fluorescence was detected by a TECAN infinite®200 microplate fluorimeter (Tecan Group, Switzerland).

4.4 Immunofluorescence assay for uptake *in vitro* studies

Immunofluorescence assay was performed in order to demonstrate the colocalization of PDPG and ASGPR in HuH7, since the polymer has galactose residues representing ligands of that receptor.

For the experiment, HuH7 cells were seeded on slides placed in each well of 6-wells plates at density of $7{,}4\times10^3$ cells/cm^2. The day after, cells were transfected with copolymers (PDPG or PDP) marked by BODIPY TR-X delivering siGL2, according to the transfection protocol as described previously for PDPG/PDP and siRNAs transfection. Copolymer/siRNA ratio was the same used in all transfection experiments (1:1) and the amount of transfected siRNA/Copolymer was 880 nM in order to facilitate the visualization of copolymers for imaging. Cells were fixed at different time point after transfection, 5 min and 1h, in order to observe the copolymer-siRNA uptake overtime. According to the fixation protocol, cells were fixed in 4% paraformaldehyde for 20 minutes at RT and then washed twice with PBS. Afterwards, cells were incubated with glycine 0.1M and washed twice with PBS. Before primary antibody incubation, cells on slides were saturated in 1% BSA/PBS and then incubated overnight in a humid chamber in dark with a specific primary antibody targeting the ASGPR at 1:100 dilution (Mouse anti-ASGPR antibody, Santa Cruz Biotechnology). After incubation, cells were washed twice with PBS and then incubated with secondary antibody (anti-mouse Alexa Fluor 488, 1:500 dilution) for 50 min at RT in a humid

chamber in dark. In the end, cells were stained with DAPI for 5 minutes at RT and mounted using Moviol Mounted solution. Images were acquired using Carl Zeiss Laser Scanning Confocal Microscopy LSM800 Zeiss Airyscan equipped with a 63×, NA=1.3 objective. Images were processed using Fiji (ImageJ) software and the Co-localization coefficient (Manders' Coefficient M1) was obtained by Coloc2 (Fiji's plugin for co-localization analysis) setting a threshold manually. Experiments were performed in duplicates and at least 6 cells for fields were analyzed in each experiment. The regions-of-interest (ROI) were designed in order to select only the transfected cells.

4.5 HuH7-EGFP stable cell line generation

To demonstrate that the copolymer is able to deliver siRNAs inside cells, a functional siRNA against a specific mRNA was used. Specifically, for *in vitro* uptake studies a stable HuH7 cell line expressing the EGFP protein was generated, in order to transfect cells with PDPG delivering a siRNA against the EGFP mRNA. If the polymer releases the siRNA inside the cell, a decrease in the fluorescence intensity of the cells expressing the EGFP protein would be observed.

A lentiviral vector was used as delivery strategy to produce the stable cell line. This type of vector is commonly used due the ability to effectively integrate the gene of interest into the host cell genome. The lentivirus containing the EGFP gene has been produced in the 293T cell line using a 3rd generation system for lentiviral production. In this system, components necessary for virus production are split across the following four plasmids:

-Lentiviral transfer plasmid encoding the EGFP gene (pLenti PGK GFP Puro (w509-5) was a gift from Eric Campeau & Paul Kaufman (Addgene plasmid #19070; http://n2t.net/addgene:19070; RRID:Addgene_19070))[399]. The EGFP gene sequence is flanked by long terminal repeat (LTR) sequences which facilitate integration of the transfer plasmid sequence into the host genome. This vector derives from the HIV-1 virus and, for safety reasons, it is replication incompetent due to deletions in 5'LTR and 3'LTR. In addition, it contains the gene conferring the Puromycin resistance, the selection marker for selection of infected cells;

-Two packaging plasmids: pMDLg/pRRE containing Gag and Pol lentivirus genes (pMDLg/pRRE was a gift from Didier Trono (Addgene plasmid #12251))[400] and pRSV-Rev containing Rev lentivirus gene (pRSV-Rev was a gift from Didier Trono (Addgene plasmid #12253))[400];

-VSV-G envelope expressing plasmid pMD2.G (pMD2.G was a gift from Didier Trono (Addgene plasmid #12259)).

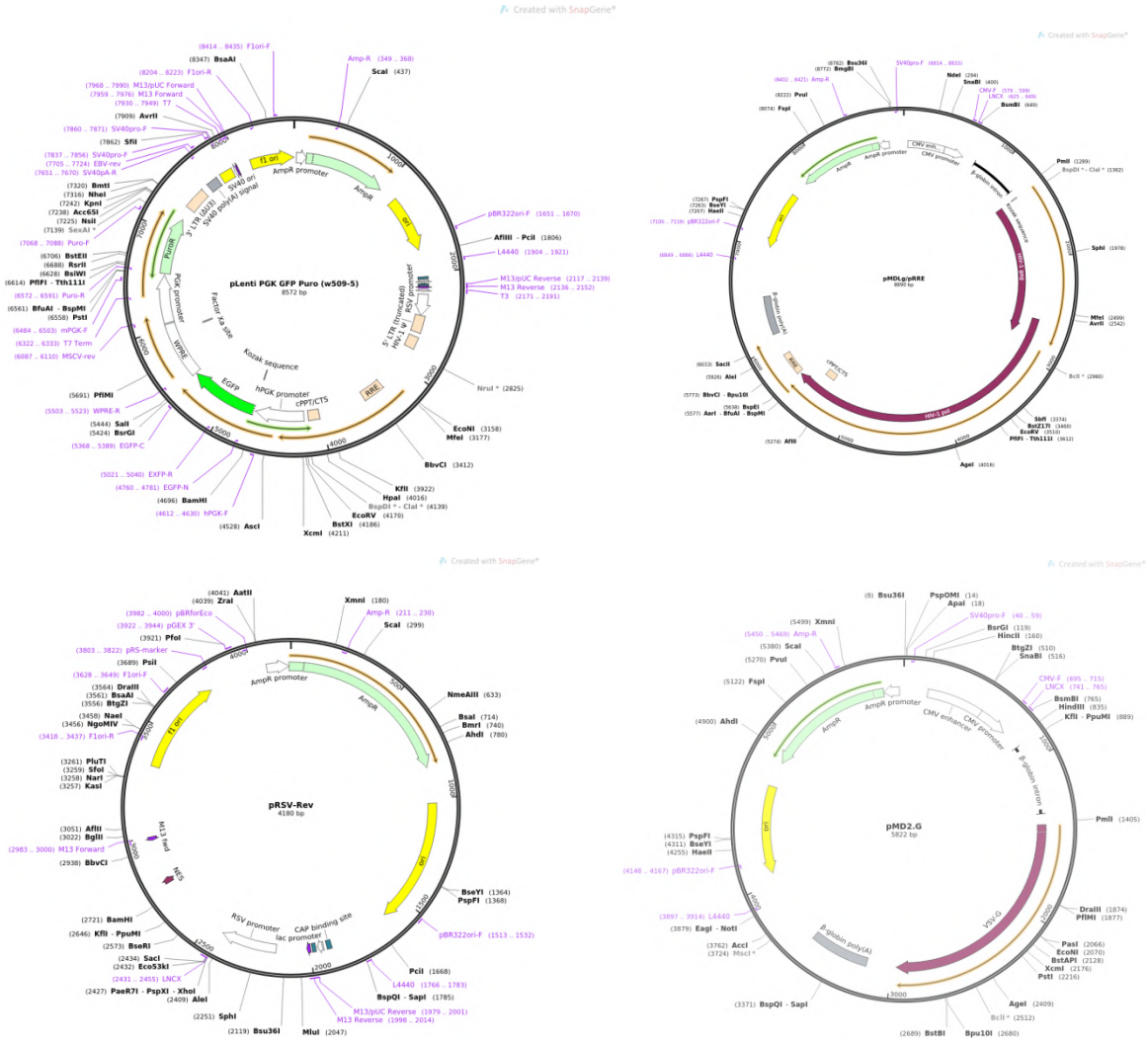

Figure 4.4. Full sequence maps of plasmids used for lentiviral particles production: pLenti PGK GFP Puro, pMDLg/pRRE, pRSV-Rev and pMD2.G plasmids (from Addgene.com).

First of all, plasmids were amplified in transformed bacterial cultures and then isolated and purified using the EndoFree Plasmid Mega Kit (Qiagen, Hilden). The plasmid DNA was eluted in endotoxin-free water (Qiagen) and the purity and the yield were determined by spectrophotometer (Epoch Microplate Spectrophotometer, Take 3^{TM} Micro-Volume Plate, BioTek, Bad Friendrichshall). Later, the identity of plasmids was verified by their digestion with specific restriction enzymes: NcoI for pLenti PGK GFP Puro, pMD2.G and pMDLg/pRRE; Xho+SfoI for pRSV-Rev (all restriction enzymes were bought from New England Biolabs (Ipswich, MA)), and digestion products were visualized by gel electrophoresis. For the transfection protocol, 293T were plated at density of 1.3×10^5 cells/cm^2 in 10 ml of medium per plate and after 12-16h the old medium was replaced with 8.0 ml of fresh DMEM complete medium (without antibiotic). For each

plate, a mix containing all plasmids in 1 ml of Optimem without serum and antibiotics was prepared as follow:

Plasmids	MIX
pMD2.G	2,4 µg
pMDLg/pRRE	4,0 µg
pRSV-Rev	1,8 µg
pLenti PGK GFP Puro	15,0 µg

The Plasmid solution was mixed with 1 ml of Optimem (without serum and antibiotics) containing 60 µl of Lipofectamine 2000, for each plate. The mix solution was incubated for 20 min at RT and added dropwise onto the medium in each dish gently swirling the plate. Then it was removed from plates 6h later and 10 mL of fresh complete DMEM medium was added in each plate. After 14-16h the medium was removed and 5 ml of complete DMEM medium was added for the lentivirus collection. Viral particles were harvested after 24h from 293T cells centrifuging the medium at 3000 rpm for 10 minutes at RT and then filtered with a 0.45 µm filter (Millipore, Bedford, MA) to remove cell debris.

For HuH7 infection, cells were seeded at density of $1{,}8\times10^4$ cells/cm^2 in 10 ml of medium per plate. The day after the medium was removed, cells were washed with PBS and 5 ml of supernatant containing viral particles were added to each plate of HuH7. After 5-6h 5 ml of fresh medium was added in each HuH7 plate. Two days after infection, the medium from plates was replaced with fresh medium and 5 µg/ml of Puromycin was added for the transduced cells selection (the antibiotic was added each time the medium was replaced). The antibiotic concentration for the selection was chosen based on the results obtained from an antibiotic dose-response curve performed on HuH7. HuH7 cells were seeded in a 12-well tissue culture plates at the density of $4{,}7\times10^3$ cells/cm^2 and after 24h, increasing amounts of Puromycin was added (Puromycin dihydrochloride from *Streptomyces alboniger*, Catalog Number P8833, Sigma-Aldrich®). The cell culture plate was examined every day and the following concentrations were tested: 2 µg/ml, 3 µg/ml, 5 µg/ml, 8 µg/ml and 10 µg/ml. Cells receiving 8 µg/ml and 10 µg/ml antibiotic concentrations died after 24h; cells receiving 5 µg/ml antibiotic concentration died after two days; instead some cells receiving 2 µg/ml and 3 µg/ml antibiotic concentrations were still alive after five days. In conclusion, 5 µg/ml was the chosen antibiotic concentration for the stable cell line

selection. In order to select cells with similar fluorescence intensity, HuH7-EGFP cells were sorted using the FACS Calibur cytofluorimeter (BD Biosciences).

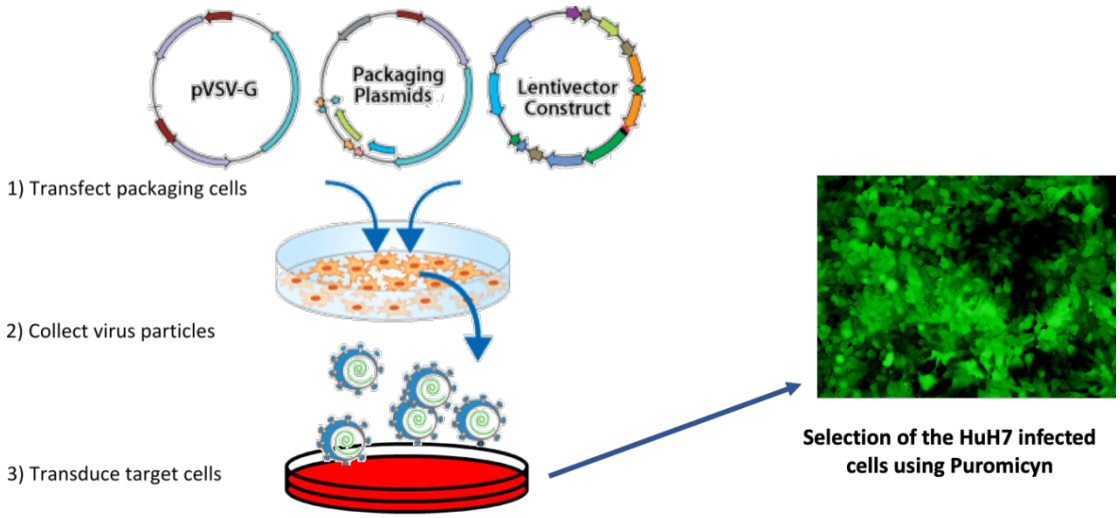

Figure 4.5. Scheme of the protocol to produce the HuH7-EGFP stable cell line using a 3rd generation system for lentiviral production.

4.6 Uptakes *in vitro* studies using HuH7-EGFP cells

In vitro uptake experiments using HuH7-EGFP cell line were performed in order to demonstrate the ability of the PDPG to deliver a siRNA targeting a specific mRNA inside the cells. For this purpose, a siRNA against the EGFP mRNA was delivered by the PDPG into HuH7-EGFP cells. Cells were seeded on slides placed in each well of 6-well plates at density of 8×10^3 cells/cm^2. The day after they were transfected with PDPG or PDP or Lipofectamine 2000 delivering siGL2 or siEGFP following the same protocol for siRNAs-polymers transfection as previously described. Lipofectamine 2000 was introduced as a positive control, because its transfection efficiency is already well documented. The PDP polymer was used in comparison to PDPG to demonstrate the specificity of the polymer, and siGL2 was used to prove the specificity of the siEGFP effect. Slides were fixed at different time points: 24h, 48h and 72h after transfection in order to follow the fluorescence intensity variation over time. Cells were fixed in 4% paraformaldehyde for 20 minutes at RT, washed twice with PBS and stained with DAPI for 5 minutes at RT. Then, slides were mounted using Moviol Mounted and images were acquired with Leica DM-2000 microscope.

To further demonstrate that the polymer is able to enter into cells through the ASGPR, the HuH7-EGFP were treated with EGTA, following the same protocol performed for HuH7.

4.7 Cell counting

Cell counting is a method to study the effect of specific treatments when the evaluated molecular targets are involved in the cell proliferation. Analysis of the cell morphology and viability are also important in order to prove the efficacy of the treatment. One of the most common method to determine the number of viable cells is the Trypan Blu exclusion assay. It is a simple method to identify and count alive cells directly in a given population. This method is based on the principle that death cells have compromised cell membrane, allowing dyes like Trypan blue to enter the cell, whereas it is excluded by alive cells[401]. Once the dye is inside the cells, it binds intracellular proteins and dead cells turn blue. Cell counting was performed diluting 1:1 a resuspension of cells (12 µl) in the Trypan blue 0.04% (Sigma-Aldrich). Then the mix was loaded in Thoma's counting chamber (Exacta-Optech) to observed and count the cells under the microscope (Nikon Eclipse TS100). To obtain a more precision counting, several independent cell counts were done. The number of cells present in 1 ml of cell resuspension was determined using the following formula

$$Xn = (nm*2*10^4)$$

where Xn represents the cell number in 1ml of medium; nm indicates the average of the different independent cell counts, 2 is the Trypan blue dilution factor and 10^4 is the conversion factor of Thoma's counting chamber.

4.8 MTT assay

MTT (3-(4,5-dimethylthiazolyl-2)-2,5-diphenyltetrazolium bromide) assay is a colorimetric test widely used to measure cell in the presence of external factors. It is an indicator of the cellular metabolic activity based on the reduction of a yellow water-soluble tetrazolium dye (MTT) into purple colored formazan crystals by mitochondrial NAD(P)H-dependent oxidoreductase enzymes[402]. This test is based on the principle that mitochondrial activity is constant for most of viable cells, thus cell viability is linearly related to mitochondrial activity.

To test siRNAs effects on decreasing cell proliferation, HuH7 cells were seeded at density of 5×10^3 cells/cm^2 in 24-wells plates. The day after cells were transfected either using the PDPG or the PDP, with weight ratio siRNA-transfectant 1:1 (w/w). More specifically, 1.27 µg of PDPG/PDP were mixed in 62.5 µl of serum-free medium Optimem (Invitrogen) for 15 minutes at RT. At the same time, 220 nM of siRNAs were incubated in 62.5 µl of Optimem medium for 15 minutes at RT. Then, the siRNA+Optimem solution was mixed with the PDPG/PDP+Optimem solution for 20 minutes at RT to allow copolymer-siRNAs complexes formation. After that, 275µl of Optimem medium were added to the mixture, to reach the final concentration of copolymers

and siRNAs of 220 nM. Cells seeded in 24 wells plates were washed with PBS and then incubated with the transfection mix for 4h at 37 °C. After the incubation the mix was removed, cells were washed with PBS and 1 ml of specific complete medium was added to the cells. MTT (MTT, 4 mg/ml in PBS, Sigma-Aldrich), at final concentration of 0.4 mg/ml, was added to cells at different time points after siRNA transfection (day 3, day 6 and day 10) in order to evaluate copolymers-siRNAs effects over time. Formed salt crystals were solubilized in DMSO and the absorbance was read at 570 nm using a spectrophotometer (Spectra Max Plus 384, Molecular Devices). To calculate the cell vitality percentage (%V) the following formula was used:

$$\%V = \left(\frac{OD\ treated\ cells}{OD\ untreated\ cells}\right) * 100$$

4.9 Lactate dehydrogenase (LDH) cytotoxicity assay

Lactate dehydrogenase (LDH) assay is a soluble cytosolic enzyme present in eukaryotic cells. When cells die, the cytoplasmic membrane is damaged and the LDH enzyme is released in the culture medium[403]. The number of lysed cells is proportional to the amount of released LDH and it can be detected using a colorimetric assay. The assay was performed in order to observe potentially necrotic effects induced by the copolymer. The LDH cytotoxic assay (Bio Vision Product, Mountain View) contains NAD^+, L-Lactate, INT and diaphrose, allowing to measure LDH activity through the reduction of NAD^+ in NADH by the LDH in the presence of L-lactate. The NADH reacts with the tetrazolium salt INT, which is reduced to a red soluble formazan salts, detectable by spectrophotometer at 490 nm.

For the experiment, cells were seeded and transfected as in MTT assay protocol and, at the end of the treatment, 100 µl of cellular supernatant were transferred to corresponding wells in an optical clear 96-well plate. Then, 100 µl of Reaction Solution, containing Catalyst Solution and Dye Solution at the ratio of 1:45, were added to each well and incubated for 30 minutes at RT in dark. Absorbance from samples was measured at 490 nm using a spectrophotometer (Spectra Max Plus 384, Molecular Devices). Free medium was considered as negative control, while as a positive control cells treated with triton X-100 (1% final concentration) were used. The percentage of the LDH levels detected in the medium was determined according to the formula:

$$Necrotic\ effect\ (\%) = \left(\frac{Test\ sample - (-CRT)}{+CRT - (-CRT)}\right) * 100$$

Where + CTR is the positive control and – CTR is the negative.

4.10 Protein extraction

In order to analyse the effect of siRNA transfection at proteins levels, HuH7 were transfected as reported in the section "siRNA *in vitro* transfection". Three days after transfection cells were trypsinized and collected by centrifugation at 1000 rpm for 5 minutes. Then the supernatant was removed, cells were resuspended in 1 ml of PBS and centrifuged at 3000 rpm for 5 min for washing. After that, cells were lysed using an extraction buffer containing Tris HCl pH 6.8 (45 mM) (Sigma-Aldrich), N-Lauroylsarcosine (0.2%) (Fluka), 0.2 mM of Phenylmethanesulfonyl fluoride (PMSF) (Sigma-Aldrich), 1mM of 1.4- Dithiothreitol (DTT) (Sigma-Aldrich), proteases inhibitors (2 µg/ml of Aprotinin and Pepstatin; Sigma-Aldrich) and phosphatases inhibitors (0.1 mM of Sodium Orthovanadate and Sodium Fluoride: Sigma-Aldrich). The amount of extraction buffer was determined based on the total cell number collected for each treatment. In particular, 20µl of extraction buffer were added every 10^5 cells and cells were incubated for 5 min at RT. Protein quantification was performed by Bicinchoninic (BCA) protein assay and protein pellets were stored at -80°C.

4.11 Bicinchoninic (BCA) protein assay for protein extracts quantification

To quantify the total concentration of proteins present in a sample, the BCA protein assay is the most used method. It is based on the principle that proteins can reduce Cu^{2+} to Cu^{1+} in the presence of an alkaline solution resulting in a color change from green to purple when the bicinchoninic solution is added. In the first reaction, proteins reduce Cu^{2+} to Cu^{1+} proportionally to the amount of proteins present in the sample. The reaction is influenced by the presence of amino acids in proteins like tyrosine, cysteine and tryptophan. In the second reaction, each Cu^{+} ions are chelated by two molecules of bicinchoninic acid causing the solution color change in purple-colored solution. The color change is proportionally correlate with protein concentration, which can be determinate by a spectrophotometer[404].

The assay was performed mixing 2 µl of the protein extract of each sample in the BCA and $CuSO_4$ solution in a ration 50:1 in a 96 wells plate. The bovine serum albumin (BSA) was used to design the standard curve to extrapolate the protein concentration for unknown samples. Each sample was loaded in duplicates and the plate was incubate at 37 °C for 30 minutes. The absorbance was measured at 562 nm using a spectrophotometer (Spectra Max Plus 384, Molecular Devices). Protein concentration for each sample was determined from a plot of concentration compared to the absorbance obtained from the BSA standard curve.

4.12 Western blotting

SDS-PAGE is a technique used to separate proteins according to their electrophoretic mobility, due to their length, conformation and molecular charge. SDS-PAGE contains the chemical denaturant Sodium Dodecyl Sulphate (SDS) which is responsible for proteins linearization breaking their natural structure. In this way, proteins mobility depends only on their length and mass-to-charge ratio. After electrophoretic separation, a specific protein of interest can be identified by Western Blot analysis in which proteins are transferred to a membrane and the incubation with specific labelled antibody allows to individuate the protein of interest[405].

SDS-PAGE were prepared according to Laemmli's procedure[406]. 30-40 µg of protein extracts were mixed with NuPAGE™ LDS Sample Buffer (4X) (ThermoFisher Scientific, Invitrogen™) containing 5% of β-mercaptoethanol, and denatured for 10 min at 70 °C. Proteins were loaded in a 8% (for PARP), or 15% (for LC3B) or 12% (for the other targets) acrylamide gel (29:1, acrylamide:bis-acrylamide) running gels after a brief running in the stacking gel (4% acrylamide gel) to compact proteins in the sample. The electrophoretic running was performed using a specific Running Buffer (0.125 M Tris-HCl pH 8.3, 0.96 M of glycine and 0.5% of SDS). An electric field of about 80 V was applied in the first instance to run the proteins in the stacking gel and then increased up to 125 V when proteins have reached the running gel. After that, proteins were transferred onto a 0.22 µm nitrocellulose membrane (Schleicher & Schuell) using a transblot semi-dry apparatus system (Pharmacia Biotech). Before sandwich assembly, membrane and filter papers used to build the sandwich were hydrated in Transfer Buffer (60 mM Tris-HCl, 40 mM glycine containing 0.05% SDS and 10% methanol). Proteins transfer was performed using an electric field of 1 mA/cm^2 for about 1h and then, membranes were stained by Ponceau S. (Sigma-Aldrich) to evaluate the efficiency of proteins transfer. Then, membranes were blocked with appropriate percentage of non-fat dried milk for 30 minutes and incubated with the specific primary antibody. The specificity of the eEF1A1 and eEF1A2 antibodies to detect selectively the respective proteins was already proved by Bosutti *et al.* (2019)[407].

A secondary antibody conjugated with the horseradish peroxidase (Bethyl Laboratories Inc) was used to detect specific primary antibodies, after washing membranes twice with PBS and 0.05% Tween 20. After secondary antibody incubation, membranes were washed twice with PBS and 0.05% Tween 20, then developed after the addition of the enhanced chemiluminescence detection system solution (SuperSignal West Pico Chemiluminescent Substrate; Thermo Scientific-Pierce) and exposed to Kodak film (Sigma-Aldrich). Band intensities were quantified by densitomer (Model GS-700 Imaging Densitometer, Biorad) and molecular Analyst software (Biorad). For

internal loading control, GAPDH protein was probed on the same membrane. The IgG and hybridization conditions used are reported in the Table 4.2.

Table 4.2. IgG and hybridization conditions.

Primary antibody	Dilution	Non-fat milk	Incubation time	Secondary antibody (1:4000)	Incubation time
eEF1A1 (AbCam)	1:1000	3% + 0.05% Tween 20	O/N at 4°C	Anti-Rabbit HRP (Bethyl Laboratories. Inc)	1h, RT
eEF1A2 (Santa Cruz)	1:500	3% + 0.05% Tween 20	O/N at 4°C	Anti-Rabbit HRP (Bethyl Laboratories. Inc)	1h, RT
E2F1(Santa Cruz)	1:200	5% + 0.05% Tween 20	O/N at 4°C	Anti-Mouse HRP (Bethyl Laboratories. Inc)	1h, RT
LC3B (Genetex)	1:1000	5% + 0.05% Tween 20	O/N at 4°C	Anti-Rabbit HRP (Bethyl Laboratories. Inc)	1h, RT
PARP (BD Pharmigen)	1:1000	5% + 0.05% Tween 20	O/N at 4°C	Anti-Mouse HRP (Bethyl Laboratories. Inc)	1h, RT
GAPDH (Santa Cruz)	1:1000	5% + 0.05% Tween 20	O/N at 4°C	Anti-Rabbit HRP (Bethyl Laboratories. Inc)	1h, RT

4.13 Total RNA extraction

Total RNA was purified from cells using the RNeasy Mini Kit (Qiagen). Cells were collected three days after transfection protocol and lysed using RLT Lysis Buffer integrated with β-mercaptoethanol. The lysis buffer contains also guanidinium thiocyanate, which inactivates RNase enzymes preventing RNA degradation. After that, 70% ethanol was added to precipitate RNA and to promote the interaction between RNA and the silica membrane of columns. The mix was loaded into spin columns and centrifuged for 25 second at 13.000 rpm. Then, the Buffer W1 was added to the columns to remove proteins and columns were washed twice using Buffer RPE. In the end, RNA was eluted from the spin column with 40 µl of RNase Free Water centrifuging for 60 seconds at 11.000 rpm. Quantification of total RNA was performed by spectrophotometric analysis (NanoDrop ND-100; CelBio).

4.14 qRT-PCR

The quantitative polymerase chain reaction (qPCR), is a technique used in molecular biology to quantify the amplification of a target gene in real time, and not like in the traditional PCR were detection and quantification of the amplified sequences are performed at the end of the reaction. For this reason, the PCR is also called real-time polymerase chain reaction (Real-Time

PCR). In this technique the detection of products can be done either using a non-specific double strand DNA intercalator fluorescence dye (Syber Green), or using a specific DNA probe which hybridized with its complementary sequence[408].

The qRT-PCR consists of two steps: reverse transcription from RNA to cDNA and the Real-Time polymerase chain reaction.

Reverse transcription protocol was performed incubating at 70 °C for 5 min 1µg of RNA of each sample with 1 µl of random hexamers in RNAse free water to reach the final volume of 10 µl. The incubation step at 70 °C unwinds the RNA secondary structures allowing random hexamers to anneal to the RNA molecules. Then 10 µl of the master mix for reverse transcription was added in each sample. Master mix composition is reported below:

Reagents	Final concentration
25mM MgCl2 Solution	5 mM
10X PCR Buffer II	1X
dGTP	1 mM
dATP	1 mM
dCTP	1 mM
dTTP	1 mM
RNase Inhibitor	1U/µl
MuLV Reverse Transcriptase	2.5 U/µl
Random Hexamers	2.5 µM

During reverse transcription, samples were incubated for 10 min at 25°C to allow the extension of random hexamer primers by reverse transcriptase. Reverse transcription will occur at 42 °C of incubation for 60 min.

Real-Time polymerase chain reaction was performed using the SYBRGreen Master Mix (Applied Biosystems) with the Step One Plus Applied Biosystems instrument. Primers sequences (MWG Eurofins) and their specific Tm are listed in Table 4.3.

Table 4.3. List of primer sequences and their Tm, qPR product length and amplification region.

Gene	Primers	Tm	Length (bp)	Amplification Region
eEF1A1	Fw 5'-AAC ATT GTC GTC ATT GGA CA-3' Rev 5'-ACT TGC TGG TCT CAA ATT TC-3'	62 °C	229	88-316
E2F1	Fw 5'-CCA GGA AAA GGT GTG AAA TC-3' Rev 5' AAG CGC TTG GTG GTG AGA TT-3'	62 °C	74	466-539
28S	Fw 5'- TGG GAA TGC AGC CCA AAG-3' Rev 5'- CCT TAC GGT ACT TGT TGA CTA TGC-3'	62 °C	84	282-365

All samples were amplified in triplicates in a final volume of 10 µl of SYBRGreen Master Mix Buffer, including 200 nM of each primer and 0.6 µl of specific cDNA. 28S rRNA was used as internal control for all samples. Real-time PCR reaction consisted of a pre-denaturation step at 95°C for 10 min and the 40 cycles of amplification (denaturation at 95°C for 15 seconds, annealing at proper temperature for 60 seconds and extension at 72°C for 30 seconds). The reaction ends with a dissociation stage (95°C/60°C/95°C 15 seconds each) to assess the homogeneity of PCR products and check the presence of primer–dimers, determining the specificity of the reaction.
For mRNAs quantitative analysis, relative amounts of the target mRNA were normalized by 28S rRNA content and compared to the respective control treatment using the ΔCt quantitative analysis method, using the following formula:

$$\Delta Ct = \text{mean of Ct gene target} - \text{mean of Ct housekeeping gene}$$

$$\Delta\Delta Ct = \Delta Ct \text{ of the treatment} - \Delta Ct \text{ of the control}$$

$$\text{Fold change} = 2^{-\Delta\Delta Ct}$$

4.15 Droplet PCR

mRNA levels of eEF1A2 were detected using the droplet PCR (ddPCR) because of the difficulties in cDNA amplification with the conventional qRT-PCR. This problem could be probably due to the very low copies of eEF1A2 mRNA present in HuH7, hardly detectable with qRT-PCR.

Droplet Digital PCR (ddPCR) is a method to perform PCR in water-oil emulsion droplet, where samples are fractionated into many droplets, and PCR amplification of the template molecules occurs in each individual droplet[409].

In the first step, the reverse transcription was performed using the iScriptTM gDNA Clear cDNA Synthesis Kit (Bio-Rad). mRNA samples were first incubated with the iScript DNase and iScript DNase Buffer to digest the DNA and then, with the iScript Reverse Transcription Supermix for the reverse transcription reaction. During reverse transcription, samples were incubated at 25°C for 5 min, then 46°C for 20 min and in the end 95°C for 1 min.

Afterward, the cDNA amplification was performed adding the mix solution composed by:

Reagents	Mix per each sample
2x ddPCR™ Supermix for Probes (no dUTP) (*Bio-Rad*)	10 µl
Mix primer&probe A2 FAM (200nM) (*Bio-Rad*)	1 µl
Mix primer&probe GAPDH HEX (200nM) (*Bio-Rad*)	1 µl
H_2O DNase free (QIAGEN)	4 µl
DNA	4 µl
Final Volume	20 µl

The Supermix for Probes contains the buffer, dNTPs and Taq polymerase, necessary for the reaction.

The reaction, performed using the QX200 Droplet Digital PCR System-Bio-Rad machine, consisted on a pre-denaturation step at 95°C for 10 min for enzyme activation and 39 cycles of amplification (denaturation at 94°C for 30 seconds and annealing at 57°C for 60 seconds). The reaction ends with a step at 98°C for 10 min for enzyme inactivation.

After the amplification step, the plate containing the samples was arranged in the QX200™ Droplet Reader machine to read the fluorescence of the primer fluorophores in order to identify the droplets containing the DNA target. Data were analysed using the QuantaSoft™ *(Bio-Rad)* software.

4.16 Dorsal window chamber assay

The dorsal skinfold window chamber is a sophisticated experimental model, which has been proven to be extremely valuable for a systematic *in vivo* analysis of the dynamic interaction of biomaterials with the surrounding host tissue in different animal models[410]. This method allows to visualize tumours in animals (like mouse), and to analyze various aspects of cancer physiology, cell migration, metastasis and vascularization. The development of the window chamber model for the investigation of cancer *in vivo* has proven an invaluable resource in the elucidation of real-time tumour inception, growth, adaptation and treatment response[411]. For this project, it represents an attractive technique for monitoring the internalization of the complex PDPG-siRNA *in vivo* and visualizing tumour cells in mice.

In the experiment, mice were anaesthetized through an intraperitoneal injection with an anesthetic solution (ketamine, 125 mg/kg; xylazine 12.5 mg/kg; acepromazine 2.5 mg/kg) with volumes adjusted to the weight of the animal. Then mice backs were shaven and depilated using a

depilatory cream and the dorsal skin fold was stretched in order to position the window chamber. For window chamber implantation, the skin fold was sandwiched between the two complementary chamber frames and fixed together by nuts, screws and sutures. Afterwards, skin and fat tissue were removed from one side of the skin fold in the window in order to expose the other layer of the skin for visual observation (Figure 4.6). Tumours were induced by injecting with a 29-G needle a solution of 5 µl of 1×10^6 HuH7-EGFP resuspended in physiological solution mixed with 5 µl of Matrigel (Corning® Matrigel® Basement Membrane Matrix Phenol Red Free) into the exposed skin layer in the window chamber. In the end, a sterile physiological solution was added and a coverslip (Glaswarenfabrik Karl Hecht, Sondheim, Germany) was placed on the exposed skin layer and fixed with a snap ring. During the surgery mice were kept on a 40°C heating pad to prevent hypothermia and all operation was done in sterile conditions using sterilized instruments. In the following days after surgery, 50 µl of analgesia (ketoprofen, 3.5 mg/kg) were injected in mice subcutaneously.

Six days after the surgery, mice were randomly divided and were treated with PDPG+siEGFP (ratio 1:1) or with PDP+siEGFP (as controls (ratio 1:1)) or without any treatment. For treatments, 1.2 µM of siEGFP was incubated with 1.2 µM of PDPG or PDP for 20 min at room temperature in a final volume of 10 µl. Then, the mix solution was injected intratumourally in each mouse. Bright-field and fluorescent images of window chambers were taken at room temperature on day 0, day 1, day 4 and day 7 using a Carl Zeiss SteREOLumar V12 (Carl Zeiss, Jena, Ger- many) fluorescence stereomicroscope equipped with a Neo- Lumar S 0.8x objective (Carl Zeiss) and a AxioCam MRc5 digital camera (Carl Zeiss). During image acquisition, animals were sedated with isoflurane inhalation anesthesia and placed on a plexiglas custom-designed holder, so that the mice rest in a lateral position during the imaging.

Images from fluorescence stereomicroscope were analysed using FiJi software in which the fluorescence of tumour cells was evaluated defining a threshold that includes the region with fluorescence and then a ROI (Region Of Interest) was drawn around the tumour mass of each mouse.

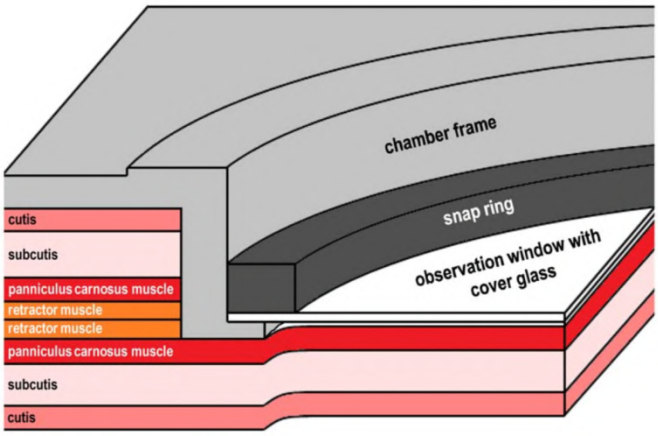

Figure 4.6. A Schematic representation of the different tissue layers of the mice skin in the dorsal skinfold window chamber experiment[410].

4.17 *In vivo* experiments in a xenograft mouse model of HCC

To prove the effect of siRNAs+PDPG treatments *in vivo*, three different experiments were performed using a xenograft mouse model of HCC. In all experiments, tumours were induced in the right flanks of 12.3 weeks old female Severe Combined Immunodeficiency (SCID) mice (Envigo, Udine, Italy, U34401-16/2017/9) by a subcutaneous injection of 10×10^6 of HuH7 cells, resuspended in 0.1 mL of saline solution. The size of the tumour masses was measured in the three perpendicular tumour diameters every second day using the digital Vernier caliper. Tumour volume was calculated using the formula for ellipsoid $V=a\times b\times c\times\pi/6$, where a, b and c represent three tumour directions. When tumours reached the volume size around 30-40 mm^3, mice were randomly divided into different treatment groups and subjected to specific experimental protocols.

In the first experiment, named *long-term experiment,* mice were divided in different groups and treated as follow:

6 animals → sieEF1A1 + PDPG

6 animals → sieEF1A2 + PDPG

6 animals → sieE2F1 + PDPG

6 animals → siGL2 + PDPG

4 animals → PDPG

2 animals → NaCl

For treatments, 50 µl of solution containing 13 µM of specific siRNAs or siGL2, incubated together with 13 µM of PDPG for 20 min at room temperature, was intratumourally injected in each mouse. For NaCl treated mice, 50 µl of physiological solution was injected. Tumour volume

was measured every second day to draw a tumour growth curve and mice were humanely sacrificed by CO_2 when tumour volume reached approximately 300 mm^3.

In the second *in vivo* experiment, named *short-term experiment*, mice were randomly divided in different experimental groups and treated as follow:

5 animals→ sieEF1A1+ PDPG

5 animals→ sieEF1A2 + PDPG

5 animals→ siE2F1 + PDPG

4 animals→ siGL2 + PDPG

Treatments were the same used for the *long-term experiment*. Tumour volume was measured every second day to draw a tumour growth curve. In this experiment mice were humanely sacrificed by CO_2 three days after treatment injection and tumours and blood were collected. The time point of the scarification was chosen according to previous *in vitro* and *in vivo* experiments, where the best activity was observed three days after transfection of siRNAs. In addition, from the first subcutaneous *in vivo* experiment it was observed that the difference between treatments and control was already evident in the first days after injections.

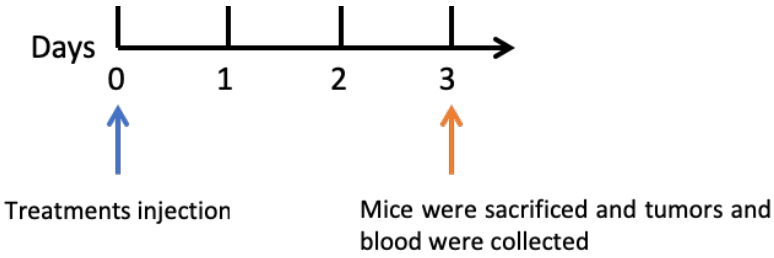

Figure 4.7. Scheme of the short-term *in vivo* experiment.

A pivotal *in vivo* experiment in which treatments were injected systemically was also performed. Tumours were induced in 12.3 weeks old female SCID mice by a subcutaneous injection of 10×10^6 of HuH7 cells, resuspended in 0.1 mL of saline solution into the right flanks of the mice. For treatments, 100 µl of mixed solution containing 8.63 µM of specific siRNAs or siGL2, incubated with 8.63 µM of PDPG for 20 min at room temperature, was injected retro-orbitally in each mouse, every two days for three times. Then, mice were humanely sacrificed by CO_2 when tumour volume reached approximately 300 mm^3.

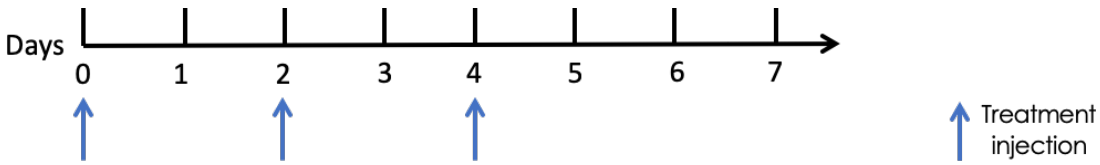

Figure 4.8. Scheme of the *in vivo* experiment where treatments were injected retro-orbitally.

Data about the tumour doubling and tripling times, indicating the time in which the tumour volume double or triplicate in term of its volume-size, and growth delay, indicating the difference in doubling/tripling time between tumours control group and tumours treated groups, were calculated. In addition, mice were weighed every second day because weight changes would have indicated a systemic toxicity caused by treatments.

4.18 Blood chemistry

In order to prove the safety of the tested delivery systems, changes in selected serum level markers were evaluated in mice from the *short-term experiment*. The peripheral blood was collected in EDTA-treated tubes (BD Microtainer® MAP) from orbital sinus of mice and stored at room temperature for approximately 30 minutes. Serum was isolated by centrifuging blood samples at 3,000 rpm for 5 min and stored at -20 °C until analysis. Samples analysis was performed at the Veterinary faculty Ljubljana using ADVIA 120 Hematology System (Siemens Healthineers, Erlangen, Germany) and values were compared to reference normal values. Levels of C reactive protein (PCR) were also analysed in order to check a possible inflammation response following treatments injection using the ELISA kit (Abcam® ab157712-C Reactive Protein (PTX-1) Mouse ELISA kit). Obtained values were compared with established normal values for mice.

4.19 Proteins and RNAs extraction from tumour masses

Tumour masses from mice were excided the day of the sacrifice and immediately frozen in liquid nitrogen for RNA and proteins preservation. All operation was conducted in RNase free conditions using sterilized instruments. Proteins and RNA were isolated from tumours collected in the *short-term-experiment in vivo* experiment using the AllPrep DNA/RNA/Protein Mini Kit (QIAGEN®). In particular, tumour samples were put in a Lysis Buffer, disrupted using a pestle and homogenized using a syringe. Samples were then centrifugated for 3 min at 13,000 rpm and the supernatant collected and transferred in an AllPrepDNA spin column in order to eliminate the DNA. Afterwards, the flow-through was used to purify the RNA adding ethanol. The solution was transferred into a RNeasy spin column and centrifuged at 10,000 rpm for 15 seconds. The flow-

through was saved for protein extraction, while the RNeasy spin column was washed several times with buffer solution and the RNA was eluted in 50 µl of RNeasy free water after centrifugation at 10,000 rpm for 1 min. Proteins were precipitated adding the Buffer APP solution for 10 min at RT and by centrifugation (13,000 rpm for 10 min). The pellet was washed with 70% ethanol by centrifugation at 13,000 rpm for 1 min and then left to dry for 15 min at RT. In the end, SDS 5% was added for protein pellet resuspension.

4.20 Statistical analysis

All data are expressed as ±SEM and they were tested for normality of distribution with the Kolmogorov–Smirnov test. P values were calculated by the GraphPad InStat tools (Graph- Pad Software, Inc., La Jolla, CA, USA) using unpaired t-test with or without Welch correction and the Mann-Whitney Test, Wilcoxon matched-pairs signed-ranks test, as appropriate. P values < 0.05 were considered statistically significant.

5 Results

5.1 Previous results

To provide siRNAs protection in the biological environment and to allow the by-passing of biological barriers, many different strategies have been explored. Among these, polymer-based strategies have been investigated[247,412,244,413,414].

Recently, we have developed different polymer based delivery systems such as PHEA-DEAEMA (α,β-poly(N-2-hydroxyethyl)-D,L-aspartamide-diethylamino ethyl methacrylate)[415] and Inu-DETA (inulin diethylene triamine)[416] that can guarantee effective siRNA protection in the biological environment. However, the solely protection against degradation cannot be considered sufficient for the effective delivery. Indeed, delivery systems should also provide specific cell targeting of the delivered siRNA. This is important to circumscribe the siRNA effects to the diseased cells thus minimizing possible systemic side effects and, in the case of liver, toxicity to the healthy hepatocytes.

To realize the targeted delivery of drugs to hepatocytes, galactosylated polymeric or lipid carriers were developed[417]. Targeting via galactosylated carriers such as polymers or nanoparticles exploits highly specific interactions of galactose (GAL) ligands with Asialoglycoprotein receptor (ASGPR). This receptor, specifically and abundantly present on hepatocytes, is over-expressed in well-differentiated forms of HCC and thus it allows enhancing the uptake of drug-loaded systems into HCC cells[418,419,398]. Because of its restricted expression, ASGPR is considered a valuable surface biomarker to target HCC cells[420].

In our previous investigation[317], we focused our attention on the development of a novel polymeric derivative of α,β-poly-(*N*-2-hydroxyethyl)-D,L-aspartamide (PHEA) for the active hepatocyte targeting. This compound was obtained by subsequent derivatization of PHEA with diethylene triamine (DETA), and with a galactosylated PEG derivative containing galactose (GAL) molecules at the end of the chain, to obtain PHEA-DETA-PEG-GAL (PDPG) (Figure 5.1).

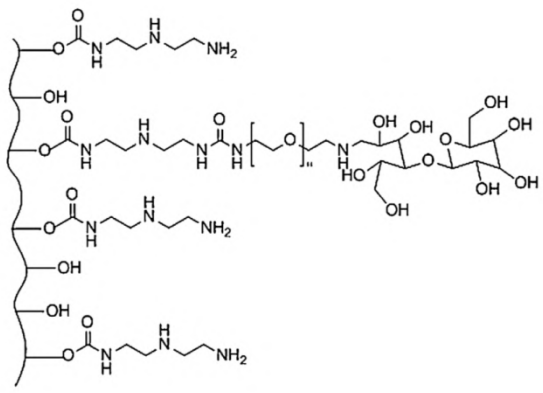

Figure 5.1. Chemical structure of PHEA-DETA-PEG-GAL (PDPG).

PDPG showed its ability to form complexes with siRNAs and to be haemo-compatible. Moreover, it was able to specifically deliver siRNA-PDPG to the HCC cell line JHH6 *in vitro*[317].

To continue our previous promising study, in this work we have tested the PDPG ability to deliver siRNA in an *in vivo* model of HCC. To this purpose, we had to change the cellular model of HCC from JHH6 to HuH7. Indeed, HuH7 but not JHH6 are suitable to generate a xenograft subcutaneous model of HCC. Notably, we have observed that HuH7 expresses ASGPR at high level[317]. Moreover, in this study we have deepened the mechanism of PDPG entrance into the target HuH7 cells. For the functional study we have used three different siRNAs directed against the mRNAs of eEF1A1, eEF1A2 and of E2F1, all implicated in HCC[300,395,299].

5.2 *In vitro* uptake studies

5.2.1 Ability of siGL2+PDPG to enter HuH7

To demonstrate the PDPG ability to specifically entering into HuH7 cell line, PDPG marked by the red fluorophore BodipyTRX was used. The copolymer PDP lacking the galactose residue and marked with BodipyTRX, was used as control of the targeting specificity. In both cases, a model siRNA directed against the luciferase mRNA (siGL2), was complexed with PDPG and PDP to generate the complexes siGL2+PDPG-BodipyTRX and siGL2+PDP-BodipyTRX, respectively. According to previous findings regarding the ASGPR turnover in hepatic cells[304], 2h and 24h after transfection were chosen as time points to observe the polymeric complexes entry into HuH7 cell line. Two hours post transfection, fluorescent confocal microscopy documented siGL2+PDPG-BodipyTRX entry into HuH7, predominantly occupying the cytoplasm of the cell (Figure 5.2). On the contrary, cells transfected by siGL2+PDP-BodipyTRX resulted in very limited ability to enter HuH7. These results highlight the importance of GAL residues for the copolymer uptake. Confocal analysis performed 24h after transfection, confirmed the siGL2+PDPG-BodipyTRX entry into the cells. However, in this case the fluorescence was less evident compared to the time point of 2h, most likely due to the processing of the copolymers within the cells (data not shown). Based on these results, all *in vitro* uptake experiments were analysed 2h after siGL2-PDPG-Bodipy-TRX transfection.

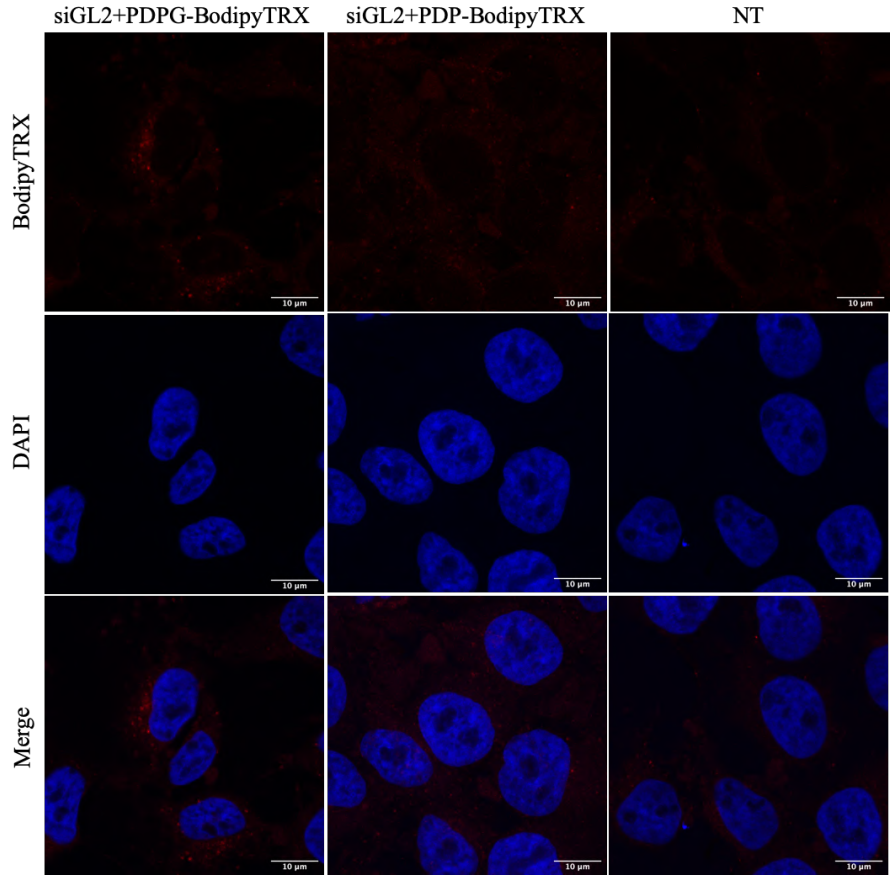

Figure 5.2. Confocal images of HuH7 transfected by siGL2+PDPG-BodipyTRX (left panel) or siGL2+PDP-BodipyTRX (middle panel). Images were taken 2h after transfection showing that the copolymer is inside the cells in siGL2+PDPG-BodipyTRX transfected cells. On the contrary, the copolymer is barely visible in images from HuH7 transfected by PDP, proving the importance of GAL residues for siRNA+copolymer uptake. Non-treated cells are shown in the right panel. Images were acquired using Carl Zeiss Laser Scanning Confocal Microscopy LSM800 Zeiss Airyscan equipped with a 63x, NA=1.3 objective. Scale bar: 10 µm. Nuclei have been labelled by DAPI (blue).

To evaluate the transfection efficiency of the PDPG, HuH7 cells were transfected with siGL2+PDPG-BodipyTRX or with siGL2+PDP-BodipyTRX and images were acquired 2h after transfection by confocal microscopy. The number of transfected cells were counted manually and compared to the total number of cells taking in consideration different fields of different slides from several independent experiments. The transfected cell count revealed that about 35% of the cells were transfected by siGL2+PDPG-BodipyTRX, while less than 10% by siGL2+PDP-BodipyTRX (Figure 5.3).

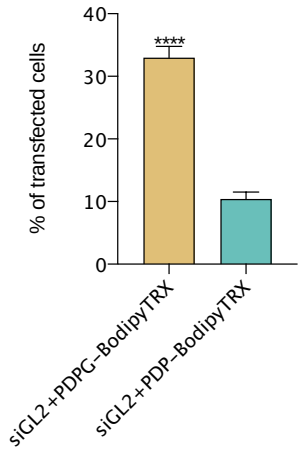

Figure 5.3. The graph shows the transfection efficiency of siGL2-PDPG-BodipyTRX compared to siGL2+PDP-BodipyTRX in HuH7 cells. Data are expressed as the % of transfected cells counted manually taking in consideration different fields of different slides from several independent experiments. Data are shown as mean ±SEM.****p<0.0001 compared to siGL2+PDP-BodipyTRX; n=2.

The above data confirm that PDPG can enter the cell. To prove that also the model siRNA siGL2 enters the cells when complexed with PDPG, HuH7 were transfected by unlabeled PDPG complexed with a FITC-labelled siGL2. For this test, we could not use fluorescent microscopy as PDPG shields the fluorescence emitted by FITC (unpublished results). Thus, we evaluated the presence of siGL2-FITC+PDPG 2h post transfection, directly in the cytoplasmic cell extract which was analyzed for FITC emission. Our results indicate the ability of PDPG to deliver siGL2 into the target cell HuH7 (Figure 5.4).

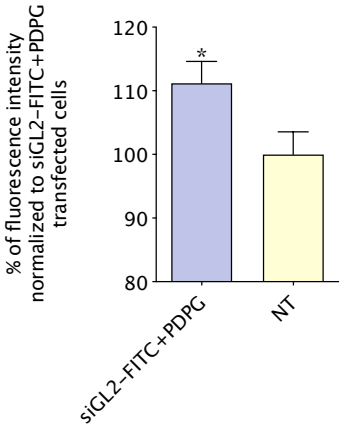

Figure 5.4. The graph shows that the fluorescence intensity of siGL2-FITC (220 nM) following siGL2-FITC+PDPG transfection in HuH7 cells. The fluorescence was measured using the TECAN infinite®200 microplate fluorimeter. Data are expressed as the % normalized to the fluorescence intensity of non-treated cells and shown as mean ±SEM.*p=0.0421, n=4.

5.2.2 The role of ASGPR in siGL2+PDPG uptake

The above data indicate the ability of siGL2+PDPG to enter the HuH7. To prove the involvement of ASGPR in the uptake process, the interaction between the ASGPR and the ligand (PDPG) was prevented by treating the HuH7 with EGTA (5 mM), 10 min before the transfection. EGTA is a chelating agent with high selective affinity for calcium ions, which are essential to allow the binding of glycopolymers to the ASGPR. The reduction of free calcium ions results in the impairment of the ability of ASGPR to bind its ligands[398]. Pre-treatment of HuH7 by EGTA, substantially impaired siGL2+PDPG-Bodipy-TRX entry into the HuH7, as evidenced by confocal analysis performed 2h after transfection (Figure 5.5). Notably, EGTA pretreatment did not modify siGL2+PDP-BodipyTRX entry into HuH7, suggesting the independence from the interaction with ASGPR. These data support the targeting ability of the copolymer PDPG in HuH7 and indicate that the entry of the siRNA+PDPG complex is a calcium-dependent mechanism. Moreover, these results suggest that the ASGPR is involved in the uptake of the siRNA-PDPG complex.

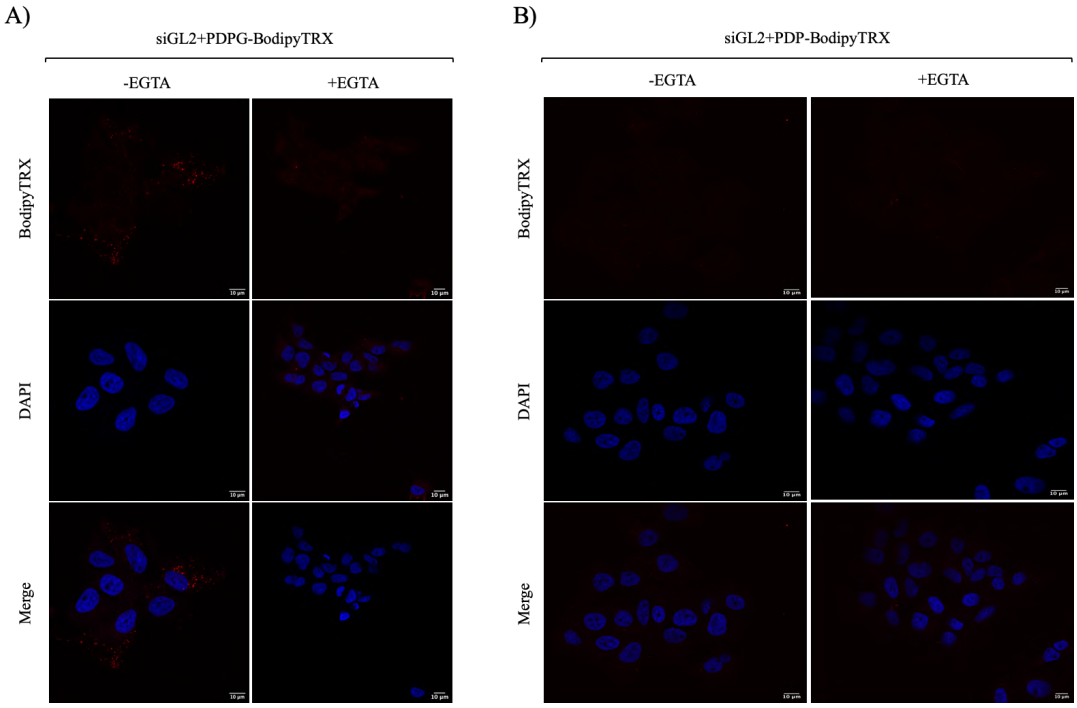

Figure 5.5. Confocal images of HuH7 transfected by siGL2+PDPG-BodipyTRX (**A**) or siGL2+PDP-BodipyTRX (**B**) with or without EGTA (5 mM) pre-treatment. Images were taken 2h after transfection showing that the PDPG can enter HuH7 when cells are not treated with EGTA. On the contrary, the copolymer is not visible following EGTA treatment. The same experiment was performed in HuH7 transfected by siGL2+PDP-BodipyTRX; confocal images show that the uptake of the copolymer lacking Gal is not affected by EGTA (right panel). Images were acquired using Carl Zeiss Laser Scanning Confocal Microscopy LSM800 Zeiss Airyscan equipped with a 63x, NA=1.3 objective. Scale bar= 10 µm.

The above data indicate the relevance of ASGPR in PDPG uptake. To further prove this aspect, we have performed co-localization experiments between siRNA+PDPG-Bodipy-TRX and ASGPR. Previous findings showed that the ASGPR is rapidly internalized after ligand binding with a first order rate constant of 3.4 x 10^{-8} M and a half-life of approximately 3 min. Moreover, the turnover of the ASGPR on hepatic cell membranes is around 20 min[304]. For these reasons, images from HuH7 were acquired by confocal microscopy at two different time points: 5 min and 1 h after the beginning of the transfection with siRNA+PDPG-BodipyTRX.

Images from the confocal microscopy and data analysis demonstrate that the co-localization of the PDPG and the receptor is evident in cells fixed 5 min and 1h after transfection. In particular, PDPG mostly co-localizes with ASGPR on the membrane surface of the cell 5 min after transfection. Instead, 1h after transfection, PDPG mainly co-localizes with ASGPR in the cytoplasm of the cell. These results support the possible interaction between PDPG and ASGPR. In addition, the images taken 1h after transfection showing PDPG/ASGPR in the cytoplasm of the cell, confirm the fast uptake rate of the ASGPR when ligands bind the receptor (Figure 5.6 A). Following confocal microscopy, images were processed for the calculation of Manders' coefficient, which indicates the degree of the overlap of the signals between two images thus representing the degree of colocalization (Figure 5.6 B). Manders' coefficient, calculated inside a ROI which delimited each single cell, revealed that around 30% of the ASGPR co-localises with PDPG-BodipyTRX (M1) 5 min after transfection and around 60% 1h after transfection (Figure 5.6 B). The increased co-localization at 1h compared to 5 minutes probably reflects the fact that 5 minutes are not enough to complete PDPG binding to ASGPR. These results further support the existence of the PDPG-ASGPR interaction. Notably, no relevant co-localization was detected in HuH7 cells transfected by siGL2+PDP-BodipyTRX (Figure 5.6).

A)

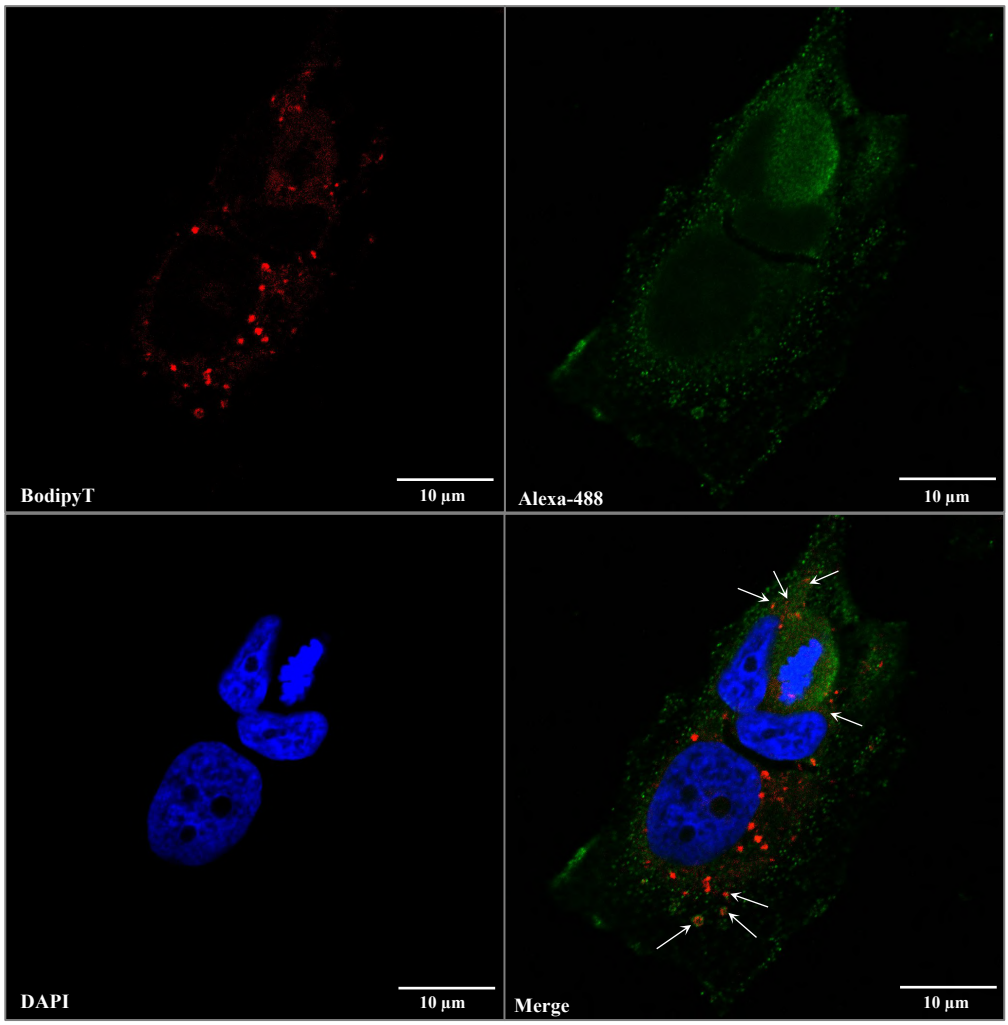

B)

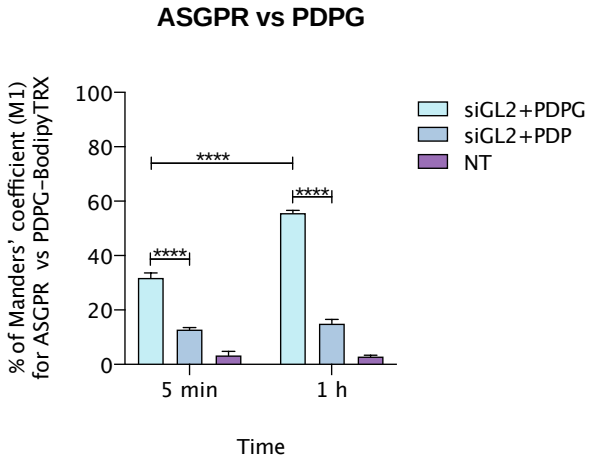

Figure 5.6. A) A confocal image showing the colocalization of PDPG-BodipyTRX (in red) and ASGPR (in green) 1h after the beginning of the transfection of siGL2+PDPG-BodipyTRX on HuH7 cells. Images were acquired using Carl Zeiss Laser Scanning Confocal Microscopy LSM800 Zeiss Airyscan equipped with a 63x, NA=1.3 objective. Scale bar= 10 µm. **B)** Manders' coefficient (M1) for ASGPR vs PDPG-BodipyTRX or PDP-BodipyTRX co-localization analysis. Manders' coefficient was calculated using the Fiji plugin Coloc2. ****p<0.0001 compared to siGL2+PDP; n=12.

5.2.3 *In vitro uptake studies using HuH7-EGFP cell line and a siEGFP*

The above data suggest that siGL2+PDPG can enter the HuH7 cells via the uptake of ASGPR. However, no evidences that the transfected siRNA is functional within the cell are provided. Thus, to explore siRNA functionality, we have used a siRNA (siEGFP) directed against the enhanced green fluorescence protein (EGFP) and tested its effectiveness in HuH7 stably expressing EGFP. As shown in the Figure 5.7, there is an evident decrease in the fluorescence intensity of the HuH7-EGFP 48h after siEGFP+PDPG transfection compared to the control siGL2+PDPG-transfected cells. As expected, no significant differences in the fluorescence intensity were observed in HuH7-EGFP following the transfection of siEGFP+PDP or siGL2+PDP. Once again, this observation highlights the inefficiency of the polymer lacking Gal residues to deliver a functional siRNA inside HuH7 cells.

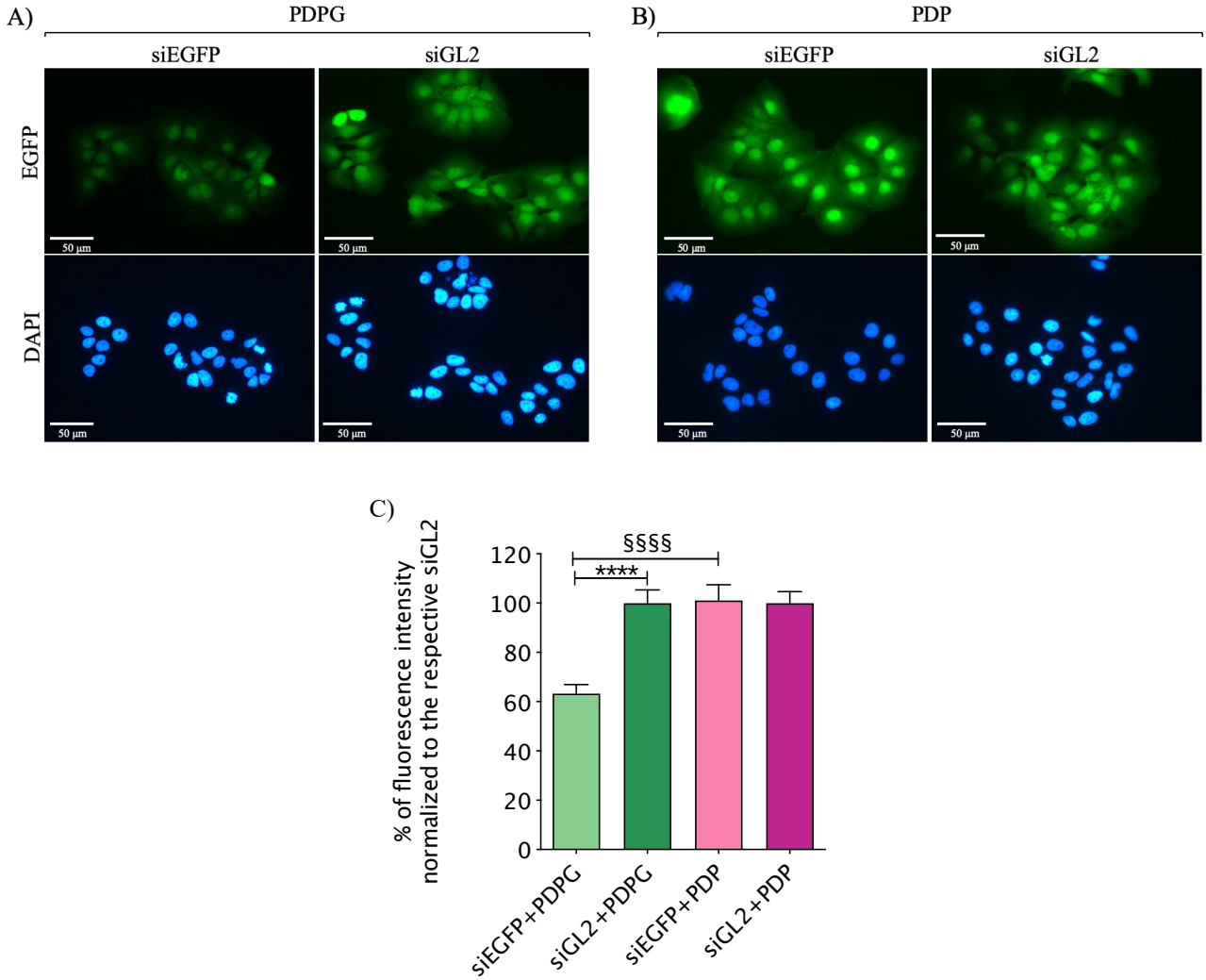

Figure 5.7. Fluorescence images of HuH7-EGFP transfected by siEGFP+PDPG (**A**) or siEGFP+PDP (**B**). **C)** A decrease on the fluorescence intensity is visible in HuH7-EGFP cells 48h following siEGFP+PDPG transfection compared to siEGFP+PDP transfected cells. Data are expressed as % of the average of the fluorescence intensity normalized to the respective siGL2 transfections and are shown as ±SEM. ****$p<0.0001$ compared to siGL2+PDPG transfected cells; $^{§§§§}p<0.0001$ compared to siEGFP+PDP transfected cells; n=3.

At longer time points following transfection (72h and more), we could not detect significant reduction in EGFP fluorescence probably because of siEGFP processing within the cells (data not shown).

To demonstrate that also using a functional siRNA+PDPG uptake is ruled by ASGPR, HuH7-EGFP cells were treated by EGTA (5 nM) for 10 min before the transfection. As above reported (section 2.10) calcium is essential for ASGPR activity and thus a reduction in its concentration impairs ASGPR functionality. In addition to comparing the effects of PDPG vs PDP, we have also introduced an additional negative control represented by Lipofectamine 2000, whose delivery is known to be independent from ASGPR. The fluorescence microscopy analysis did not evidence significant differences in the green fluorescence intensity in HuH7-EGFP cells transfected by siEGFP+PDPG and pre-treated with EGTA, compared to the HuH7-EGFP transfected by siGL2+PDPG and pre-treated with EGTA (Figure 5.8). In contrast, in the absence of EGTA pre-treatment, an evident decrease in the fluorescence intensity was observed in HuH7-EGFP transfected by siEGFP+PDPG but not in cells transfected by siEGFP+PDP, compared to the respective siGL2+PDPG/siGL2+PDP control transfected HuH7. Notably, a decrease in the fluorescence intensity was evident following siEGFP+Lipofectamine 2000 transfection regardless of EGTA pre-treatment, compared to siGL2+Lipofectamine 2000 transfected cells. These results strongly indicate that ASGPR independent uptake is not affected by free-calcium depletion. Moreover, this observation proves the specificity of the EGTA test to detect ASGPR dependent and independent uptake and indirectly confirms ASGPR dependent uptake for PDPG.

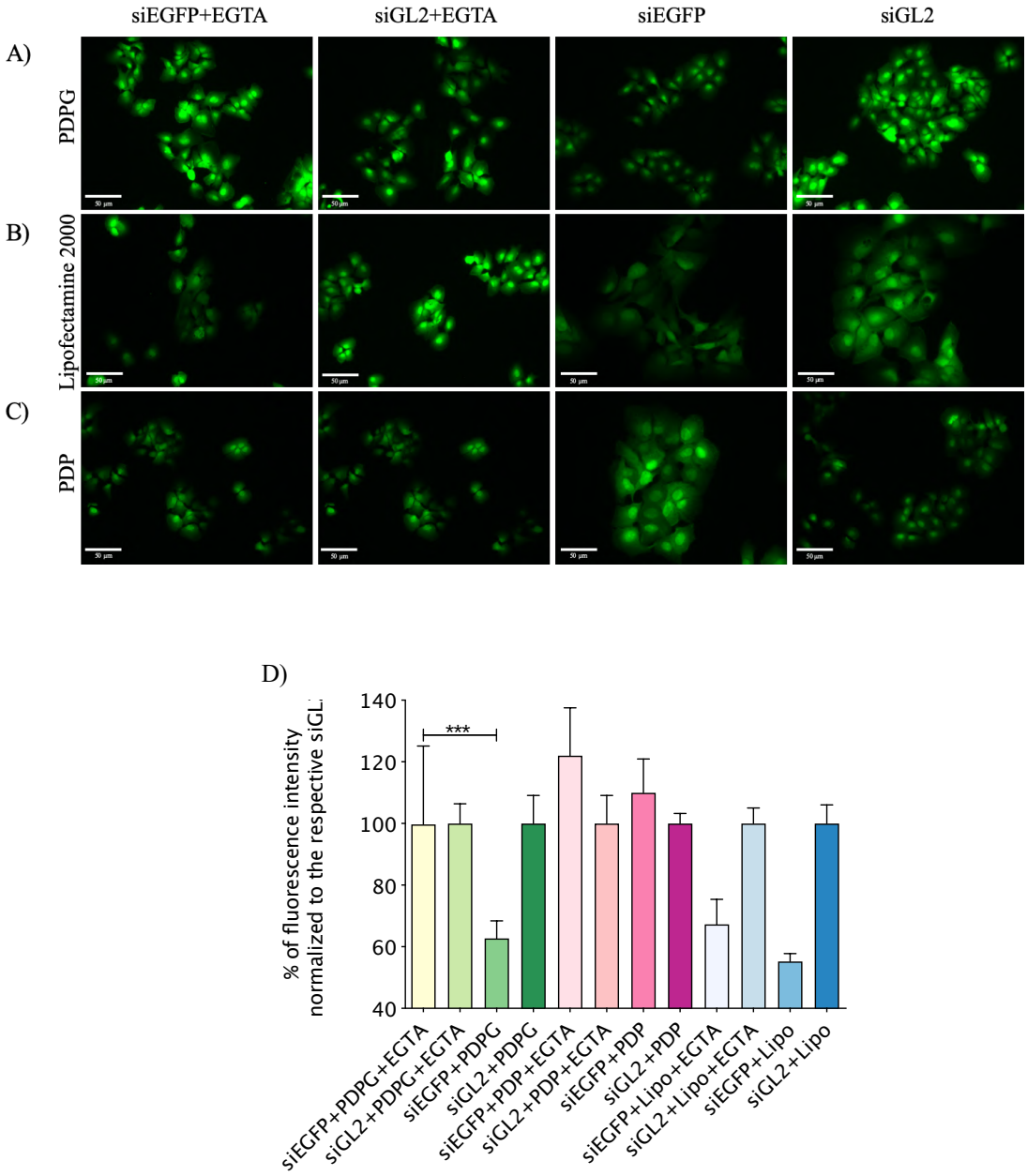

Figure 5.8. Fluorescence images of HuH7-EGFP transfected by siEGFP/siGL2+PDPG (**A**), siEGFP/siGL2+Lipofectamine 2000 (**B**) or siEGFP/siGL2+PDP (**C**) with (+) or without EGTA (-) (5 mM) treatment. **D)** A decrease on the fluorescence intensity is visible 48h only in HuH7-EGFP cells following siEGFP+PDPG transfection without EGTA treatment compared to siGL2+PDPG transfected cells. A decrease on the fluorescence intensity is visible in HuH7-EGFP cells 48h following siEGFP+Lipofectamine 2000 transfection with and without EGTA treatment compared to siGL2+Lipofectamine 2000 transfected cells. No significant differences in the fluorescence intensity are visible following siEGFP+PDP transfection compared to siGL2+PDP transfected cells, with and without EGTA treatment. Data are expressed as % of the average of the fluorescence intensity normalized to the respective siGL2 transfections and are shown as ±SEM. ***p=0.0006 compared to siEGFP+PDPG; n=3.

5.3 *In vitro* functional studies

Following the demonstration of the effective and specific (ASGPR dependent) uptake of PDPG in HuH7, we tested the effects of the delivery of three siRNAs targeted against the mRNAs of HCC related genes. In particular, we focused the attention on the targeting of the mRNA of eEF1A1, eEF1A2 and E2F1. These genes are considered valuable targets for HCC treatments, since they are overexpressed in HCC and we observed that the reduction of the respective mRNA and protein levels could induce a reduction in tumour cells growth[366,395,342].

5.3.1 siRNA+PDPG effects on cell viability

Being eEF1A1, eEF1A2 and E2F1 involved in the cell proliferation process, effects on cell viability and cell number were analyzed following the transfection of HuH7 by sieEF1A1, sieEF1A2 and siE2F1, respectively. An evident decrease in HuH7 cell viability was observed three days from the transfection by sieEF1A1, sieEF1A2 and siE2F1 delivered by PDPG, compared to the control siGL2-PDPG transfected cells (Figure 5.9). In particular, siRNAs effects were more evident three days after siRNAs+PDPG transfection, showing a decrease of cell viability down to about 70% for sieEF1A2+PDPG and siE2F1+PDPG transfected cells and 80% for sieEF1A1+PDPG transfected cells. The effects were time dependent being reduced at day 6 from transfection and substantially not detectable at day 10. Based on these data, three days after siRNAs transfection was chosen as the optimal time point for further evaluation of siRNA effects.

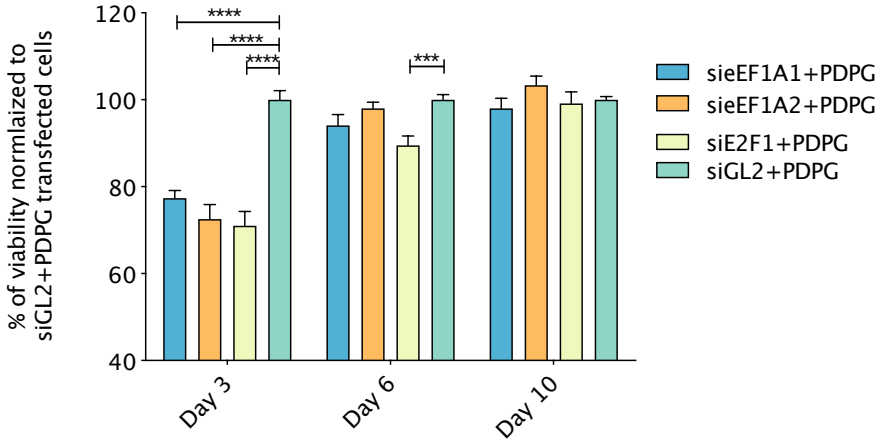

Figure 5.9. siRNAs targeting either eEF1A1 (220 nM), eEF1A2 (220 nM) or E2F1 (220 nM) mRNAs were delivered by PDPG in HuH7 cells. Effects on cell viability were evaluated by MTT test at different time points following siRNAs+PDPG transfection and compared to siGL2 (control siRNA against the luciferase mRNA, 220 nM)+PDPG transfected cells. Data are expressed as % of the average of cells transfected by siGL2+PDPG and shown as mean ±SEM. ****p< 0.0001 and ***p<0.0008 compared to control siGL2+PDPG transfected cells; n=6.

In line with the viability tests, a significant reduction in cell number was observed three days following the transfection of the PDPG loaded by sieEF1A1, sieEF1A2 or siE2F1 in HuH7 (Figure 5.10), compared to siGL2-PDPG transfected cells.

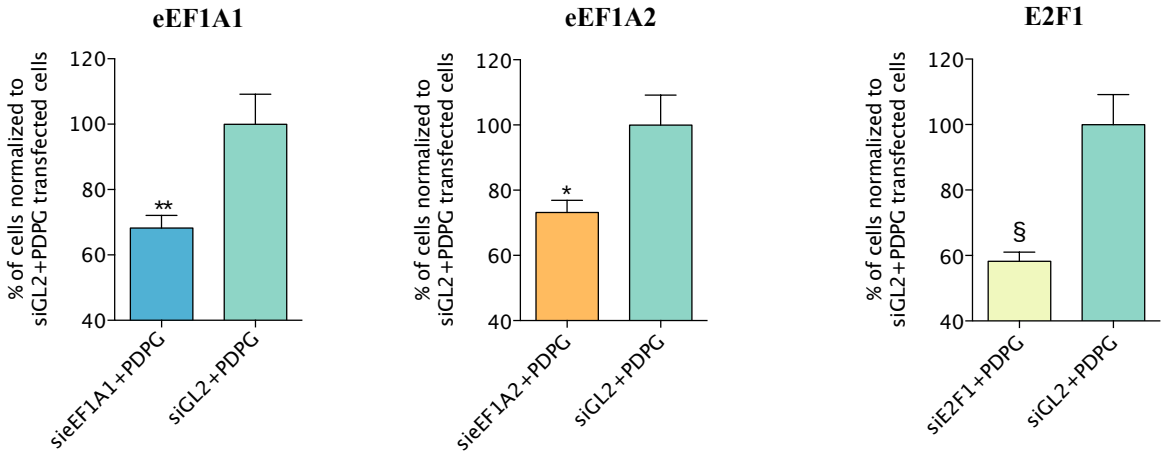

Figure 5.10. Three days after transfection by siRNAs+PDPG, sieEF1A1(220 nM), sieEF1A2(220 nM) or siE2F1(220 nM) a significant reduction in the cell number was observed in HuH7 cells compared to siGL2+PDPG-transfected cells. Data, expressed as the % of the average of siGL2+PDPG transfected cells, are shown as mean ±SEM; **p< 0.0160, *p< 0.316 and §p<0.0049 compared to control siGL2+PDPG transfected cells; n = 6.

5.3.2 siRNA+PDPG effects on target genes expression

To prove the specific action of the siRNAs against their targets, the mRNA levels of eEF1A1, eEF1A2 and E2F1 were evaluated following sieEF1A1+PDPG, sieEF1A2+PDPG or siE2F1+PDPG transfection, respectively. Three days after siRNAs transfection, a significant reduction in the mRNA of eEF1A1, eEF1A2 and E2F1 was observed compared to siGL2+PDPG transfected cells (Figure 5.11). In particular, a decrease of around 80% was observed for eEF1A1 mRNA levels, 40% for eEF1A2 mRNA levels and 60% for E2F1 mRNA levels. Notably, the mRNA levels of eEF1A2 were evaluated using the droplet PCR, because of the difficulties in cDNA amplification by conventional qRT-PCR due to the very low amount of mRNA levels in the cell.

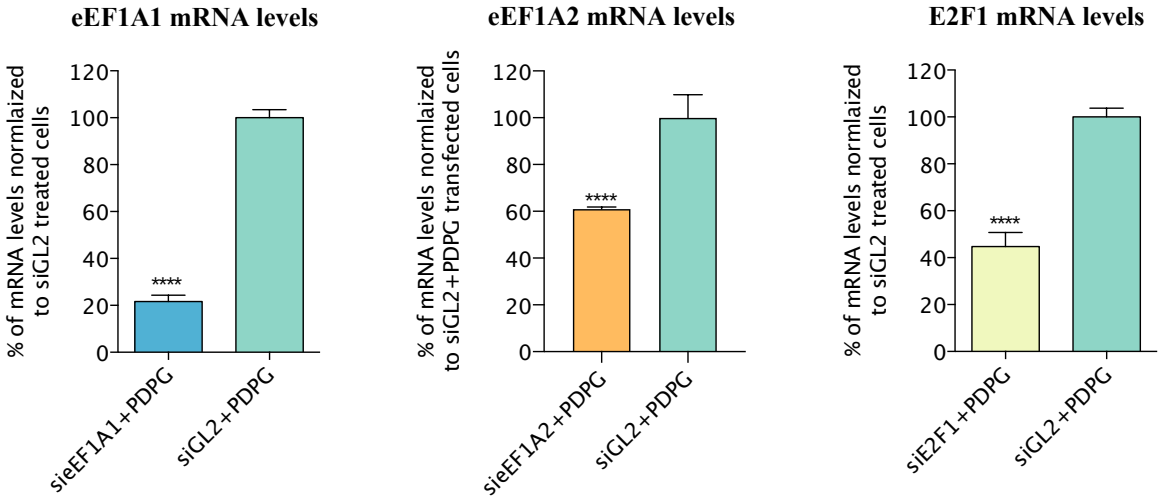

Figure 5.11. Three days after the transfection of sieEF1A1(220 nM) or siE2F1(220 nM) delivered by the PDPG, a significant reduction of mRNA levels of the respective targets was observed in HuH7 cells compared to siRNA-control transfected cells (siGL2, 220 nM). eEF1A1 and E2F1 mRNA data were normalized to 28S rRNA levels, while eEF1A2 mRNA data were normalized to GAPDH mRNA levels. Data are expressed as the % of the average of the respective siGL2+PDPG-transfected cells, are shown as mean ± SEM; ****$p < 0.0001$ compared to control siGL2+PDPG transfected cells; $n = 6$.

With regard to the protein levels, western blot analysis showed a significant decrease of E2F1 protein levels following siE2F1+PDPG transfection compared to siGL2+PDPG transfected cells of about 30%. sieEF1A1+PDPG or sieEF1A2+PDPG showed a decrease of eEF1A1 or eEF1A2 protein levels of around 20-25% (Figure 5.12).

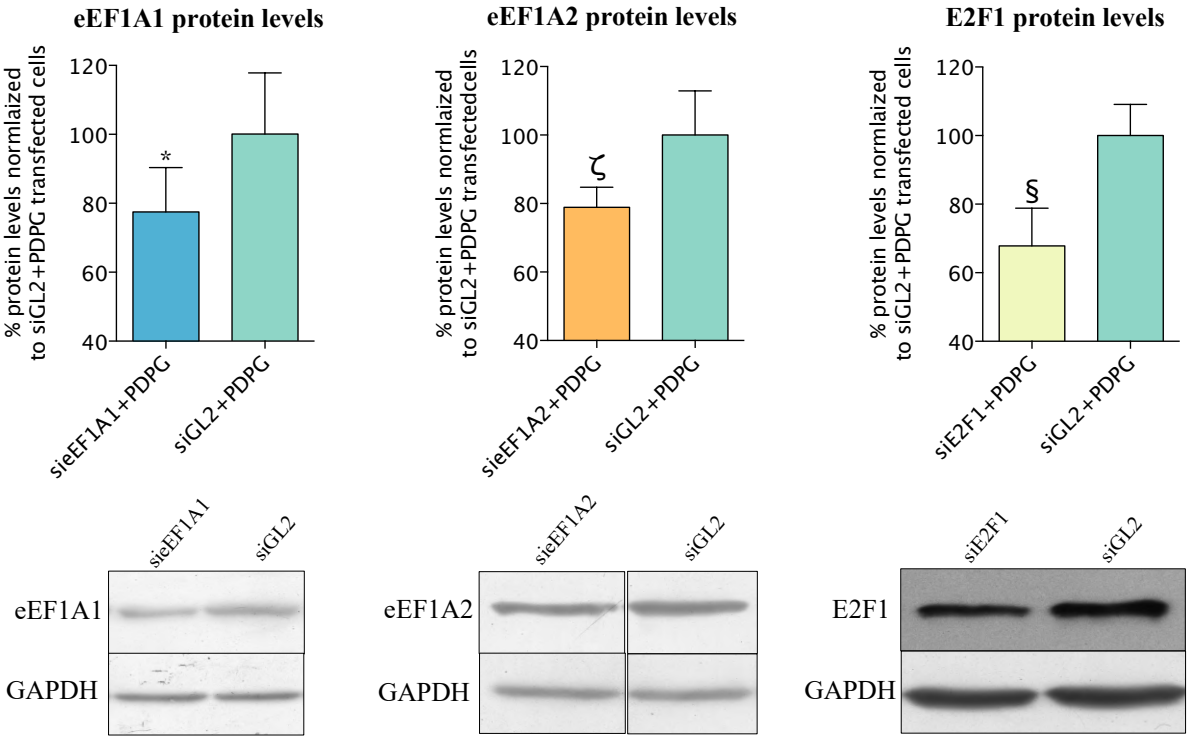

Figure 5.12. Three days after the transfection of sieEF1A1, sieEF1A2 and siE2F1 (220 nM) delivered by the PDPG, a significant reduction of protein levels of specific targets was observed on HuH7 cells compared to siRNA-control transfected cells (siGL2, 220 nM). Data, normalized to GAPDH levels and expressed as % of the respective siGL2+PDPG-transfected cells, are shown as mean ±SEM; *p<0.0431, ζp<0.0313 and §p<0.0462 compared to control siGL2+PDPG (paired t test) transfected cells; n = 6.

5.3.3 siRNA+PDP effects on cell viability and on target genes expression

Uptake studies *in vitro* strongly indicate the targeting ability of PDPG vs PDP. To verify this PDPG feature at the functional level, we have tested the functional effects of sieEF1A1 delivered by PDP. sieEF1A1 was randomly chosen among the three siRNA (sieEF1A1, sieEF1A2 and siE2F1) tested in combination with PDPG. sieEF1A1+PDP effect on cell viability was neither detectable at day 3 nor 10 post transfection (Figure 5.13). Only a tendency towards viability reduction was observed at day 6. Additionally, no clear reduction in cell number and protein levels were detected. Finally, just a tendency in the reduction of eEF1A1 mRNA level was observed.

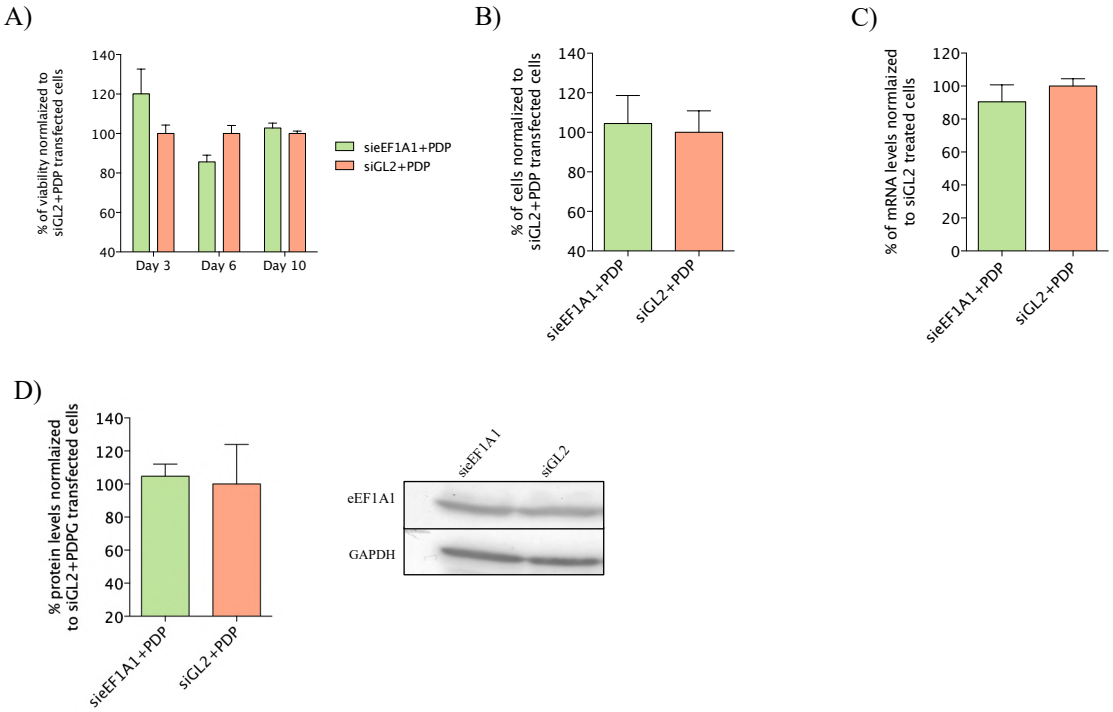

Figure 5.13. Evaluation of the sieEF1A1+PDP effectiveness in HuH7 cells. **A)** Effects on cell viability were evaluated by MTT test at different time points following sieEF1A1+PDP delivery in comparison to siGL2+PDP transfected cells. Data are expressed as % of the average of cells transfected by siGL2+PDP and shown as mean ±SEM; n=3. **B)** sieEF1A1+PDP (220 nM) transfection did not result in a significant decrease of the cell number three days after transfection compared to siGL2+PDP-transfected cells. Data, expressed as the % of the average of siGL2+PDP transfected cells, are shown as mean ±SEM; n=6. **C)** sieEF1A1+PDP (220 nM) transfection just resulted in a tendency towards a decrease of eEF1A1 mRNA levels three days after transfection compared to siGL2+PDP-transfected cells. Data, normalized to 28S rRNA levels and expressed as the % of the average of the respective siGL2+PDP-transfected cells, are shown as mean ± SEM; n = 2. **D)** sieEF1A1+PDP (220 nM) transfection did not result in a significant decrease of eEF1A1 proteins levels three days after transfection compared to siGL2+PDP-transfected cells. Data, normalized to GAPDH levels and expressed as % of the respective siGL2+PDPG-transfected cells, are shown as mean ±SEM; n = 3.

All together, these results further highlight the targeting ability of the developed PDPG as a delivery system for siRNAs into HCC cell line and the importance of the galactose, which confers to PDPG the ability to bind ASGPR.

5.4 Evaluation of possible siRNAs+PDPG side effects *in vitro*

The functional data above reported for siRNA+PDPG (section 5.3.1), strongly support the concept that the observed viability reduction is due to the down regulation in the expression of the target genes eEF1A1, eEF1A2 or E2F1, all related to the promotion of HuH7 growth. To further confirm the specificity of action of our siRNA+PDPG, we investigated the possible activation of cell death. For this purpose, we evaluated the induction of cell necrosis, autophagy and apoptosis, representing the most common mechanisms of cell death.

To explore whether siRNAs+PDPG transfection could have induced any necrotic effects on HuH7, the LDH assay was performed. This test allows to measuring Lactate Dehydrogenase (LDH) levels that, upon the occurrence of cell necrosis, is released outside the cell in the culture medium. Cells treated by Triton-X-100, a non-ionic surfactant able to induce cell lysis, was introduced as positive controls for necrosis induction. The evaluation of the LDH levels on HuH7 transfected by siRNAs+PDPG or sieEF1A1+PDP performed 3 days and 6 days after transfection, did not evidence any significant increase of LDH levels compared to siGL2+PDPG transfected cells and non-treated cells (Figure 5.14). This data show that the specific siRNAs delivered by PDPG do not elicit any unspecific cell necrosis. Notably, the levels of LDH evaluated 10 days after siRNAs+PDPG or sieEF1A1+PDP transfection were higher than those detected on day 3 and day 6. This is probably because cells overgrew on day 10 inducing cell death and thus releasing LDH in the medium.

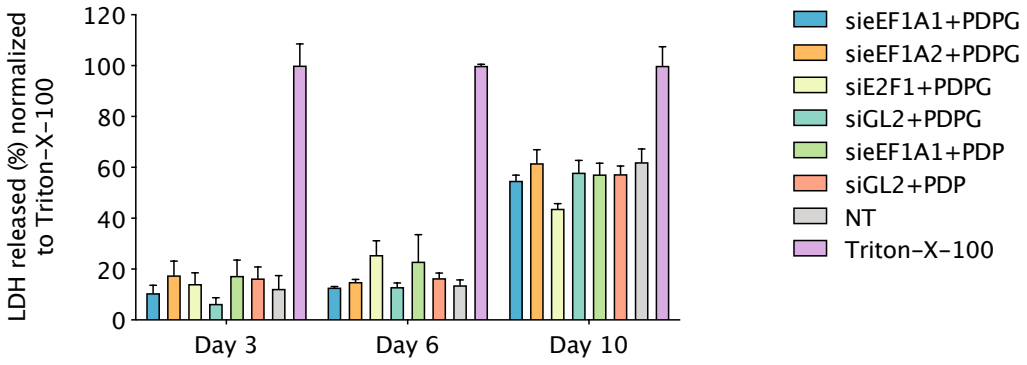

Figure 5.14. Evaluation of necrosis induction in HuH7 cells after siRNAs+PDPG or siRNAs+PDP transfection. LDH assay was performed at different time points following transfection. The measure of LDH levels released after either sieEF1A1+PDPG, sieEF1A2+PDPG, siE2F1+PDPG or sieEF1A1+PDP transfection did not evidence any significant necrotic effects. Data, normalized to Triton X-100, are expressed as mean ± SEM; n=3.

LC3B is a soluble protein detectable as a single band in normal condition. When autophagy is activated, the protein can be detected as two bands in western blotting, one representing the cytosolic form (LC3B-I, 16 kDa), and the other (LC3B-II, 14 kDa) the conjugated form[421]. The

evaluation of the LC3B autophagy marker showed a tendency in the autophagy induction following siRNAs+PDPG transfection compared to siGL2+PDPG transfected cells and NT cells. Indeed, the LC3B-II/LC3B-I ratio for the specific siRNA+PDPG is lower to those of the control siGL2+PDPG-transfected cells and non-treated cells (Figure 5.15).

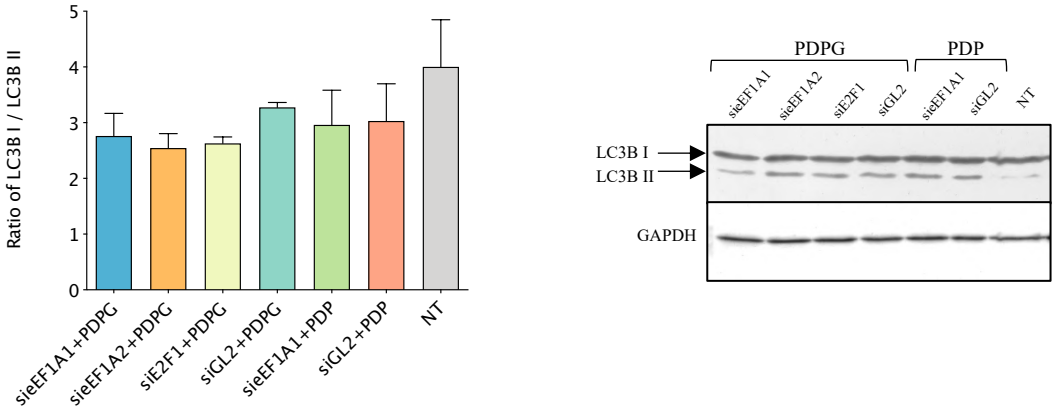

Figure 5.15. Three days after either sieEF1A1+PDPG, sieEF1A2+PDPG, siE2F1+PDPG or sieEF1A1+PDP transfection in HuH7 cells, the induction of cell autophagy was monitored evaluating the levels of the autophagy marker LC3B forms (LC3B-I and LC3B-II). The transfection of siRNAs+PDPG resulted in a tendency of autophagy induction compared to siGL2+PDPG transfected cells. Data are represented as LC3B-I/LC3B-II ratio and shown as ±SEM; n=3.

We finally evaluated apoptosis induction by measuring the cleaved/unleaded forms of PARP, a known marker of apoptosis. PARP is a protein mainly involved in the DNA repair process in the single-strand DNA breaks. It is cleaved in two fragments of 24 kDa and 89 kDa by Caspase 3 and 7 during the late apoptosis, inactivating the protein[422]. Our data suggest that no significant apoptosis is induced by siRNAs+PDPG (Figure 5.16).

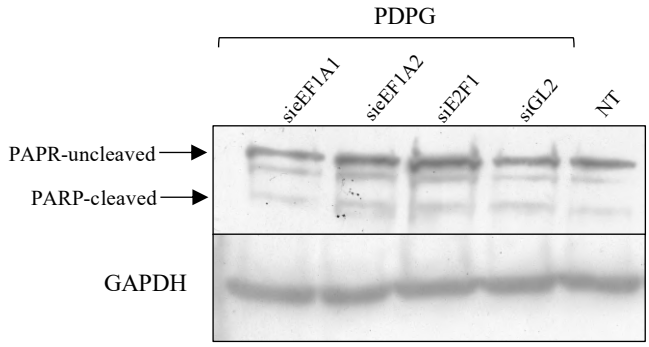

Figure 5.16. Three days after either sieEF1A1+PDPG, sieEF1A2+PDPG, siE2F1+PDPG or sieEF1A1+PDP transfection in HuH7 cells, the induction of cell apoptosis was monitored evaluating the levels of the apoptosis marker PARP forms, cleaved (89 kDa) and uncleaved (118 kDa). The transfection of siRNAs+PDPG did not result in the apoptosis induction compared to siGL2+PDPG transfected cells.

5.5 *In vivo* uptake: Dorsal skinfold window chamber in SCID mice

The promising results obtained in *in vitro* experiments, prompted us to investigate the effectiveness of the delivery system also *in vivo* using a xenograft mouse model of HCC, SCID mice. In particular, to study the ability of the PDPG to deliver siRNAs *in vivo,* the dorsal skinfold window chamber experiment was performed. The technique allowed to monitor the internalization of the complex siRNAs+PDPG *in vivo* and to visualize tumour cells in animals. In order to monitor the tumour growth over time and to decide the correct time point to start the treatments, in a preliminary experiment, in one group of female SCID mice the tumour was induced injecting HuH7-EGFP cells, and the growth followed over time. Images from the window chamber were taken every two/three days using the stereomicroscope. HuH7-EGFP cells could graft into the animal and the tumour mass was present for at least 12 days after HuH7-EGFP cells injection (Figure 5.17).

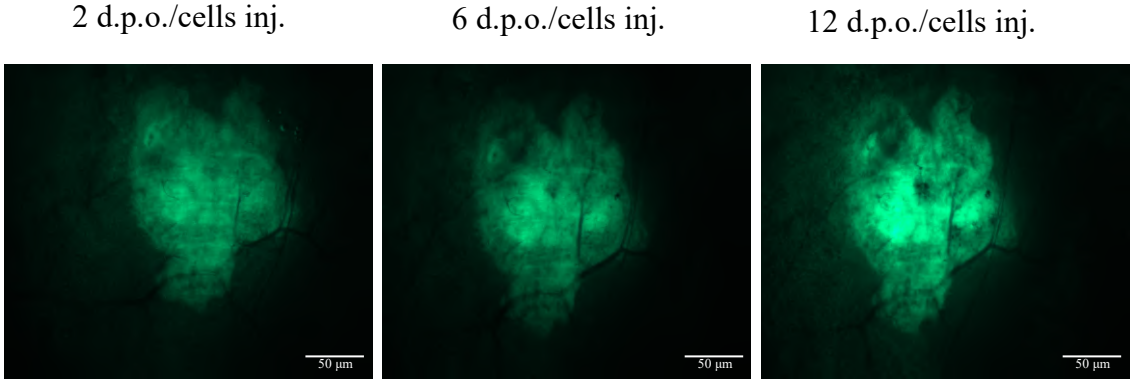

Figure 5.17. Fluorescence images of tumours (green) from the dorsal window chamber of mice 2, 6 and 12 days post operation/cell injection (d.p.o/cells inj.). Scale bar= 50 µm.

Since the implantation of window chambers apparatus for a long time can induce inflammation and mice suffering, six days after cells inoculation was chosen as time point to start the intratumour injection of siRNA+PDPG or siRNA+PDP. A siRNA against the EGFP (siEGFP) mRNA was used, as already utilized in *in vitro* uptake tests. With this experimental system, it was possible to monitor cell growth by simply evaluating the green fluorescence. Images from the stereomicroscope were taken the day of the treatment (day 0) and then on day 1, day 4 and day 7. With this test, a more pronounced decrease of the fluorescence intensity following siEGFP+PDPG treatment compared to siEGFP+PDP (Figure 5.18) was observed. In conclusion, this experiment demonstrated the ability of the PDPG to effectively target HuH7-EGFP cells *in vivo* compared to PDP and to deliver siEGFP inside tumour cells.

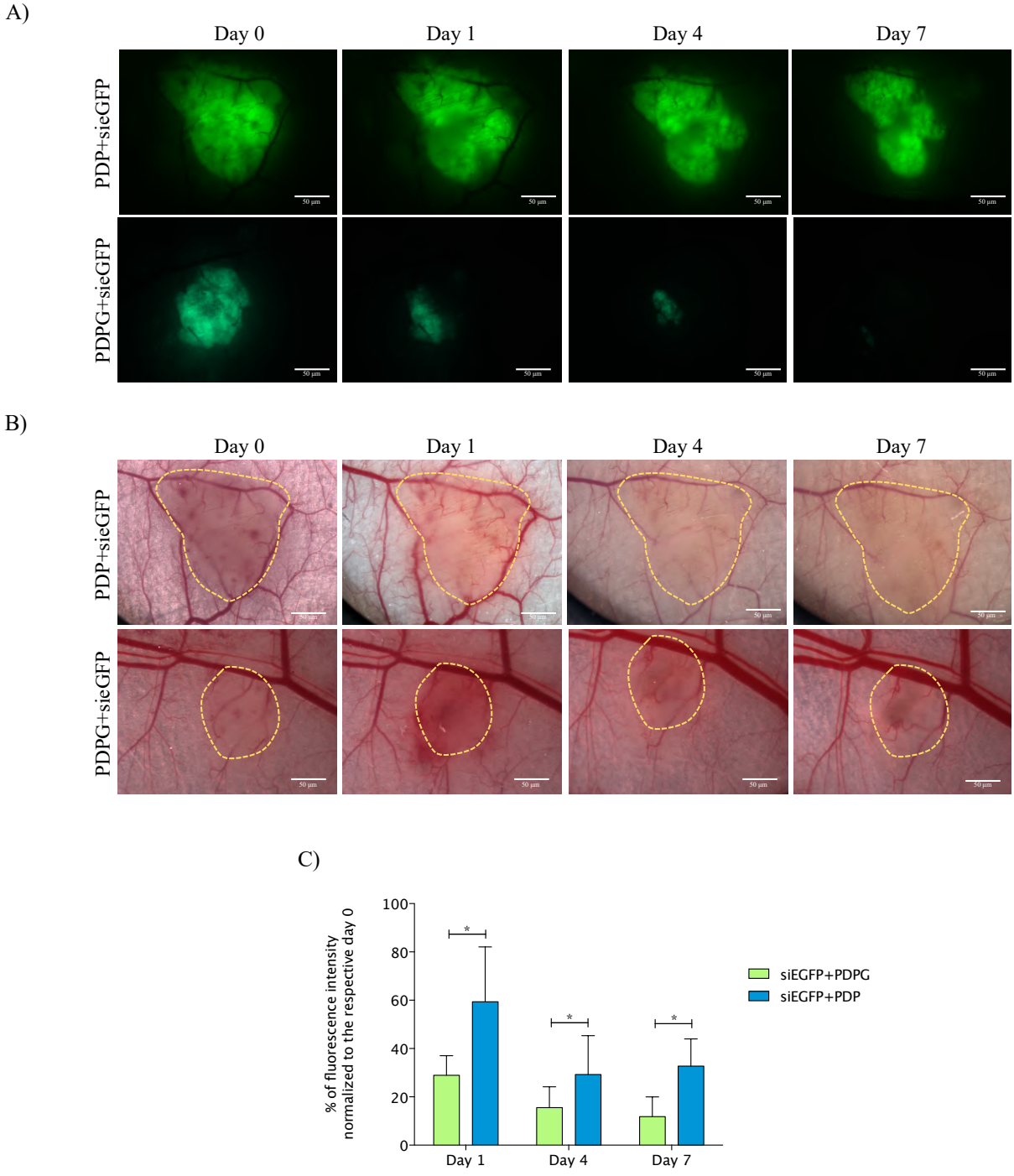

Figure 5.18. A and B) Representative images of tumours in mice treated with siEGFP+PDPG and siEGFP+PDP. Fluorescence images of tumours (**A, green**) and Bright-field images (**B**) from the dorsal window chamber of mice before therapy injection (Day 0) and 1 day, 4 days and 7 days after intratumour injection of siEGFP+PDPG or siEGFP+PDP treatments. Scale bar= 50 µm. **C)** A decrease of the fluorescence intensity of tumours in dorsal window chamber after siEGFP+PDPG treatment is visible from day 1 to day 7, compared to siEGFP+PDP treated mice. Data, shown as ±SEM, are normalized to the fluorescence intensity of siEGFP+PDP-treated-tumours on the day 0 and expressed as %; n=5 *p=0.0463 (paired t test).

5.6 *In vivo* functional studies

5.6.1 Long-term experiment

The dorsal skinfold window chamber showed the ability of siRNA+PDPG to specifically target tumour cells and to be effective *in vivo*. In analogy to the *in vitro* uptake studies, we then moved to test the effectiveness of our specific siRNA *in vivo*. We started with a *long-term experiment* in SCID mice that were randomly divided into six groups and treated by PDPG, NaCl, sieEF1A1+PDPG, sieEF1A2+PDPG, siE2F1+PDPG or siGL2+PDPG. The tumour volume was measured every second day from the day of intratumour injection and a tumour growth curve was draw. The results showed an evident slowdown of the tumour volume growth in mice treated by sieEF1A1+PDPG, sieEF1A2+PDPG and siE2F1+PDPG compared to the control group siGL2+PDPG, PDPG and NaCl. Notably, the difference between specific treatments and controls started already at day 1 and was maintained up to day 6-7 (Figure 5.19). PDPG and siGL2+PDPG treatments showed the similar results with a slight slowdown in the tumour growth compared to the NaCl treated mice. This is probably related to the copolymer itself, which could induce a decrease in cell proliferation.

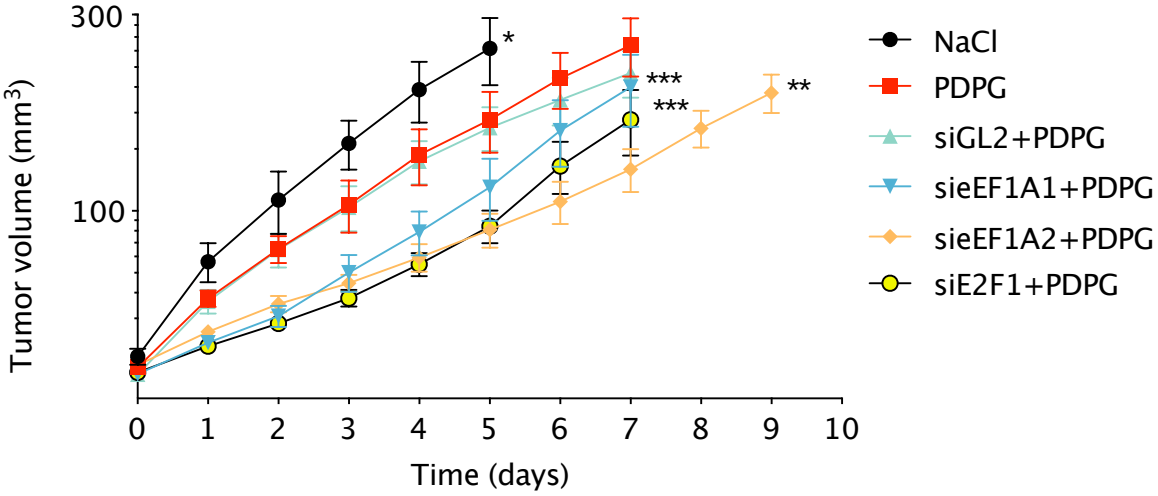

Figure 5.19. A slowdown in tumour growth is visible following for sieEF1A1+PDPG, sieEF1A2+PDPG and siE2F1+PDPG intratumour injections compared to siGL2+PDPG treated mice. Data are shown as ±SEM; *p=0.0264, **p=0.0030; ***p=0.0004 compared to siGL2+PDPG treated mice (paired t test).

Data from tumour growth curve allowed to calculate the doubling time, indicating the time in which the tumour volume double in term of its volume-size and in turn, to extrapolate data for the tumour growth delay calculation. The results demonstrated that mice treated by sieEF1A1+PDPG, sieEF1A2+PDPG and siE2F+PDPG showed a tumour growth delay of around 3 days compared to siGL2+PDPG and PDPG treated mice (Figure 5.20)

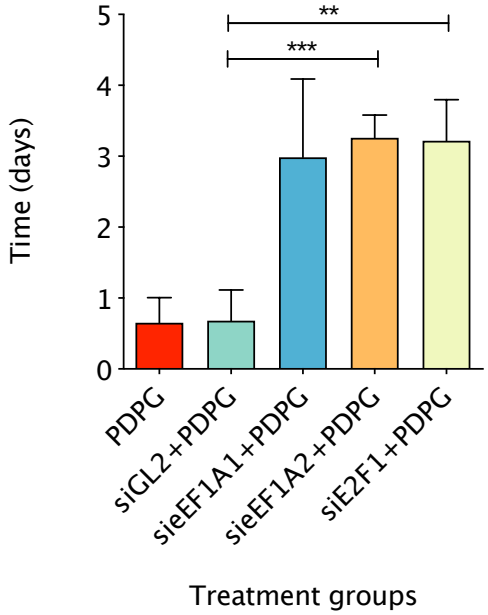

Figure 5.20. siRNA+PDPG treatments resulted in a tumour growth delay of around three days compared to siGL2+PDPG treated mice. Data are shown as ±SEM. ***p=0,009 and **p=0,0063 compared to siGL2+PDPG treated mice.

6.2 Short-term experiment

The *long-term experiment* provided information about the phenotypic effects of our siRNA+PDPG. We then wanted to prove that also *in vivo* the mechanism of action was based on the reduction of target gene expression. For this purpose, we performed a *short-term experiment* limited to day three post intra tumour injection. This time point was chosen based on the *in vitro* and *in vivo* experiments, where day three allowed to detect the phenotypic/molecular effects of siRNA+PDPG (*in vitro*) and the reduction of tumour growth (*in vivo*). We did not consider a longer time point as we believe the molecular effects of the siRNA could have been lost both due to siRNA processing in the cells and to the growth of un-transfected cells. Mice were randomly divided into four groups, and treated by either sieEF1A1+PDPG, sieEF1A2+PDPG, siE2F1+PDPG or siGL2+PDPG. At day three post injection, animals were then sacrificed. The size of the tumours was measured the day of siRNAs injections (day 0) and the day of the sacrifice (day 3). The trend of the tumour growth curve is comparable to that of the *long-term experiment*. In particular, a slowdown in the tumour growth is evident following sieEF1A1+PDPG, sieEF1A2+PDPG and siE2F1+PDPG treatments compared to siGL2+PDPG-treated mice (control group) (Figure 5.21)

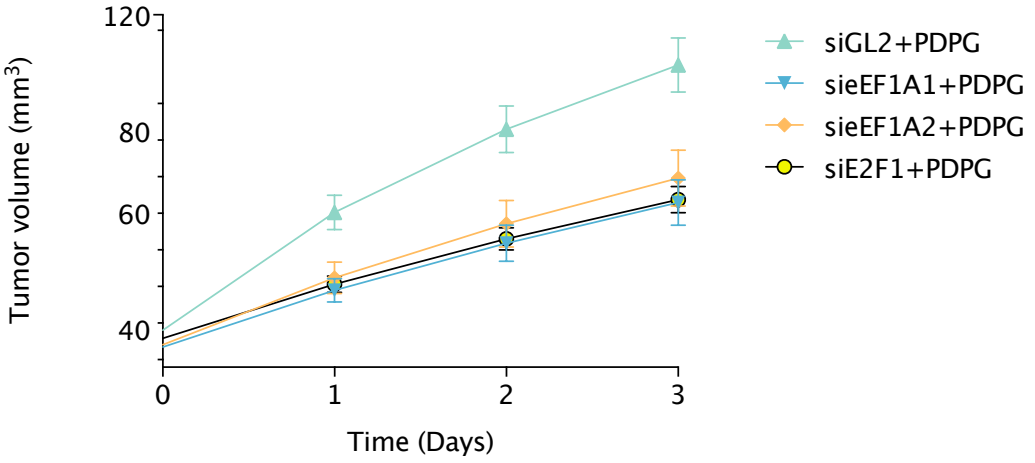

Figure 5.21. A slowdown in tumour growth is visible following either sieEF1A1+PDPG, sieEF1A2+PDPG or siE2F1+PDPG intratumour injections compared to siGL2+PDPG treated mice. Data are compared to siGL2+PDPG treated mice and shown as ±SEM.

Tumour were then collected and tested for the levels of the mRNA and protein of the specific targets. A decrease in eEF1A1, eEF1A2 and E2F1 mRNA levels was observed in mice treated by sieEF1A1+PDPG and sieEF1A2+PDPG respectively (Figure 5.22) compared to siGL2+PDPG treated mice.

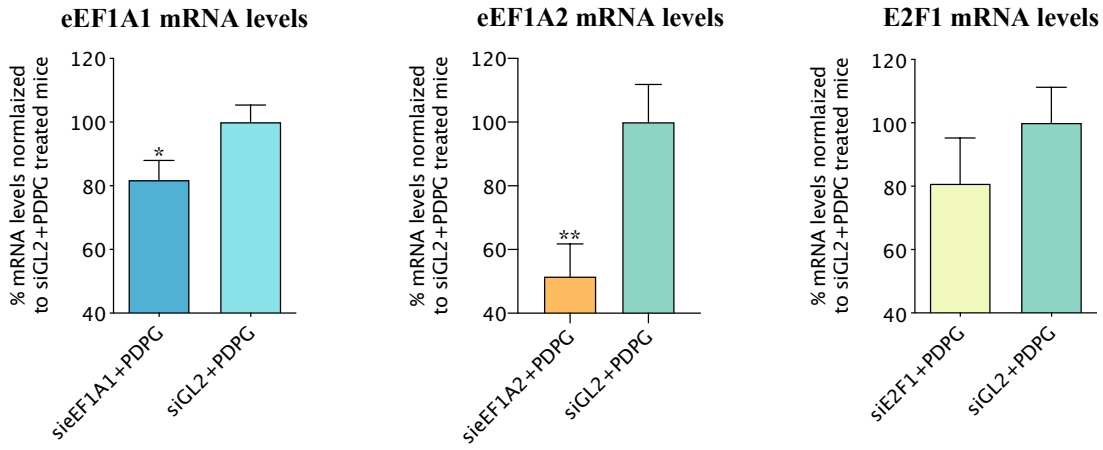

Figure 5.22. mRNA levels of eEF1A1 and eEF1A2 decrease following sieEF1A1+PDPG and sieEF1A2+PDPG treatment injections in SCID mice respectively, compared to siGL2+PDPD treated mice. On the contrary, E2F1 mRNA levels did not decrease following siE2F1+PDPG treatment injection. Data, normalized to 28S rRNA levels and expressed as the % of the average of the respective siGL2+PDPG-treated-mice, are shown as mean ± SEM; *p = 0.0439 and **p=0.0159 compared to control siGL2+PDPG treated mice.

Western blot showed a slight decrease of eEF1A1, eEF1A2 and E2F1 protein levels in mice treated by the specific siRNAs delivered by PDPG compared to siGL2+PDPG treated mice (Figure 5.23).

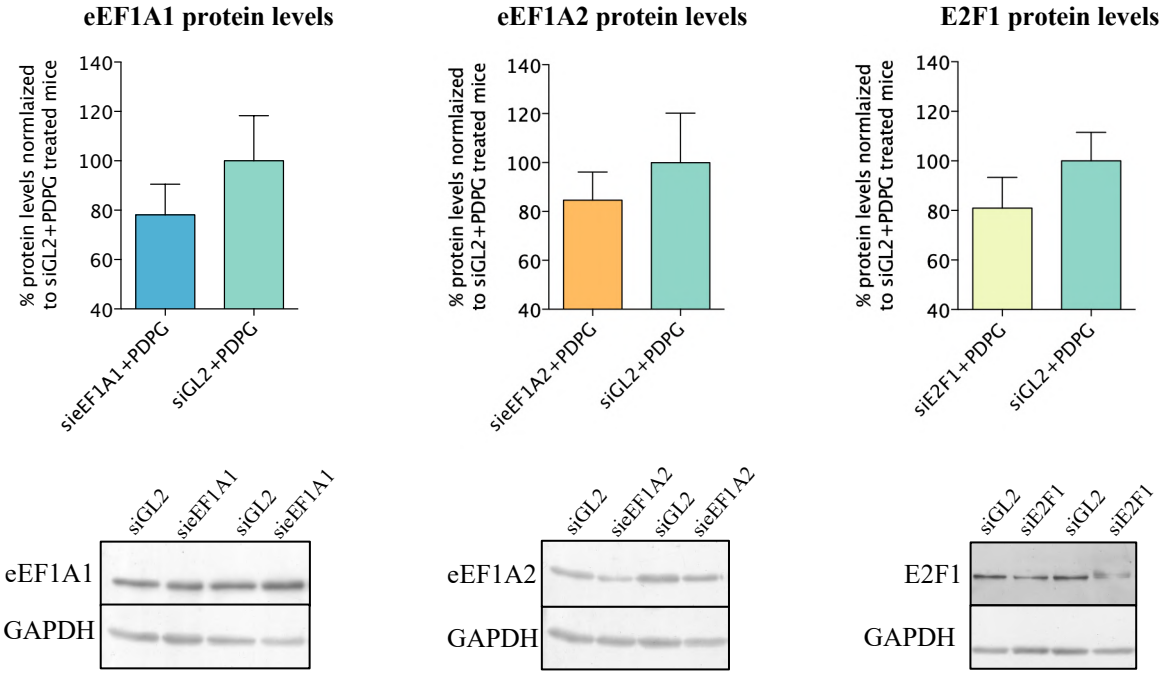

Figure 5.23. Results show a slight decrease of eEF1A1, eEF1A2 and E2F1 protein levels three days after sieEF1A+PDPG, sieEF1A2+PDPG and siE2F1+PDPG treatment injections in SCID mice respectively, compared to siGL2+PDPD treated mice. Data, normalized to GAPDH levels and expressed as % of the respective siGL2+PDPG-treated mice, are shown as mean ±SEM.

5.7 Evaluation of possible siRNAs+PDPG side effects *in vivo*

Major side effects were not detected *in vitro*. To prove the same *in vivo*, levels of blood markers indicating systemic toxicity were analyzed in the animal that underwent the *short-term experiment*. In particular, albumin, Aspartate transaminases (AST) and Alanine aminotransferases (ALT) blood levels were measured to explore liver function. C-reactive protein levels were analyzed to investigate any possible pro-inflammatory induction by our siRNA+PDPG. Glucose blood levels were measured to the evaluate glycemic homeostasis. Finally, creatinine blood levels were evaluated to test the kidney function. Results show no significant siRNAs+PDPG toxic effects in mice, since no significant differences in marker levels were detected in all experimental groups compared to the control group (siGL2+PDPG) treated mice (Figure 5.24 A, B, C, D, E and F). Moreover, levels of the analyzed markers were not altered compared to values of the same markers in non-treated SCID mice (Table 5.1)[423]. Finally, no relevant variations in mice weight were observed, further proving the safety of the injected treatments (Figure 5.24 G and H) in both, *long-term* and *short-term experiments*.

All together, these data demonstrated that the polymer is not toxic for mice and that it is safe for future *in vivo* applications.

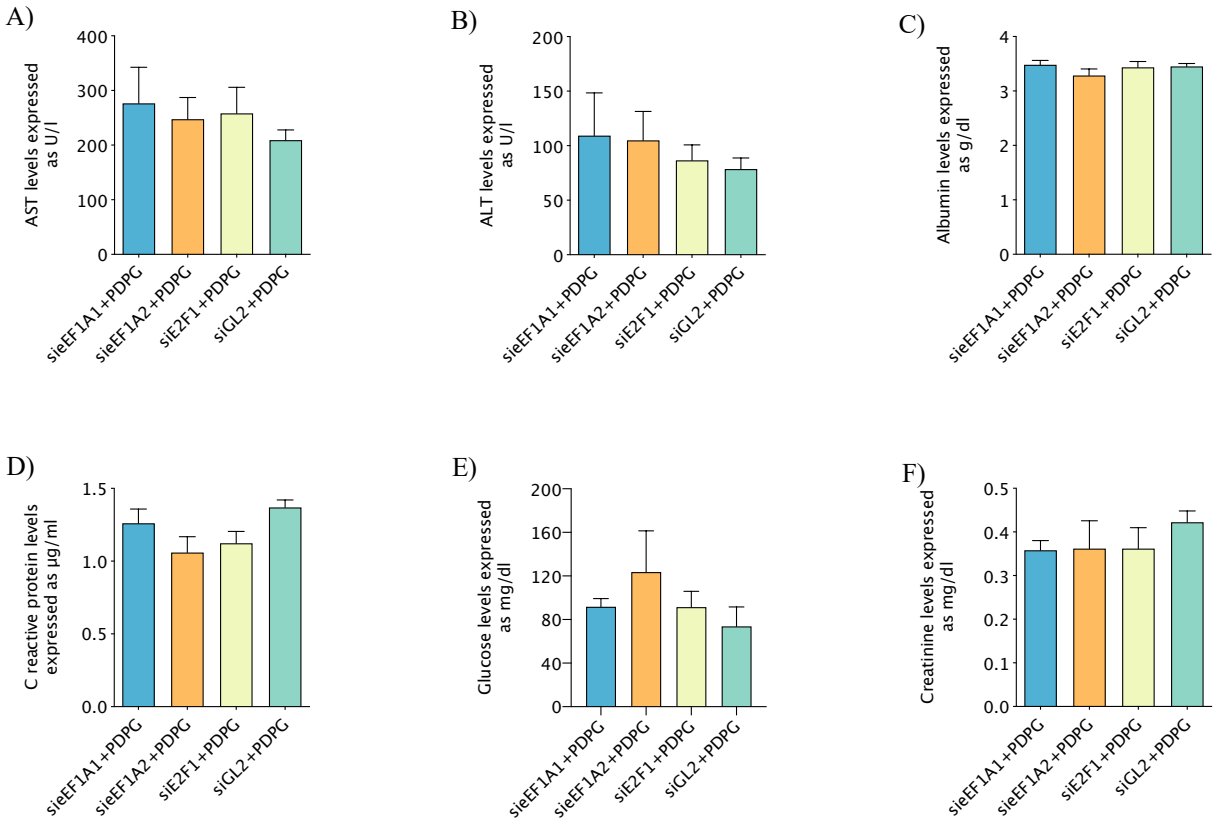

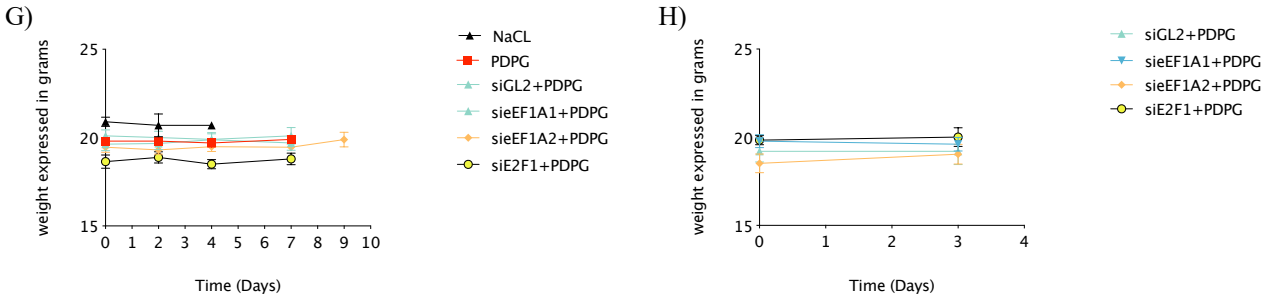

Figure 5.24. Levels of AST (**A**), ALT (**B**), albumin (**C**), C reactive protein (**D**), Glucose (**E**) and Creatinine (**F**) did not show any significant siRNA/PDPG-related toxic effects in mice following sieEF1A1+PDPG, sieEF1A2+PDPG and siE2F1+PDPG compared to siGL2+PDPG treated mice. Values were also compared to the normal mice values, which are shown in the Table 5.1. Data, represented with the respective unit values, are shown as ±SEM. **G and H)** Graphs showing mice weight from the *long-term experiment* and *short-term experiment,* respectively. Data are shown as ±SEM.

Table 5.1. Reference values in normal mice of some blood markers[423].

Blood marker	Range of values in normal mice
Creatinine	0.2-0.6 mg/dl
Albumin	3.3-4.6 g/dl
ALT	30-113 U/L
AST	57-393 U/L
Glucose	128-277 mg/dl

5.7.1 Systemic injection of treatments in mice

Following the promising data obtained by the intra tumour injection, we tried a pivotal experiment in which siE2F1+PDPG was delivered systemically by retro-orbital injection. We tested only one dosage injected three times every second day. Unfortunately, we could not observe significant differences between the mice treated by siE2F1+PDPG compared to the control group, siGL2+PDPG treated mice (Figure 5.25 A). Whereas the reasons for this result can be numerous, we cannot exclude that the amount of siRNA used was sub-optimal and thus the amount of polymer that reached the tumour could have been too low to show an evident effect. Nevertheless, systemic treatments injections did not result in toxic effects on mice, since no loss of weigh was not observed during the experiment (Figure 5.25 B).

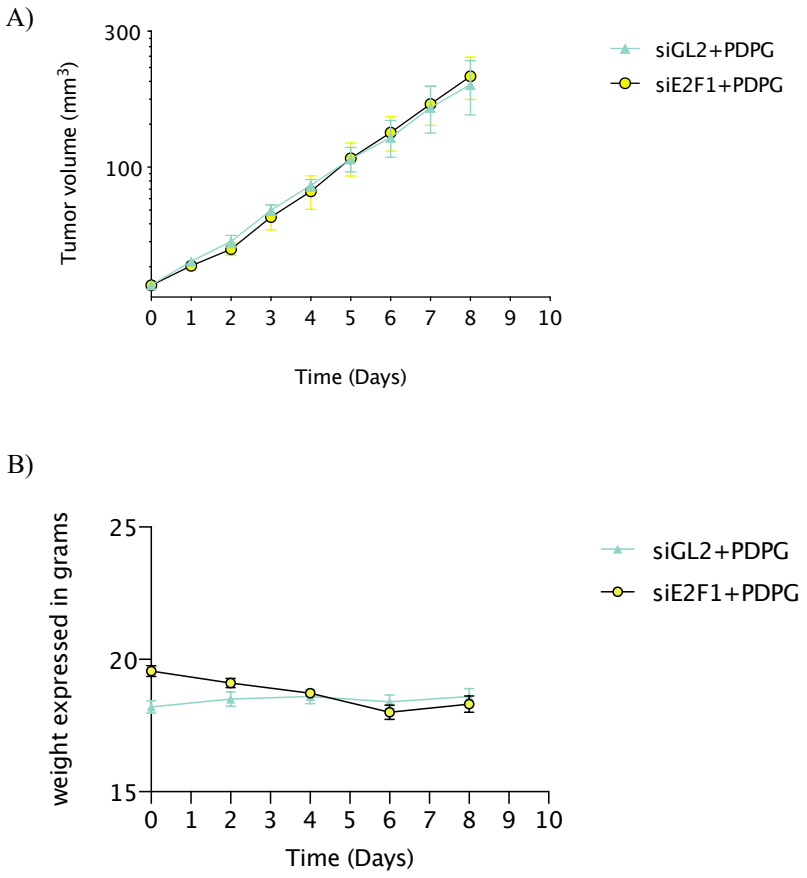

Figure 5.25. A) Tumour growth curve of mice treated with retro-orbitally injection of siE2F1+PDPG. Data are compared to siGL2+PDPG treated mice and shown as ±SEM. **B)** The graph, showing the weight of mice measured every second day, did not evidence any changes in mice weight during the experiment. Data are shown as ±SEM.

6 Discussion

6.1 Background

HCC is the most frequent primary malignant neoplasm of the liver and one of the most lethal human cancer type[424]. The prognosis is very poor with a 5-year overall survival rate estimated at less than 12%[425]. HCC displays high resistance to chemotherapy and radiation treatments[426,427]. Surgical resection, transplantation and ablation are treatments restricted to very early stages of the disease[428,429]. The first line systemic chemotherapy approved by the FDA is based on the use of Sorafenib[200,430]. However, Sorafenib clinical advantage is modest, prolonging both relapse-free survival and overall survival by only 2-3 months with a response rate of less than 5%[431,426].

Based on the above consideration it is evident that novel therapeutic approaches are urgently needed. In this regard, significant improvements in treatment efficacy may come from the enhancement of drug specificity. This goal may be achieved by combining the use of therapeutic molecules with tumour specific effects and delivery carriers with tumour targeting ability. siRNAs are attractive molecules due to the possibility to be engineered to target specific tumour genes. Polymeric-based delivery systems are emerging as versatile carriers to generate tumour-targeted delivery systems. Based on this background, we have investigated the therapeutic potential of siRNAs directed against HCC related genes (eEF1A1, eEF1A2 and E2F1) delivered by a polymer able to target ASGPR, overexpressed in HCC cells.

6.2 Rational of the investigation

6.2.1 Target genes

The choice of the target genes is based on the following consideration. We reported that eEF1A1 overexpression relates with HCC cell growth and differentiation phenotype[342]. Moreover, eEF1A1 seems to mediate the tumourigenic functions of the human HLA-F adjacent transcript 10 (FAT10) protein in HCC[348]. We also showed that eEF1A1 targeting by an aptamer or a siRNA, resulted in the profound impairment of the viability of cultured HCC cell lines[395,351]. eEF1A2 is overexpressed in HCC and the overexpression correlates with cancer cell growth and differentiation phenotype[342]. Moreover, eEF1A2 overexpression has been detected in HCC human tumour specimens[432,433]. eEF1A2 also takes part in the eEF1A2/PI3K/AKT/mTOR-dependent stabilization of MDM4 (Mouse Double Minute homolog 4) which in turn inactivates the anti-oncogene p53 thus resulting in a pro-tumourigenic effect in HCC[344]. eEF1A2 has been also

implicated in the oncogenic function of the mammalian timeless (TIM) protein in HCC[345]. The involvement of E2F1 in HCC[434,435] is rather articulated being its role dependent on HCC stage[146]. Despite this, the overall effect on HCC promotion is now recognized for E2F1. Finally, we observed that in HCC, eEF1A1 depletion results in the down regulation of E2F1 expression[395] thus displaying the E2F1 correlation with eEF1A1 in HCC. Together these findings show the rational to choose as siRNA targets eEF1A1, eEF1A2 and E2F1, all implicated in HCC.

6.2.2 Delivery material

Despite the great therapeutic potential of siRNAs, their practical use is limited by the chemical structure that does not allow the administration in the naked form[300]. In particular, they are subjected to fast degradation by the nucleases present in the biological environment. Moreover, cell membrane crossing is hindered by the electrostatic repulsion between the negatively charged phosphate groups present in siRNAs and the negatively charged surface of cellular membranes. In addition, siRNA hydrophilic nature substantially prevents the crossing of the hydrophobic layer of the cell membranes. Thus, to exert their biological functions they need to be protected. So far, many different siRNA delivery options have been developed, among which polymer-based material.

Polymers have been used in siRNA delivery due to: 1) the relatively low costs of production/isolation, 2) the possibility to undergo a wide range of chemical modifications that allow the optimization for the specific application, 3) the fact that they are biocompatible, biodegradable and have low immunogenic properties[300]. The high plasticity of the molecular structure of polymers is probably at the base of their success as delivery systems for different drugs including, but not limited to, siRNAs. In this work we have chosen a polymer we previously developed[317] based on a core of α,β-poly-(N-2-hydroxyethyl)-D,L-aspartamide (PHEA). PHEA was then derivatized by diethylene triamine (DETA) and by a galactosylated PEG derivative containing galactose (GAL) molecules, to obtain PHEA-DETA-PEG-GAL. This positively charged polymer was chosen for the ability to carry negatively charged siRNAs, for the hemocompatibility and for the potential to target ASGPR, overexpressed in HCC cells.

6.3 Results

6.3.1 Uptake

The studies we performed demonstrated an excellent uptake specificity for PDPG compared to PDP (Figure 5.2), related to the presence of the Gal residue. The role of the Gal is

shown by the fact that EGTA, a Ca^{2+} chelating agent, down regulates PDPG uptake due to the impairment of ASGPR (Figure 5.5) which is Ca^{2+} dependent. Moreover, we have evidences of a co-localization between PDPG and ASGPR (Figure 5.6). Whereas co-localization per se does not necessarily demonstrate a physical binding, it is highly suggestive of an PDPG-ASGPR interaction. Our uptake data also indicate that the siRNAs carried/released by PDPG are functional. This is shown by the siEGFP-PDPG complex, which is able to down regulate the EGFP expression in the HuH7-EGFP model. siRNA functionality is also confirmed by the functional *in vitro* and *in vivo* studies (sieEF1A1, sieEF21A2, siE2F1) showing a significant reduction in HuH7 expansion. Once again, Ca^{2+} chelation substantially prevents siEGFP-PDPG effect, as a consequence of ASGPR impairment. Notably this was not the case for the Lipofectamine, whose delivery mechanism does not depend on ASGPR and Ca^{2+}. The robustness of our data is further corroborated by the *in vivo* uptake studies (Figure 5.18). At all the time points considered, siEGFP+PDPG is superior in reducing EGFP expression compared to siEGFP+PDP. Notably, in these experiments, the green fluorescence of HuH7-EGFP tended to decrease over time also for siEGFP+PDP. This may depend on the fact that a certain amount of siEGFP+PDP can enter HuH7 as observed by the uptake study (confocal microscopy, Figure 5.3). Moreover, functional studies in cultured HuH7 (Figure 5.13) indicate a somewhat decrease of eEF1A1 mRNA following sieEF1A1+PDP treatment. Together these observations suggest that, although at a low level, PDP can enter into HuH7. Whatever the mechanism, our data indicate that PDP is poorly efficient in siRNA transfection and its cell entry is not depending on ASGPR. It is possible that at the basis of the phenomenon there is a passive uptake mechanism, common to positively charged molecules.

The above considerations support the ASGPR-dependent uptake of siRNA/PDPG, representing the first level of specificity of our approach. A second level of specificity occurs for sieEF1A2 and siE2F1. Besides being overexpressed in HCC, eEF1A2 is not expressed in the normal hepatocytes. E2F1 not only is overexpressed in HCC compared to healthy liver[146], it is not crucial for the growth of normal hepatocytes[436] where another family member, E2F4, plays the major role. Thus, the lack of eEF1A2 expression in the normal hepatocytes and the minor contribution of E2F1 to normal hepatocytes growth, suggest that sieEF1A2/siE2F1 may predominantly exert their effect in HCC cells but not in normal hepatocytes, thus preserving their functions.

6.4 Functional studies

6.4.1 In vitro

The *in vitro* studies indicate a clear time dependent effect on the reduction of cell viability for all the siRNAs tested (Figure 5.9), which well fits with the down regulation of cell cycle progression we have previously observed[437,395]. Viability down regulation peaks three days after transfection, as also confirmed by the decrease in cell number (Figure 5.10). The time dependent effect most likely descends from the processing of siRNA into the cells. Additionally, it is possible that the expansion of non-transduced cells contributes to "dilute" the downregulation of the viability of transduced cells. We observed these phenomena also when same siRNAs were delivered by Lipofectamine to HuH7[437,395], suggesting the independence from the transfection material employed. Obviously, the time dependent effect suggests that multiple injections would been necessary to permanently down regulate tumour cell viability. Despite these considerations, here we aimed to provide the proof of principle that the system siRNA-PDPG can be effective in down regulating cell viability.

The uptake efficiencies detected *in vitro* (about 30% evaluated by confocal microscopy – Figure 5.3), was paralleled by a target mRNA decrease induced by sieEF1A1/sieEF1A2/siE2F1-PDPG of 80%, 40% and 60%, respectively (Figure 5.11). As the mRNA levels of the siRNA target represent the gold standard to evaluate siRNA effectiveness, we can state that the silencing effect was remarkable. Target mRNA down-regulation was superior (in %) compared to the amount (in %) of transfected cells, as evaluated by confocal microscopy counting. We believe this just reflects the different sensibility between fluorescent microscopy and quantitative real time PCR, with this last technique being more sensible. Despite this aspect, a similar reduction in eEF1A1/A2 mRNA levels was detected in HuH7 (same sieEF1A1/A2 concentration and time point) when sieEF1A1/A2 were delivered by Lipofectamine[395]. Thus, with our novel copolymer PDPG we could reproduce Lipofectamine effectiveness but introducing the element of an extraordinary increased specificity of delivery. In the case of siE2F1, our previous data[437] performed in HuH7 where siE2F1 was delivered by Lipofectamine (same concentration and time point as here), indicate an E2F1 mRNA reduction of about 80% vs 60% of the current investigation. We believe that the modest reduction in target mRNA down-regulation can be paid in favour of a remarkable increased delivery specificity.

The considerable decrease in the eEF1A1 mRNA (80%) induced by sieEF1A1+PDPG, seems to be in disagreement with the more contained reduction (25%) in the protein level (Figure 5.12). We believe this may be explained by the huge abundance of eEF1A1[323] and its long half-life. We believe that the apparent discrepancy mRNA/protein cannot be ascribed to the delivery

system used, rather it may depend on the biology of the protein. This hypothesis is in line with our previous data[395] where sieEF1A1 (same concentration and time point as here) delivered by Lipofectamine to HuH7, resulted in a similar pattern of protein reduction (25%) *in vitro*. For sieEF1A2+PDPG and siE2F1+PDPG we observe a more contained divergence between the mRNA (40 or 55%, respectively) and protein (20 or 30%, respectively) reduction (Figures 5.11 and 5.12), most likely related to the higher turnover of the two proteins compared to eEF1A1. These differences are in line with our previous data where sieEF1A2[395,437] were delivered by Lipofectamine (same sieEF1A2/siE2F1 concentration and time point) to HuH7.

Regardless of the extent of the divergence between mRNA and protein down regulation for eEF1A1/A2 or E2F1, here, like in our previous study[437,395], we notice that a submaximal protein reduction is sufficient to induce a significant slow-down of HuH7 growth both *in vitro* (Figures 5.9 and 5.10) and *in vivo* (Figure 5.19). The question is how a submaximal reduction in protein target level can result in a clear impairment in cell growth? Whereas we do not have an unequivocal answer to this question, our previous observation about eEF1A1 may provide a hypothesis. We noticed that below a certain eEF1A1 protein decrease (around 40% decrease), the number of cells was no further reduced[438]. For example, despite a decrease of eEF1A1 protein level of about 80%, the reduction in cell number was comparable to that of a protein decrease around 40%. It is thus possible that for gene products strictly related to cell proliferation (like eEF1A1/A2 and E2F1) a submaximal decrease in their protein level is sufficient to perturb the delicate equilibrium of the proliferative pathway resulting in cell growth slow down.

Besides being siRNAs+PDPG effective and specific, they do not elicit any major side effects such as the induction of unexpected cell necrosis or apoptosis (Figures 5.14 and 5.16). This observation is in line with our previous works where we showed that sieEF1A1, sieEF1A2[395] and siE2F1[437] (neither induced unspecific cell necrosis nor apoptosis in HuH7 when delivered by Lipofectamine). Importantly, here we show that the negligible toxicity is confirmed also *in vivo* following both local intratumour injection of siRNA+PDPG (as evaluated by monitoring animal weight and different biochemical markers of organ functionality, Figure 5.24) and following systemic administration (as evaluated by monitoring animal weight Figure 5.25).

Whereas no evident signs of cell necrosis/apoptosis are detected, we observed a tendency towards autophagy induction by siRNA-PDPG (figure 5.15). Autophagy is a process by which cytoplasmic components are delivered into the lysosome for degradation leading to cell death[439]. Does autophagy induction mean that our siRNA-PDPG elicit nonspecifically a certain type of cell death? We do not believe this is the case. Indeed, we have evidences that in Mec-1 cell line (Chronic Lymphocytic Leukaemia cells, Dapas et al IJP, in print) and PC-3 (Prostatic

adenocarcinoma cell line, Bosutti et al submitted) sieEF1A1 elicits autophagy. The phenomenon seems to be totally unrelated to the delivery agent as in Mec-1 and PC-3 we used electroporation and lipofection, respectively, as delivery strategies. Which is the connection of eEF1A1/A2/E2F1 depletion with autophagy induction? So far it is not clear, however, for example, eEF1A1 is known to form complex with actin[440] which in turn is related to autophagy since its filamentous form is requested for autophagy to progress[441]. Thus, it is possible that perturbation of eEF1A1 (and perhaps eEF1A2, which shares with eEF1A1 many functions) levels affects actin leading to autophagy. The connection of E2F1 with autophagy may be related to the fact that in HuH7 we observed a functional crosstalk between eEF1A1 and E2F1[395].

6.4.2 In vivo

The effectiveness of sieEF1A1, sieEF1A2 and siE2F1 observed *in vitro* is fully confirmed *in vivo* following a single injection into the tumour mass (*long-term experiment*, Figure 5.19). The effect starts already one day post injection and lasts for 6, 7 or 9 days for sieEF1A1, sieEF1A2 and siE2F1, respectively. Compared to the *in vitro* data, the *in vivo* ones seem to have a longer duration, as from day 6 *in vitro* the effects are significantly decreased. Considering the differences between the two experimental set up, many variables can be responsible for this observation. For example, it is possible to hypothesize that *in vivo* siRNA-PDPG can stay longer (days) in contact with tumour cells compared to the *in vitro* situation, where the optimized contact time was set to 4 h. Thus, the longer interaction tumour cells-siRNA/PDPG could have enhanced transfection. This improved effectiveness of nucleic acid-based molecules *in vivo* compared to *in vitro* is a phenomenon we have already observed. In particular, the transfection of a DNA aptamer *in vivo* into the tumour mass formed by Mec-1 cells, resulted in a longer down regulation in cell growth compared to the same aptamer delivered to cultured MEC-1 cells (Dapas et all, IJP, in print).

The *in vivo* effectiveness of our siRNAs is confirmed in the *short-term experiments* (Figure 5.21), which was mainly used to investigate at the molecular level the effects of the tested siRNAs, in analogy to what done *in vitro*. For this reason, the time point of day 3 was chosen to mimic the in *vitro* data. For all the siRNA tested, we observed the reduction in the mRNA and protein levels of the respective targets (Figure 5.22). However, we could not observe a clear statistical decrease. We believe this can be due to two reasons. The first is that *in vitro* we could produce more replicates for each evaluation, compared to *in vivo* where we had to limit the number of replicates to the number of animal (kept low -5/6 animals for ethical reasons). The second is that in the tumour sample analyzed probably many mouse cells (endothelial, fibroblasts, white blood cells

etc) in addition to the injected human HuH7 where present. We do not know if our PDPG can transfect the different types of mice cells. Thus, it is possible that the mRNA/protein from the contaminating mouse cells could have increased the levels of the target mRNA and protein. Notably, the reagents used to detect the target mRNA/protein cannot discriminate between human and mice variants. Despite this aspect, the observed tendency to the reduction of the expression levels of the targets suggests that also *in vivo* the mechanisms of siRNA-PDPG action is comparable to the *in vitro* situation.

In this work, we have also performed a prelaminar experiment where siRNA-PDPG was systemically delivered. The data obtained (Figure 5.25) indicate non-significant differences in tumour growth between siGL2-PDPG (control) and siE2F1-PDPG, randomly chosen among the three siRNAs available. Many reasons can account for this observation, including the amount of siE2F1-PDPG administered. In the literature we have found that for siRNA delivered by ASGPR-targeted delivery systems the doses ranges from 1000 mg/Kg[442] to 36 mg/Kg[266] and 1 mg/Kg of animal[443]. We decided to start with a rather low dosage choosing 15 mg/Kg. It is thus possible that we have use a suboptimal dosage. We believe that for each particular delivery system the dosage should be experimentally optimized. Thus, in the next future we will progressively scale up the dose evaluating in parallel possible toxicity.

Finally, the data presented support the concept that our ASGPR-targeted PDPG, loaded by sieEF1A1, sieEF1A2 and siE2F1 displays high specificity and a remarkable anti-tumour effect both *in vitro* and *in vivo*. Our data are in line with the effects observed for other ASGPR-targeted delivery systems containing chemically synthesized siRNAs only[443,444,442,266]. The methodologies undertaken in the published works differ significantly from our (chemical nature of the deliver material, siRNA targets, HCC animal model, delivery route, siRNA amount administered etc.). However, it seems that the use of delivery materials with the common feature of being ASGPR targeted, leads to an effective HCC targeting with growth down regulation. This strongly indicates that ASGPR targeting is particularly promising for the development of future siRNA-based anti HCC therapeutic approaches.

7 References

1. Abdel-Misih, S. R. Z., Bloomston, M. & Bismuth, H. Liver Anatomy. (2010). doi:10.1016/j.suc.2010.04.017
2. Ozougwu, J. C. *Physiology of the liver*. *International Journal of Research in Pharmacy and Biosciences* **4**, (2017).
3. *Anatomy and Physiology of the Liver 2.1 Anatomy*.
4. Sun, S., Song, Z., Cotler, S. J. & Cho, M. Biomechanics and functionality of hepatocytes in liver cirrhosis. *J. Biomech.* **47**, 2205–2210 (2014).
5. Zhou, Z., Xu, M.-J. & Gao, B. Hepatocytes: a key cell type for innate immunity. *Cell. Mol. Immunol.* **13**, 301–315 (2016).
6. Poisson, J. *et al.* Liver sinusoidal endothelial cells: Physiology and role in liver diseases. *J. Hepatol.* **66**, 212–227 (2017).
7. Shetty, S., Lalor, P. F. & Adams, D. H. Liver sinusoidal endothelial cells — gatekeepers of hepatic immunity. *Nat. Rev. Gastroenterol. Hepatol.* **15**, 555–567 (2018).
8. Bilzer, M., Roggel, F. & Gerbes, A. L. Role of Kupffer cells in host defense and liver disease. *Liver Int.* **26**, 1175–1186 (2006).
9. Dixon, L. J., Barnes, M., Tang, H., Pritchard, M. T. & Nagy, L. E. Kupffer cells in the liver. *Compr. Physiol.* **3**, 785–97 (2013).
10. Kawada, N. The hepatic perisinusoidal stellate cell. *Histol. Histopathol.* **12**, 1069–80 (1997).
11. Oakley, F. & Mann, D. A. Stellate Cell Depletion Models. *Stellate Cells Heal. Dis.* 251–270 (2015). doi:10.1016/B978-0-12-800134-9.00015-4
12. Charlton, M. R. Protein metabolism and liver disease. *Baillieres. Clin. Endocrinol. Metab.* **10**, 617–35 (1996).
13. Rui, L. Energy metabolism in the liver. *Compr. Physiol.* **4**, 177–97 (2014).
14. Enjoji, M., Kohjima, M. & Nakamuta, M. Lipid Metabolism and the Liver. in *The Liver in Systemic Diseases* 105–122 (Springer Japan, 2016). doi:10.1007/978-4-431-55790-6_6
15. Roberts, E. A. & Sarkar, B. Liver as a key organ in the supply, storage, and excretion of copper. *Am. J. Clin. Nutr.* **88**, 851S-854S (2008).
16. Langer, M. & Chiandussi, L. Hormones and Liver: Some Aspects of the Problem. in *Assessment and Management of Hepatobiliary Disease* 217–225 (Springer Berlin Heidelberg, 1987). doi:10.1007/978-3-642-72631-6_29
17. Sookoian, S. & Pirola, C. J. Alanine and aspartate aminotransferase and glutamine-cycling pathway: Their roles in pathogenesis of metabolic syndrome. *World J. Gastroenterol.* **18**, 3775 (2012).
18. Chiang, J. Y. L. & Ferrell, J. M. Bile Acid Metabolism in Liver Pathobiology. *Gene Expr.* **18**, 71–87 (2018).
19. Hundt, M., Basit, H. & John, S. *Physiology, Bile Secretion*. *StatPearls* (StatPearls Publishing, 2019).
20. Payushina, O. V. Hematopoietic Microenvironment in the Fetal Liver: Roles of Different Cell Populations. *ISRN Cell Biol.* **2012**, 1–7 (2012).
21. Sajid, M. IB Singh - Textbook of Human Histology, 6th Edition.
22. Park, B.-J., Lee, Y.-J. & Lee, H.-R. Chronic liver inflammation: clinical implications beyond alcoholic liver disease. *World J. Gastroenterol.* **20**, 2168–75 (2014).
23. Ramadori, G., Moriconi, F., Malik, I. & Dudas, J. Physiology and pathophysiology of liver inflammation, damage and repair. *J. Physiol. Pharmacol.* **59 Suppl 1**, 107–17 (2008).
24. Cooper, G. M. The Development and Causes of Cancer. (2000).
25. Venturelli, S. *et al.* Epigenetic combination therapy as a tumor-selective treatment approach for hepatocellular carcinoma. *Cancer* **109**, 2132–2141 (2007).

26. Ghouri, Y. A., Mian, I. & Rowe, J. H. Review of hepatocellular carcinoma: Epidemiology, etiology, and carcinogenesis. *J. Carcinog.* **16**, 1 (2017).
27. Tang, A., Hallouch, O., Chernyak, V., Kamaya, A. & Sirlin, C. B. Epidemiology of hepatocellular carcinoma: target population for surveillance and diagnosis. *Abdom. Radiol.* **43**, 13–25 (2018).
28. Vitale, A. *et al. Personalized treatment of patients with very early hepatocellular carcinoma*. *Journal of Hepatology* **66**, (2017).
29. Chacko, S. & Samanta, S. "Hepatocellular carcinoma: A life-threatening disease". *Biomed. Pharmacother.* **84**, 1679–1688 (2016).
30. Zamor, P. J., Delemos, A. S. & Russo, M. W. Viral hepatitis and hepatocellular carcinoma: etiology and management. *J Gastrointest Oncol* **8**, 229–242 (2017).
31. El-Serag, H. B. Epidemiology of Viral Hepatitis and Hepatocellular Carcinoma. (2012). doi:10.1053/j.gastro.2011.12.061
32. Shouval, D. Hepatitis B vaccines. doi:10.1016/S0168-8278(03)00152-1
33. Niederhauser, C., Burnouf, T., Andonov, A. P., Candotti, D. & Laperche, S. Hepatitis B virus Blood Screening: Need for Reappraisal of Blood Safety Measures? *Article* **5**, 1 (2018).
34. Ma, L., Alla, N. R., Li, X., Mynbaev, O. A. & Shi, Z. Mother-to-child transmission of HBV: review of current clinical management and prevention strategies. *Rev. Med. Virol.* **24**, 396–406 (2014).
35. Lin, C.-L. & Kao, J.-H. Hepatitis B Virus Genotypes and Variants. doi:10.1101/cshperspect.a021436
36. Liang, T. J. Hepatitis B: the virus and disease. *Hepatology* **49**, S13-21 (2009).
37. Wynne, S. ., Crowther, R. . & Leslie, A. G. . The Crystal Structure of the Human Hepatitis B Virus Capsid. *Mol. Cell* **3**, 771–780 (1999).
38. Venkatakrishnan, B. & Zlotnick, A. The Structural Biology of Hepatitis B Virus: Form and Function. doi:10.1146/annurev-virology-110615-042238
39. Lamontagne, R. J., Bagga, S. & Bouchard, M. J. Hepatitis B virus molecular biology and pathogenesis. *Hepatoma Res.* **2**, 163 (2016).
40. Datta, S., Chatterjee, S., Veer, V. & Chakravarty, R. Molecular Biology of the Hepatitis B Virus for Clinicians BRIEF HISTORY OF INFECTIOUS HEPATITIS. *J. Clin. Exp. Hepatol.* **2**, 353–365 (2012).
41. Tavis, J. E. *et al.* The Hepatitis B Virus Ribonuclease H Is Sensitive to Inhibitors of the Human Immunodeficiency Virus Ribonuclease H and Integrase Enzymes. *PLoS Pathog.* **9**, e1003125 (2013).
42. Milich, D. & Liang, T. J. Exploring the biological basis of hepatitis B e antigen in hepatitis B virus infection. *Hepatology* **38**, 1075–1086 (2003).
43. Huang, C.-F., Lin, S.-S., Ho, Y.-C., Chen, F.-L. & Yang, C.-C. The immune response induced by hepatitis B virus principal antigens. *Cell. Mol. Immunol.* **3**, 97–106 (2006).
44. Brunetto, M. R. *et al.* Wild-type and e antigen-minus hepatitis B viruses and course of chronic hepatitis. *Proc. Natl. Acad. Sci. U. S. A.* **88**, 4186–90 (1991).
45. Shi, Y.-H., Shi, C.-H. & Bock, T. Molecular characteristics and stages of chronic hepatitis B virus infection. *World J Gastroenterol* **15**, 3099–3105 (2009).
46. Sureau, C. & Salisse, J. A conformational heparan sulfate binding site essential to infectivity overlaps with the conserved hepatitis B virus A-determinant. *Hepatology* **57**, 985–994 (2013).
47. Yan, H. *et al.* Sodium taurocholate cotransporting polypeptide is a functional receptor for human hepatitis B and D virus. *Elife* **1**, e00049 (2012).
48. Yuen, M.-F. *et al.* Hepatitis B virus infection. *Nat. Rev. Dis. Prim.* **4**, 18035 (2018).
49. Levrero, M. *et al.* Control of cccDNA function in hepatitis B virus infection. *J. Hepatol.* **51**, 581–592 (2009).
50. Zhao, X.-L. *et al.* Serum viral duplex-linear DNA proportion increases with the progression

of liver disease in patients infected with HBV. *Gut* **65**, 502–511 (2016).
51. Di Bisceglie, A. M. Hepatitis B And Hepatocellular Carcinoma. doi:10.1002/hep.22962
52. Muroyama, R. *et al.* Nucleotide change of codon 38 in the X gene of hepatitis B virus genotype C is associated with an increased risk of hepatocellular carcinoma. *J. Hepatol.* **45**, 805–812 (2006).
53. Li, L. *et al.* The Ras/Raf/MEK/ERK signaling pathway and its role in the occurrence and development of HCC (Review). *Oncology Letters* (2016). doi:10.3892/ol.2016.5110
54. Zucman-Rossi, J., Villanueva, A., Nault, J.-C. & Llovet, J. M. Genetic Landscape and Biomarkers of Hepatocellular Carcinoma. *Gastroenterology* **149**, 1226-1239.e4 (2015).
55. Kumar, S., Mani, K. & Andrisani, O. Hepatitis B Virus-Associated Hepatocellular Carcinoma and Hepatic Cancer Stem Cells. (2018). doi:10.3390/genes9030137
56. Li, H.-C. & Lo, S.-Y. Hepatitis C virus: Virology, diagnosis and treatment. *World J. Hepatol.* **7**, 1377–89 (2015).
57. Petruzziello, A., Marigliano, S., Loquercio, G., Cozzolino, A. & Cacciapuoti, C. Global epidemiology of hepatitis C virus infection: An up-date of the distribution and circulation of hepatitis C virus genotypes. *World J. Gastroenterol.* **22**, 7824–40 (2016).
58. Moosavy, S. H. *et al.* Epidemiology, transmission, diagnosis, and outcome of Hepatitis C virus infection. *Electron. physician* **9**, 5646–5656 (2017).
59. Alter, M. J. Epidemiology of hepatitis C virus infection. *World J. Gastroenterol.* **13**, 2436–41 (2007).
60. Manns, M. P., Wedemeyer, H. & Cornberg, M. Treating viral hepatitis C: efficacy, side effects, and complications. *Gut* **55**, 1350–9 (2006).
61. Rong, L. & Perelson, A. S. Treatment of hepatitis C virus infection with interferon and small molecule direct antivirals: viral kinetics and modeling. *Crit. Rev. Immunol.* **30**, 131–48 (2010).
62. Childs-Kean, L. M., Brumwell, N. A. & Lodl, E. F. Profile of sofosbuvir/velpatasvir/voxilaprevir in the treatment of hepatitis C. *Infection and Drug Resistance* **12**, 2259–2268 (2019).
63. Cory, T. J., Mu, Y., Gong, Y., Kodidela, S. & Kumar, S. Sofosbuvir + velpatasvir + voxilaprevir for the treatment of hepatitis C infection. *Expert Opin. Pharmacother.* **19**, 749–757 (2018).
64. Bukh, J. *The history of hepatitis C virus (HCV): Basic research reveals unique features in phylogeny, evolution and the viral life cycle with new perspectives for epidemic control*. *Journal of Hepatology* **65**, (2016).
65. Kumar, A. *et al.* Genotyping & diagnostic methods for hepatitis C virus: A need of low-resource countries. *Indian J. Med. Res.* **147**, 445–455 (2018).
66. Ashfaq, U. A., Javed, T., Rehman, S., Nawaz, Z. & Riazuddin, S. *An overview of HCV molecular biology, replication and immune responses*. *Virology Journal* **8**, (2011).
67. Catanese, M. T. *et al.* Ultrastructural analysis of hepatitis C virus particles. *Proc. Natl. Acad. Sci. U. S. A.* **110**, 9505–10 (2013).
68. Ashfaq, U. A., Javed, T., Rehman, S., Nawaz, Z. & Riazuddin, S. An overview of HCV molecular biology, replication and immune responses. *Virol. J.* **8**, 161 (2011).
69. Abdel-Hakeem, M. S. & Shoukry, N. H. Protective Immunity Against Hepatitis C: Many Shades of Gray. *Front. Immunol.* **5**, (2014).
70. Dustin, L. B., Bartolini, B., Capobianchi, M. R. & Pistello, M. Hepatitis C virus: life cycle in cells, infection and host response, and analysis of molecular markers influencing the outcome of infection and response to therapy. *Clin. Microbiol. Infect.* **22**, 826–832 (2016).
71. Virzì, A., Roca Suarez, A. A., Baumert, T. F. & Lupberger, J. Oncogenic Signaling Induced by HCV Infection. *Viruses* **10**, (2018).
72. Hoshida, Y., Fuchs, B. C., Bardeesy, N., Baumert, T. F. & Chung, R. T. Pathogenesis and prevention of hepatitis C virus-induced hepatocellular carcinoma. *J. Hepatol.* **61**, S79-90

(2014).
73. Fattovich, G., Stroffolini, T., Zagni, I. & Donato, F. Hepatocellular carcinoma in cirrhosis: Incidence and risk factors. *Gastroenterology* **127**, S35–S50 (2004).
74. Goossens, N. & Hoshida, Y. Hepatitis C virus-induced hepatocellular carcinoma. *Clin. Mol. Hepatol.* **21**, 105 (2015).
75. Street, A., Macdonald, A., McCormick, C. & Harris, M. Hepatitis C virus NS5A-mediated activation of phosphoinositide 3-kinase results in stabilization of cellular beta-catenin and stimulation of beta-catenin-responsive transcription. *J. Virol.* **79**, 5006–16 (2005).
76. Choi, S.-H. & Hwang, S. B. Modulation of the Transforming Growth Factor-β Signal Transduction Pathway by Hepatitis C Virus Nonstructural 5A Protein. *J. Biol. Chem.* **281**, 7468–7478 (2006).
77. Herbig, U., Jobling, W. A., Chen, B. P. C., Chen, D. J. & Sedivy, J. M. Telomere shortening triggers senescence of human cells through a pathway involving ATM, p53, and p21(CIP1), but not p16(INK4a). *Mol. Cell* **14**, 501–13 (2004).
78. Lim, J. S., Park, S.-H. & Jang, K. L. Hepatitis C virus Core protein overcomes stress-induced premature senescence by down-regulating p16 expression via DNA methylation. *Cancer Lett.* **321**, 154–161 (2012).
79. American Diabetes Association, A. D. Diagnosis and classification of diabetes mellitus. *Diabetes Care* **33 Suppl 1**, S62-9 (2010).
80. Baynest, H. W. & Baynes, H. W. Citation: Baynes HW (2015) Classification, Pathophysiology, Diagnosis and Management of Diabetes Mellitus. *Baynes J Diabetes Metab* **6**, 541 (2015).
81. Liu, C. Y. & Feng, G.-S. NCOA5, a molecular link between type 2 diabetes and liver cancer. *Hepatobiliary Surg. Nutr.* **3**, 106–8 (2014).
82. Bertolani, C. & Marra, F. The role of adipokines in liver fibrosis. *Pathophysiology* **15**, 91–101 (2008).
83. Mantovani, A. & Targher, G. Type 2 diabetes mellitus and risk of hepatocellular carcinoma: spotlight on nonalcoholic fatty liver disease. *Ann. Transl. Med.* **5**, 270 (2017).
84. Dharmalingam, M. & Yamasandhi, P. G. Nonalcoholic Fatty Liver Disease and Type 2 Diabetes Mellitus. *Indian J. Endocrinol. Metab.* **22**, 421–428 (2018).
85. Li, X., Wang, X. & Gao, P. Diabetes Mellitus and Risk of Hepatocellular Carcinoma. *Biomed Res. Int.* **2017**, 5202684 (2017).
86. Yang, J. D. *et al.* Diabetes Mellitus Heightens the Risk of Hepatocellular Carcinoma Except in Patients With Hepatitis C Cirrhosis. *Am. J. Gastroenterol.* **111**, 1573–1580 (2016).
87. Montella, M., Crispo, A. & Giudice, A. HCC, diet and metabolic factors: Diet and HCC. *Hepat. Mon.* **11**, 159–62 (2011).
88. Rega, G. *et al.* Vascular Endothelial Growth Factor Is Induced by the Inflammatory Cytokines Interleukin-6 and Oncostatin M in Human Adipose Tissue In Vitro and in Murine Adipose Tissue In Vivo. *Arterioscler. Thromb. Vasc. Biol.* **27**, 1587–1595 (2007).
89. Matsushita, H. & Takaki, A. Alcohol and hepatocellular carcinoma. *BMJ Open Gastroenterol.* **6**, e000260 (2019).
90. Ramadori, P., Cubero, F. J., Liedtke, C., Trautwein, C. & Nevzorova, Y. A. Alcohol and Hepatocellular Carcinoma: Adding Fuel to the Flame. *Cancers (Basel).* **9**, (2017).
91. Kikuchi, M. *et al.* Alcoholic Liver Cirrhosis and Significant Risk Factors for the Development of Alcohol-related Hepatocellular Carcinoma--Japan, 2012. *Nihon Arukoru Yakubutsu Igakkai Zasshi* **50**, 222–34 (2015).
92. Scotet, V. *et al.* Hereditary Hemochromatosis: Effect of Excessive Alcohol Consumption on Disease Expression in Patients Homozygous for the C282Y Mutation. *Am. J. Epidemiol.* **158**, 129–134 (2003).
93. Mobarra, N. *et al.* A Review on Iron Chelators in Treatment of Iron Overload Syndromes. *Int. J. Hematol. stem cell Res.* **10**, 239–247 (2016).

94. Kew, M. C. Hepatic iron overload and hepatocellular carcinoma. *Liver cancer* **3**, 31–40 (2014).
95. Vecchia, C. La. Coffee, liver enzymes, cirrhosis and liver cancer. *J. Hepatol.* **42**, 444–446 (2005).
96. Polesel, J. *et al.* Nutrients intake and the risk of hepatocellular carcinoma in Italy. *Eur. J. Cancer* **43**, 2381–2387 (2007).
97. Freedman, N. D. *et al.* Association of meat and fat intake with liver disease and hepatocellular carcinoma in the NIH-AARP cohort. *J. Natl. Cancer Inst.* **102**, 1354–65 (2010).
98. Sauvaget, C. *et al.* Vegetables and fruit intake and cancer mortality in the Hiroshima/Nagasaki Life Span Study. *Br. J. Cancer* **88**, 689–694 (2003).
99. Schütte, K., Schulz, C. & Malfertheiner, P. Nutrition and Hepatocellular Cancer. *Gastrointest. Tumors* **2**, 188 (2016).
100. Liu, Y. & Wu, F. Global Burden of Aflatoxin-Induced Hepatocellular Carcinoma: A Risk Assessment. *Environ. Health Perspect.* **118**, 818 (2010).
101. Fedeles, B. I. & Essigmann, J. M. Impact of DNA lesion repair, replication and formation on the mutational spectra of environmental carcinogens: Aflatoxin B1 as a case study. *DNA Repair (Amst).* **71**, 12–22 (2018).
102. Devereux, T. R. *et al.* CTNNB1 mutations and ?-catenin protein accumulation in human hepatocellular carcinomas associated with high exposure to aflatoxin B1. *Mol. Carcinog.* **31**, 68–73 (2001).
103. Pappachan, J. M., Babu, S., Krishnan, B. & Ravindran, N. C. Non-alcoholic Fatty Liver Disease: A Clinical Update. *J. Clin. Transl. Hepatol.* **5**, 384–393 (2017).
104. Romero-Gómez, M., Zelber-Sagi, S. & Trenell, M. Treatment of NAFLD with diet, physical activity and exercise. *J. Hepatol.* **67**, 829–846 (2017).
105. Andronescu, C. I., Purcarea, M. R. & Babes, P. A. Nonalcoholic fatty liver disease: epidemiology, pathogenesis and therapeutic implications. *J. Med. Life* **11**, 20–23 (2018).
106. Kikuchi, L., Oliveira, C. P. & Carrilho, F. J. Nonalcoholic fatty liver disease and hepatocellular carcinoma. *Biomed Res. Int.* **2014**, 106247 (2014).
107. Adams, L. A., Angulo, P. & Lindor, K. D. Nonalcoholic fatty liver disease. *CMAJ* **172**, 899–905 (2005).
108. Said, A. & Ghufran, A. Epidemic of non-alcoholic fatty liver disease and hepatocellular carcinoma. *World J. Clin. Oncol.* **8**, 429–436 (2017).
109. Wang, P., Kang, D., Cao, W., Wang, Y. & Liu, Z. Diabetes mellitus and risk of hepatocellular carcinoma: a systematic review and meta-analysis. *Diabetes. Metab. Res. Rev.* **28**, 109–122 (2012).
110. Francque, S. M. The Role of Non-alcoholic Fatty Liver Disease in Cardiovascular Disease. *Eur. Cardiol.* **9**, 10–15 (2014).
111. Powell, L. W. & Yapp, T. R. HEMOCHROMATOSIS. *Clin. Liver Dis.* **4**, 211–228 (2000).
112. Gattermann, N. The treatment of secondary hemochromatosis. *Dtsch. Arztebl. Int.* **106**, 499–504, I (2009).
113. Fargion, S., Valenti, L. & Fracanzani, A. L. Role of iron in hepatocellular carcinoma. *Clin. Liver Dis.* **3**, 108–110 (2014).
114. Schlageter, M., Terracciano, L. M., D'Angelo, S. & Sorrentino, P. Histopathology of hepatocellular carcinoma. *World J. Gastroenterol.* **20**, 15955–64 (2014).
115. Leong, T. Y.-M. & Leong, A. S.-Y. Epidemiology and carcinogenesis of hepatocellular carcinoma. *HPB (Oxford).* **7**, 5–15 (2005).
116. Libbrecht, L., Desmet, V. & Roskams, T. Preneoplastic lesions in human hepatocarcinogenesis. *Liver Int.* **25**, 16–27 (2005).
117. Kojiro, M. & Roskams, T. Early Hepatocellular Carcinoma and Dysplastic Nodules. *Semin. Liver Dis.* **25**, 133–142 (2005).

118. Park, Y. N. Hepatocellular dysplasia: large and small cell changes. *Pathology* **46**, S23 (2014).
119. Tinkle, C. L. & Haas-Kogan, D. Hepatocellular carcinoma: natural history, current management, and emerging tools. *Biologics* **6**, 207–19 (2012).
120. Teoh, N. C. Proliferative drive and liver carcinogenesis: Too much of a good thing? *J. Gastroenterol. Hepatol.* **24**, 1817–1825 (2009).
121. Yano, O. *et al.* The cytological characteristics of small cell change of dysplasia in small hepatic nodules. *Oncol. Rep.* **23**, 1229–32 (2010).
122. Watanabe, S. *et al.* Morphologic studies of the liver cell dysplasia. *Cancer* **51**, 2197–205 (1983).
123. Nascimento, C., Bottino, A., Nogueira, C. & Pannain, V. Analysis of morphological variables and arterialization in the differential diagnosis of hepatic nodules in explanted cirrhotic livers. *Diagn. Pathol.* **2**, 51 (2007).
124. Park, Y. N. *Update on Precursor and Early Lesions of Hepatocellular Carcinomas*.
125. Niu, Z.-S., Niu, X.-J. & Wang, W.-H. Genetic alterations in hepatocellular carcinoma: An update. *World J. Gastroenterol.* **22**, 9069–9095 (2016).
126. Kan, Z. *et al.* Whole-genome sequencing identifies recurrent mutations in hepatocellular carcinoma. *Genome Res.* **23**, 1422–1433 (2013).
127. Homayounfar, K. *et al.* Etiologic influence on chromosomal aberrations in European hepatocellular carcinoma identified by CGH. *Pathol. - Res. Pract.* **209**, 380–387 (2013).
128. Kaposi-Novak, P. *et al.* Central Role of c-Myc during Malignant Conversion in Human Hepatocarcinogenesis. *Cancer Res.* **69**, 2775–2782 (2009).
129. Jia, D. *et al.* Genome-wide copy number analyses identified novel cancer genes in hepatocellular carcinoma. *Hepatology* **54**, 1227–1236 (2011).
130. Xie, C.-R. *et al.* Significance of genetic variants in DLC1 and their association with hepatocellular carcinoma. *Mol. Med. Rep.* **12**, 4203–4209 (2015).
131. Tsuji, K. *et al.* PEG10 is a probable target for the amplification at 7q21 detected in hepatocellular carcinoma. *Cancer Genet. Cytogenet.* **198**, 118–125 (2010).
132. Dong, H. *et al.* Digital karyotyping reveals probable target genes at 7q21.3 locus in hepatocellular carcinoma. *BMC Med. Genomics* **4**, 60 (2011).
133. Ryland, G. L. *et al.* Loss of heterozygosity: what is it good for? *BMC Med. Genomics* **8**, 45 (2015).
134. Fu, L. *et al.* Down-regulation of tyrosine aminotransferase at a frequently deleted region 16q22 contributes to the pathogenesis of hepatocellular carcinoma. *Hepatology* **51**, 1624–1634 (2010).
135. Kanai, Y. *et al.* The E-cadherin gene is silenced by CpG methylation in human hepatocellular carcinomas. *Int. J. cancer* **71**, 355–9 (1997).
136. Slattery, M. L. *et al.* The co-regulatory networks of tumor suppressor genes, oncogenes, and miRNAs in colorectal cancer. *Genes. Chromosomes Cancer* **56**, 769–787 (2017).
137. Shen, L., Shi, Q. & Wang, W. Double agents: genes with both oncogenic and tumor-suppressor functions. *Oncogenesis* **7**, 25 (2018).
138. Martin, J. & Dufour, J.-F. Tumor suppressor and hepatocellular carcinoma. *World J. Gastroenterol.* **14**, 1720–33 (2008).
139. Matsui, D., Nagai, H., Mukozu, T., Ogino, Y. U. & Sumino, Y. VEGF in patients with advanced hepatocellular carcinoma receiving intra-arterial chemotherapy. *Anticancer Res.* **35**, 2205–10 (2015).
140. Zhu, A. X., Duda, D. G., Sahani, D. V. & Jain, R. K. HCC and angiogenesis: possible targets and future directions. *Nat. Rev. Clin. Oncol.* **8**, 292–301 (2011).
141. Chen, C. & Lou, T. Hypoxia inducible factors in hepatocellular carcinoma. *Oncotarget* **8**, 46691–46703 (2017).
142. Bisteau, X., Caldez, M. J. & Kaldis, P. The Complex Relationship between Liver Cancer

and the Cell Cycle: A Story of Multiple Regulations. *Cancers (Basel).* **6**, 79–111 (2014).
143. Yang, K., Hitomi, M. & Stacey, D. W. Variations in cyclin D1 levels through the cell cycle determine the proliferative fate of a cell. *Cell Div.* **1**, 32 (2006).
144. Wu, S.-Y. *et al.* Hepatocellular carcinoma-related cyclin D1 is selectively regulated by autophagy degradation system. *Hepatology* **68**, 141–154 (2018).
145. Huang, Y.-L. *et al.* Promising diagnostic and prognostic value of E2Fs in human hepatocellular carcinoma. *Cancer Manag. Res.* **11**, 1725–1740 (2019).
146. Rossella, F. *et al.* The Role of the Transcription Factor E2F1 in Hepatocellular Carcinoma. *Curr. Drug Deliv.* **13**, 1–1 (2016).
147. MacDonald, B. T., Tamai, K. & He, X. Wnt/beta-catenin signaling: components, mechanisms, and diseases. *Dev. Cell* **17**, 9–26 (2009).
148. Gao, C. *et al.* Exon 3 mutations of CTNNB1 drive tumorigenesis: a review. *Oncotarget* **9**, 5492–5508 (2018).
149. Khalaf, A. M. *et al.* Role of Wnt/β-catenin signaling in hepatocellular carcinoma, pathogenesis, and clinical significance. *J. Hepatocell. carcinoma* **5**, 61–73 (2018).
150. Waisberg, J. & Saba, G. T. Wnt-/-β-catenin pathway signaling in human hepatocellular carcinoma. *World J. Hepatol.* **7**, 2631 (2015).
151. Wang, W., Pan, Q., Fuhler, G. M., Smits, R. & Peppelenbosch, M. P. Action and function of Wnt/β-catenin signaling in the progression from chronic hepatitis C to hepatocellular carcinoma. *J. Gastroenterol.* **52**, 419–431 (2017).
152. Hao, J., Chen, D., Hao, J. & Chen, D. TGF-β signaling in hepatocellular carcinoma suppression and progression. *Tradit. Med. Res.* **3**, 10–21 (2018).
153. Syed, V. TGF-β Signaling in Cancer. *J. Cell. Biochem.* **117**, 1279–1287 (2016).
154. Hernanda, P. Y. *et al.* SMAD4 exerts a tumor-promoting role in hepatocellular carcinoma. *Oncogene* **34**, 5055–5068 (2015).
155. Katz, L. H. *et al.* TGF-β signaling in liver and gastrointestinal cancers. *Cancer Lett.* **379**, 166–72 (2016).
156. Yang, S. & Liu, G. Targeting the Ras/Raf/MEK/ERK pathway in hepatocellular carcinoma. *Oncol. Lett.* **13**, 1041–1047 (2017).
157. Gedaly, R. *et al.* The role of PI3K/mTOR inhibition in combination with sorafenib in hepatocellular carcinoma treatment. *Anticancer Res.* **32**, 2531–6 (2012).
158. Peyrou, M., Bourgoin, L. & Foti, M. PTEN in liver diseases and cancer. *World J. Gastroenterol.* **16**, 4627–33 (2010).
159. Jia, Y., Wang, Y. & Xie, J. The Hedgehog pathway: role in cell differentiation, polarity and proliferation. *Arch. Toxicol.* **89**, 179–91 (2015).
160. Della Corte, C. M. *et al.* Implication of the Hedgehog pathway in hepatocellular carcinoma. *World J. Gastroenterol.* **23**, 4330–4340 (2017).
161. Dupont, C., Armant, D. R. & Brenner, C. A. Epigenetics: definition, mechanisms and clinical perspective. *Semin. Reprod. Med.* **27**, 351–7 (2009).
162. Weinhold, B. Epigenetics: the science of change. *Environ. Health Perspect.* **114**, A160-7 (2006).
163. Moore, L. D., Le, T. & Fan, G. DNA methylation and its basic function. *Neuropsychopharmacology* **38**, 23–38 (2013).
164. Ehrlich, M., Lacey, M., Ehrlich, M. & Lacey, M. Epigenetic Alterations in Oncogenesis. *Adv. Exp. Med. Biol.* **754**,
165. Sun, G. *et al.* Methylation analysis of p16, SLIT2, SCARA5, and Runx3 genes in hepatocellular carcinoma. *Medicine (Baltimore).* **96**, e8279 (2017).
166. Zhang, X. *et al.* Analysis of Liver Tumor-Prone Mouse Models of the Hippo Kinase Scaffold Proteins RASSF1A and SAV1. *Cancer Res.* **76**, 2824–2835 (2016).
167. Ishak, C. A. *et al.* An RB-EZH2 Complex Mediates Silencing of Repetitive DNA Sequences. *Mol. Cell* **64**, 1074–1087 (2016).

168. Nishida, N. & Kudo, M. Alteration of Epigenetic Profile in Human Hepatocellular Carcinoma and Its Clinical Implications. *Liver cancer* **3**, 417–27 (2014).
169. Lim, S.-O. *et al.* Epigenetic Changes Induced by Reactive Oxygen Species in Hepatocellular Carcinoma: Methylation of the E-cadherin Promoter. *Gastroenterology* **135**, 2128-2140.e8 (2008).
170. Okamoto, Y. *et al.* Hepatitis Virus Infection Affects DNA Methylation in Mice With Humanized Livers. *Gastroenterology* **146**, 562–572 (2014).
171. Murphy, S. K. *et al.* Relationship Between Methylome and Transcriptome in Patients With Nonalcoholic Fatty Liver Disease. *Gastroenterology* **145**, 1076–1087 (2013).
172. Gao, W. *et al.* Variable DNA methylation patterns associated with progression of disease in hepatocellular carcinomas. *Carcinogenesis* **29**, 1901–1910 (2008).
173. Liu, M., Jiang, L. & Guan, X.-Y. The genetic and epigenetic alterations in human hepatocellular carcinoma: a recent update. *Protein Cell* **5**, 673–91 (2014).
174. Haggarty, S. J. & Tsai, L.-H. Probing the role of HDACs and mechanisms of chromatin-mediated neuroplasticity. *Neurobiol. Learn. Mem.* **96**, 41–52 (2011).
175. Wahid, B., Ali, A., Rafique, S. & Idrees, M. New Insights into the Epigenetics of Hepatocellular Carcinoma. *Biomed Res. Int.* **2017**, 1609575 (2017).
176. Magerl, C. *et al.* H3K4 dimethylation in hepatocellular carcinoma is rare compared with other hepatobiliary and gastrointestinal carcinomas and correlates with expression of the methylase Ash2 and the demethylase LSD1. *Hum. Pathol.* **41**, 181–189 (2010).
177. Shon, J. K. *et al.* Hepatitis B virus-X protein recruits histone deacetylase 1 to repress insulin-like growth factor binding protein 3 transcription. *Virus Res.* **139**, 14–21 (2009).
178. Schulze, K. *et al.* Exome sequencing of hepatocellular carcinomas identifies new mutational signatures and potential therapeutic targets. *Nat. Genet.* **47**, 505–511 (2015).
179. Wong, C.-M. *et al.* Up-regulation of histone methyltransferase SETDB1 by multiple mechanisms in hepatocellular carcinoma promotes cancer metastasis. *Hepatology* **63**, 474–487 (2016).
180. Chen, H. P., Zhao, Y. T. & Zhao, T. C. Histone deacetylases and mechanisms of regulation of gene expression. *Crit. Rev. Oncog.* **20**, 35–47 (2015).
181. Liu, K.-Y., Wang, L.-T. & Hsu, S.-H. Modification of Epigenetic Histone Acetylation in Hepatocellular Carcinoma. *Cancers (Basel).* **10**, (2018).
182. Linnekamp, J. F., Butter, R., Spijker, R., Medema, J. P. & van Laarhoven, H. W. M. Clinical and biological effects of demethylating agents on solid tumours – A systematic review. *Cancer Treat. Rev.* **54**, 10–23 (2017).
183. Kung, J. T. Y., Colognori, D. & Lee, J. T. Long noncoding RNAs: past, present, and future. *Genetics* **193**, 651–69 (2013).
184. Mehra, M. & Chauhan, R. Long Noncoding RNAs as a Key Player in Hepatocellular Carcinoma. *Biomark. Cancer* **9**, 1179299X17737301 (2017).
185. Peng, L. *et al.* The emergence of long non-coding RNAs in hepatocellular carcinoma: an update. *J. Cancer* **9**, 2549–2558 (2018).
186. Quagliata, L. *et al.* Long noncoding RNA HOTTIP/HOXA13 expression is associated with disease progression and predicts outcome in hepatocellular carcinoma patients. *Hepatology* **59**, 911–923 (2014).
187. He, X. *et al.* Long non-coding RNA AK058003, as a precursor of miR-15a, interacts with HuR to inhibit the expression of γ-synuclein in hepatocellular carcinoma cells. *Oncotarget* **8**, 9451–9465 (2017).
188. Shi, H., Xu, Y., Yi, X., Fang, D. & Hou, X. Current Research Progress on Long Noncoding RNAs Associated with Hepatocellular Carcinoma. *Anal. Cell. Pathol. (Amst).* **2019**, 1534607 (2019).
189. Tellapuri, S., Sutphin, P. D., Beg, M. S., Singal, A. G. & Kalva, S. P. Staging systems of hepatocellular carcinoma: A review. *Indian J. Gastroenterol.* **37**, 481–491 (2018).

190. Llovet, J. M., Burroughs, A. & Bruix, J. Hepatocellular carcinoma. *Lancet* **362**, 1907–1917 (2003).
191. Llovet, J. M. *et al.* Design and Endpoints of Clinical Trials in Hepatocellular Carcinoma. *JNCI J. Natl. Cancer Inst.* **100**, 698–711 (2008).
192. Bruix, J., Reig, M. & Sherman, M. Evidence-Based Diagnosis, Staging, and Treatment of Patients With Hepatocellular Carcinoma. *Gastroenterology* **150**, 835–853 (2016).
193. Llovet, J. M., Fuster, J. & Bruix, J. The Barcelona Approach: Diagnosis, Staging, and Treatment of Hepatocellular Carcinoma. (2004). doi:10.1002/lt.20034
194. Chedid, M. F. *et al.* HEPATOCELLULAR CARCINOMA: DIAGNOSIS AND OPERATIVE MANAGEMENT. *Arq. Bras. Cir. Dig.* **30**, 272–278 (2017).
195. Bolondi, L. *et al.* Heterogeneity of Patients with Intermediate (BCLC B) Hepatocellular Carcinoma: Proposal for a Subclassification to Facilitate Treatment Decisions. *Semin. Liver Dis.* **32**, 348–359 (2013).
196. Carr, B. I. *Hepatocellular carcinoma : diagnosis and treatment*.
197. Lurje, I. *et al.* Treatment Strategies for Hepatocellular Carcinoma – a Multidisciplinary Approach. *Int. J. Mol. Sci.* **20**, (2019).
198. Gervais, D. A. & Arellano, R. S. Percutaneous Tumor Ablation for Hepatocellular Carcinoma. *Am. J. Roentgenol.* **197**, 789–794 (2011).
199. Lee, E. W. & Khan, S. Recent advances in transarterial embolotherapies in the treatment of hepatocellular carcinoma. *Clin. Mol. Hepatol.* **23**, 265–272 (2017).
200. Llovet, J. & Bruix, J. Systematic review of randomized trials for unresectable hepatocellular carcinoma: Chemoembolization improves survival. *Hepatology* **37**, 429–442 (2003).
201. Schirrmacher, V. From chemotherapy to biological therapy: A review of novel concepts to reduce the side effects of systemic cancer treatment (Review). *Int. J. Oncol.* **54**, 407–419 (2019).
202. Okusaka, T. & Ikeda, M. Immunotherapy for hepatocellular carcinoma: current status and future perspectives. *ESMO Open* **3**, e000455 (2018).
203. Ikeda, M. *et al.* Chemotherapy for hepatocellular carcinoma: current status and future perspectives. *Jpn. J. Clin. Oncol.* **48**, 103–114 (2018).
204. Ikeda, M. *et al.* Systemic Chemotherapy for Advanced Hepatocellular Carcinoma: Past, Present, and Future. *Dis. (Basel, Switzerland)* **3**, 360–381 (2015).
205. Keating, G. M. Sorafenib: A Review in Hepatocellular Carcinoma. *Target. Oncol.* **12**, 243–253 (2017).
206. Gholam, P. The Role of Sorafenib in Hepatocellular Carcinoma. *Gastroenterol. Hepatol. (N. Y).* **11**, 253–5 (2015).
207. Cheng, A.-L. *et al.* Efficacy and safety of sorafenib in patients in the Asia-Pacific region with advanced hepatocellular carcinoma: a phase III randomised, double-blind, placebo-controlled trial. *Lancet Oncol.* **10**, 25–34 (2009).
208. Longo, L., de Freitas, L. B. R., Santos, D., Grivicich, I. & Álvares-da-Silva, M. R. Sorafenib for Advanced Hepatocellular Carcinoma: A Real-Life Experience. *Dig. Dis.* **36**, 377–384 (2018).
209. Llovet, J. M. *et al.* Sorafenib in Advanced Hepatocellular Carcinoma. *N. Engl. J. Med.* **359**, 378–390 (2008).
210. Xie, B., Wang, D. H. & Spechler, S. J. Sorafenib for treatment of hepatocellular carcinoma: a systematic review. *Dig. Dis. Sci.* **57**, 1122–9 (2012).
211. Lei, X.-F. *et al.* Effect and safety of sorafenib in patients with intermediate hepatocellular carcinoma who received transarterial chemoembolization: A retrospective comparative study. *World J. Clin. cases* **6**, 74–83 (2018).
212. Chen, J. *et al.* Potential molecular, cellular and microenvironmental mechanism of sorafenib resistance in hepatocellular carcinoma. *Cancer Lett.* **367**, 1–11 (2015).
213. Abdel-Aziz, A. K., Abdel-Naim, A. B., Shouman, S., Minucci, S. & Elgendy, M. From

Resistance to Sensitivity: Insights and Implications of Biphasic Modulation of Autophagy by Sunitinib. *Front. Pharmacol.* **8**, 718 (2017).
214. Wörns, M. A. *et al.* Sunitinib in Patients with Advanced Hepatocellular Carcinoma after Progression under Sorafenib Treatment. *Oncology* **79**, 85–92 (2010).
215. Toh, H. C. *et al.* Phase 2 trial of linifanib (ABT-869) in patients with unresectable or metastatic hepatocellular carcinoma. *Cancer* **119**, 380–387 (2013).
216. Cainap, C. *et al.* Linifanib Versus Sorafenib in Patients With Advanced Hepatocellular Carcinoma: Results of a Randomized Phase III Trial. *J. Clin. Oncol.* **33**, 172 (2015).
217. Finn, R. S. *et al.* Phase II, Open-Label Study of Brivanib as Second-Line Therapy in Patients with Advanced Hepatocellular Carcinoma. *Clin. Cancer Res.* **18**, 2090–2098 (2012).
218. Yap, T. A. *et al.* Phase I Trial of a Selective c-MET Inhibitor ARQ 197 Incorporating Proof of Mechanism Pharmacodynamic Studies. *J. Clin. Oncol.* **29**, 1271–1279 (2011).
219. Santoro, A. *et al.* Tivantinib for second-line treatment of advanced hepatocellular carcinoma: a randomised, placebo-controlled phase 2 study. *Lancet Oncol.* **14**, 55–63 (2013).
220. Zhu, A. X. *et al.* EVOLVE-1: Phase 3 study of everolimus for advanced HCC that progressed during or after sorafenib. *J. Clin. Oncol.* **32**, 172–172 (2014).
221. Finkelmeier, F., Waidmann, O. & Trojan, J. Nivolumab for the treatment of hepatocellular carcinoma. *Expert Rev. Anticancer Ther.* **18**, 1169–1175 (2018).
222. Reig, M., da Fonseca, L. G. & Faivre, S. New trials and results in systemic treatment of HCC. *J. Hepatol.* **69**, 525–533 (2018).
223. Le Grazie, M., Biagini, M. R., Tarocchi, M., Polvani, S. & Galli, A. Chemotherapy for hepatocellular carcinoma: The present and the future. *World J. Hepatol.* **9**, 907–920 (2017).
224. Howell, P. M., Liu, Z., Khong, H. T. & Khong, H. T. Demethylating Agents in the Treatment of Cancer. *Pharmaceuticals (Basel).* **3**, 2022–2044 (2010).
225. Derissen, E. J. B., Beijnen, J. H. & Schellens, J. H. M. Concise drug review: azacitidine and decitabine. *Oncologist* **18**, 619–24 (2013).
226. Diesch, J. *et al.* A clinical-molecular update on azanucleoside-based therapy for the treatment of hematologic cancers. *Clin. Epigenetics* **8**, 71 (2016).
227. Venturelli, S. *et al.* Dual antitumour effect of 5-azacytidine by inducing a breakdown of resistance-mediating factors and epigenetic modulation. doi:10.1136/gut.2010.208041
228. Mocellin, S. & Provenzano, M. RNA interference: learning gene knock-down from cell physiology. *J. Transl. Med.* **2**, 39 (2004).
229. Fire, A. *et al.* Potent and specific genetic interference by double-stranded RNA in Caenorhabditis elegans. *Nature* **391**, 806–811 (1998).
230. Perrimon, N., Ni, J.-Q. & Perkins, L. In vivo RNAi: today and tomorrow. *Cold Spring Harb. Perspect. Biol.* **2**, a003640 (2010).
231. Song, M.-S. & Rossi, J. J. Molecular mechanisms of Dicer: endonuclease and enzymatic activity. *Biochem. J.* **474**, 1603–1618 (2017).
232. Kurzynska-Kokorniak, A. *et al.* Revealing a new activity of the human Dicer DUF283 domain in vitro. *Sci. Rep.* **6**, 23989 (2016).
233. Svobodova, E., Kubikova, J. & Svoboda, P. Production of small RNAs by mammalian Dicer. *Pflugers Arch. Eur. J. Physiol.* 1–14 (2016). doi:10.1007/s00424-016-1817-6
234. Dominska, M. & Dykxhoorn, D. M. Breaking down the barriers: siRNA delivery and endosome escape. *J Cell Sci* **123**, 1183–1189 (2010).
235. MacRae, I. J. *et al.* Structural Basis for Double-Stranded RNA Processing by Dicer. *Science (80-.).* **311**, 195–198 (2006).
236. Carthew, R. W. & Sontheimer, E. J. Origins and Mechanisms of miRNAs and siRNAs. *Cell* **136**, 642–55 (2009).
237. Lam, J. K. W., Chow, M. Y. T., Zhang, Y. & Leung, S. W. S. siRNA Versus miRNA as Therapeutics for Gene Silencing. *Mol. Ther. Nucleic Acids* **4**, e252 (2015).

238. Perwitasari, O., Bakre, A., Tompkins, S. M. & Tripp, R. A. siRNA Genome Screening Approaches to Therapeutic Drug Repositioning. *Pharmaceuticals (Basel).* **6**, 124–60 (2013).
239. Guo, W., Chen, W., Yu, W., Huang, W. & Deng, W. Small interfering RNA-based molecular therapy of cancers. *Chin. J. Cancer* **32**, 488–93 (2013).
240. Scaggiante, B. *et al.* Improving siRNA Bio-Distribution and Minimizing Side Effects. *Curr. Drug Metab.* **12**, 11–23 (2011).
241. Farra, R. *et al.* Strategies for Delivery of siRNAs to Ovarian Cancer Cells. *Pharmaceutics* **11**, (2019).
242. Huang, Y. *et al.* Elimination pathways of systemically delivered siRNA. *Mol. Ther.* **19**, 381–385 (2011).
243. Jackson, A. L. & Linsley, P. S. Recognizing and avoiding siRNA off-target effects for target identification and therapeutic application. *Nature Reviews Drug Discovery* **9**, 57–67 (2010).
244. Grassi, M. *et al.* Current Strategies to Improve the Efficacy and the Delivery of Nucleic Acid Based Drugs. *doi.org* 92–120 (2010). doi:10.2174/157436210791112163
245. Barba, A. A. *et al.* Engineering approaches in siRNA delivery. *Int. J. Pharm.* **525**, 343–358 (2017).
246. Sun, J., Wang, J. & Yang, Z. Supramolecular assembly models of siRNA delivery systems. *Chinese J. Chem.* **33**, 79–89 (2015).
247. Barba, A. *et al.* Novel Lipid and Polymeric Materials as Delivery Systems for Nucleic Acid Based Drugs. *Curr. Drug Metab.* **16**, 427–452 (2015).
248. Zatsepin, T. S., Kotelevtsev, Y. V & Koteliansky, V. Lipid nanoparticles for targeted siRNA delivery – going from bench to bedside. *Int. J. Nanomedicine* **11**, 3077 (2016).
249. Xue, H. Y., Guo, P., Wen, W.-C. & Wong, H. L. Lipid-Based Nanocarriers for RNA Delivery. *Curr. Pharm. Des.* **21**, 3140–7 (2015).
250. Sercombe, L. *et al.* Advances and challenges of liposome assisted drug delivery. *Front. Pharmacol.* **6**, 1–13 (2015).
251. Xu, C. & Wang, J. Delivery systems for siRNA drug development in cancer therapy. *Asian J. Pharm. Sci.* **10**, 1–12 (2015).
252. Barba, A. A., Bochicchio, S., Dalmoro, A. & Lamberti, G. Lipid Delivery Systems for Nucleic-Acid-Based-Drugs: From Production to Clinical Applications. *Pharmaceutics* **11**, 360 (2019).
253. Xia, Y., Tian, J. & Chen, X. Effect of surface properties on liposomal siRNA delivery. *Biomaterials* **79**, 56–68 (2016).
254. Kapoor, M. & Burgess, D. J. Efficient and safe delivery of siRNA using anionic lipids: Formulation optimization studies. *Int. J. Pharm.* **432**, 80–90 (2012).
255. Kapoor, M., Burgess, D. J. & Patil, S. D. Physicochemical characterization techniques for lipid based delivery systems for siRNA. *Int. J. Pharm.* **427**, 35–57 (2012).
256. Naseri, N., Valizadeh, H. & Zakeri-Milani, P. Solid Lipid Nanoparticles and Nanostructured Lipid Carriers: Structure,Preparation and Application. *Adv. Pharm. Bull.* **5**, 305 (2015).
257. Mukherjee, S., Ray, S. & Thakur, R. Solid lipid nanoparticles: A modern formulation approach in drug delivery system. *Indian J. Pharm. Sci.* **71**, 349 (2009).
258. Kim, J. H. *et al.* Tumor-targeted delivery of paclitaxel using low density lipoprotein-mimetic solid lipid nanoparticles. *Mol. Pharm.* **12**, 1230–1241 (2015).
259. McMahon, K. M. *et al.* Synthetic High-Density Lipoprotein-Like Nanoparticles as Cancer Therapy. in *Cancer treatment and research* **166**, 129–150 (2015).
260. Bozzuto, G. & Molinari, A. Liposomes as nanomedical devices. *Int. J. Nanomedicine* **10**, 975–99 (2015).
261. Trofimov, A., Ivanova, A., Zyuzin, M. & Timin, A. Porous Inorganic Carriers Based on Silica, Calcium Carbonate and Calcium Phosphate for Controlled/Modulated Drug

Delivery: Fresh Outlook and Future Perspectives. *Pharmaceutics* **10**, 167 (2018).
262. Jafari, S. *et al.* Mesoporous silica nanoparticles for therapeutic/diagnostic applications. *Biomed. Pharmacother.* **109**, 1100–1111 (2019).
263. Tarn, D. *et al.* Mesoporous silica nanoparticle nanocarriers: Biofunctionality and biocompatibility. *Acc. Chem. Res.* **46**, 792–801 (2013).
264. Narayan, R., Nayak, U., Raichur, A. & Garg, S. Mesoporous Silica Nanoparticles: A Comprehensive Review on Synthesis and Recent Advances. *Pharmaceutics* **10**, 118 (2018).
265. Hanafy, N. A. N., El-Kemary, M. & Leporatti, S. Micelles Structure Development as a Strategy to Improve Smart Cancer Therapy. *Cancers (Basel).* **10**, (2018).
266. Wang, H. X., Xiong, M. H., Wang, Y. C., Zhu, J. & Wang, J. N-acetylgalactosamine functionalized mixed micellar nanoparticles for targeted delivery of siRNA to liver. *J. Control. Release* **166**, 106–114 (2013).
267. Lee, S.-Y. *et al.* A theranostic micelleplex co-delivering SN-38 and VEGF siRNA for colorectal cancer therapy. *Biomaterials* **86**, 92–105 (2016).
268. Zhao, Y.-Z., Du, L.-N., Lu, C.-T., Jin, Y.-G. & Ge, S.-P. Potential and problems in ultrasound-responsive drug delivery systems. *Int. J. Nanomedicine* **8**, 1621–33 (2013).
269. Tian, J. *et al.* A novel approach to making the gas-filled liposome real: Based on the interaction of lipid with free nanobubble within the solution. *ACS Appl. Mater. Interfaces* **7**, 26579–26584 (2015).
270. Mullin, L. B., Phillips, L. C. & Dayton, P. A. Nanoparticle delivery enhancement with acoustically activated microbubbles. *IEEE Trans. Ultrason. Ferroelectr. Freq. Control* **60**, 65–77 (2013).
271. Shapiro, G. *et al.* Multiparameter evaluation of in vivo gene delivery using ultrasound-guided, microbubble-enhanced sonoporation. *J. Control. Release* **223**, 157–164 (2016).
272. Sirsi, S. R. & Borden, M. A. Advances in ultrasound mediated gene therapy using microbubble contrast agents. *Theranostics* **2**, 1208–1222 (2012).
273. Delalande, A. *et al.* Cationic gas-filled microbubbles for ultrasound-based nucleic acids delivery. *Biosci. Rep.* **37**, (2017).
274. Santhosh, P. B. & Ulrih, N. P. Multifunctional superparamagnetic iron oxide nanoparticles: Promising tools in cancer theranostics. *Cancer Lett.* **336**, 8–17 (2013).
275. Zou, P. *et al.* Superparamagnetic Iron Oxide Nanotheranostics for Targeted Cancer Cell Imaging and pH-Dependent Intracellular Drug Release. *Mol. Pharm.* **7**, 1974–1984 (2010).
276. Indira, T. Magnetic Nanoparticles: A Review. *Int. J. Pharm.* **3**, 1035–1042 (2010).
277. Wahajuddin & Arora, S. Superparamagnetic iron oxide nanoparticles: magnetic nanoplatforms as drug carriers. *Int J Nanomedicine.* **7**, 3445–3471 (2012).
278. Hoang, M. D. *et al.* Branched Polyethylenimine-Superparamagnetic Iron Oxide Nanoparticles (bPEI-SPIONs) Improve the Immunogenicity of Tumor Antigens and Enhance Th1 Polarization of Dendritic Cells. *J. Immunol. Res.* **2015**, (2015).
279. Sarett, S. M., Nelson, C. E. & Duvall, C. L. Technologies for controlled, local delivery of siRNA. *J. Control. Release* **218**, 94–113 (2015).
280. Lee, Y. H., Park, H. I. & Choi, J. S. Novel glycol chitosan-based polymeric gene carrier synthesized by a Michael addition reaction with low molecular weight polyethylenimine. *Carbohydr. Polym.* **137**, 669–677 (2016).
281. Höbel, S. & Aigner, A. Polyethylenimines for siRNA and miRNA delivery *in vivo*. *Wiley Interdiscip. Rev. Nanomedicine Nanobiotechnology* **5**, 484–501 (2013).
282. Liu, L. *et al.* Efficient and Tumor Targeted siRNA Delivery by Polyethylenimine-graft-polycaprolactone-block-poly(ethylene glycol)-folate (PEI-PCL-PEG-Fol). *Mol. Pharm.* **13**, 134–143 (2016).
283. Muralidharan, P., Mallory, E., Malapit, M., Don, H. & Mansour, H. M. Inhalable PEGylated phospholipid nanocarriers and PEGylated therapeutics for respiratory delivery as aerosolized colloidal dispersions and dry powder inhalers. *Pharmaceutics* **6**, 333–353

(2014).
284. Kolate, A. *et al.* PEG - A versatile conjugating ligand for drugs and drug delivery systems. *J. Control. Release* **192**, 67–81 (2014).
285. Bao, Y. *et al.* Effect of PEGylation on Biodistribution and Gene Silencing of siRNA/Lipid Nanoparticle Complexes. *Pharm. Res.* **30**, 342–351 (2013).
286. Usman, A. *et al.* Chitin and chitosan based polyurethanes: A review of recent advances and prospective biomedical applications. *Int. J. Biol. Macromol.* **86**, 630–645 (2016).
287. Ahmed, T. & Aljaeid, B. Preparation, characterization, and potential application of chitosan, chitosan derivatives, and chitosan metal nanoparticles in pharmaceutical drug delivery. *Drug Des. Devel. Ther.* 483 (2016). doi:10.2147/DDDT.S99651
288. Zhong, J. *et al.* Development of hybrid-type modified chitosan derivative nanoparticles for the intracellular delivery of midkine-siRNA in hepatocellular carcinoma cells. *Hepatobiliary Pancreat. Dis. Int.* **14**, 82–89 (2015).
289. Gidwani, B. & Vyas, A. A Comprehensive Review on Cyclodextrin-Based Carriers for Delivery of Chemotherapeutic Cytotoxic Anticancer Drugs. *Biomed Res. Int.* **2015**, (2015).
290. Chaturvedi, K. *et al.* Cyclodextrin-based siRNA delivery nanocarriers: a state-of-the-art review. *Expert Opin. Drug Deliv.* **8**, 1455–1468 (2011).
291. Fitzgerald, K. A. *et al.* A novel, anisamide-targeted cyclodextrin nanoformulation for siRNA delivery to prostate cancer cells expressing the sigma-1 receptor. *Int. J. Pharm.* **499**, 131–145 (2016).
292. Yang, Y. *et al.* Ligand-directed stearic acid grafted chitosan micelles to increase therapeutic efficacy in hepatic cancer. *Mol. Pharm.* **12**, 644–52 (2015).
293. Cavallaro, G., Licciardi, M., Caliceti, P., Salmaso, S. & Giammona, G. Synthesis, physico-chemical and biological characterization of a paclitaxel macromolecular prodrug. *Eur. J. Pharm. Biopharm.* **58**, 151–159 (2004).
294. Pitarresi, G., Fiorica, C., Palumbo, F. S., Calascibetta, F. & Giammona, G. Polyaspartamide-polylactide electrospun scaffolds for potential topical release of Ibuprofen. *J. Biomed. Mater. Res. Part A* **100A**, 1565–1572 (2012).
295. Lv, S. *et al.* Investigation on the controlled synthesis and post-modification of poly-[(N-2-hydroxyethyl)-aspartamide]-based polymers. *Polym. Chem.* **8**, 1872–1877 (2017).
296. Lohitesh, K., Chowdhury, R. & Mukherjee, S. Resistance a major hindrance to chemotherapy in hepatocellular carcinoma: an insight. *Cancer Cell Int.* **18**, 44 (2018).
297. Ke, X. & Shen, L. Molecular targeted therapy of cancer: The progress and future prospect. *Front. Lab. Med.* **1**, 69–75 (2017).
298. Zhang, X. *et al.* Drug delivery system targeting advanced hepatocellular carcinoma: Current and future. *Nanomedicine Nanotechnology, Biol. Med.* **12**, 853–869 (2016).
299. Scarabel, L. *et al.* Strategies to optimize siRNA delivery to hepatocellular carcinoma cells. *Expert Opin. Drug Deliv.* **14**, 797–810 (2017).
300. Farra, R. *et al.* Polymer-Mediated Delivery of siRNAs to Hepatocellular Carcinoma: Variables Affecting Specificity and Effectiveness. *Molecules* **23**, 777 (2018).
301. Baumhoer, D. *et al.* Glypican 3 Expression in Human Nonneoplastic, Preneoplastic, and Neoplastic Tissues. *Am. J. Clin. Pathol.* **129**, 899–906 (2008).
302. Moradpour, D., Compagnon, B., Wilson, B. E., Nicolau, C. & Wands, J. R. Specific targeting of human hepatocellular carcinoma cells by immunoliposomes in vitro. *Hepatology* **22**, 1527–1537 (1995).
303. Shi, B., Abrams, M. & Sepp-Lorenzino, L. Expression of Asialoglycoprotein Receptor 1 in Human Hepatocellular Carcinoma. *J. Histochem. Cytochem.* **61**, 901–909 (2013).
304. D'Souza, A. A. & Devarajan, P. V. Asialoglycoprotein receptor mediated hepatocyte targeting — Strategies and applications. *J. Control. Release* **203**, 126–139 (2015).
305. Stockert, R. J. The asialoglycoprotein receptor: relationships between structure, function, and expression. *Physiol. Rev.* **75**, 591–609 (1995).

306. Onizuka, T. *et al.* NMR study of ligand release from asialoglycoprotein receptor under solution conditions in early endosomes. *FEBS J.* **279**, 2645–2656 (2012).
307. Huang, T., Deng, H., Wolkoff, A. W. & Stockert, R. J. Phosphorylation-dependent interaction of the asialoglycoprotein receptor with molecular chaperones. *J. Biol. Chem.* **277**, 37798–803 (2002).
308. Ishibashi, S., Hammer, R. E. & Herz, J. Asialoglycoprotein receptor deficiency in mice lacking the minor receptor subunit. *J. Biol. Chem.* **269**, 27803–6 (1994).
309. Monestier, M. *et al.* ASGPR-Mediated Uptake of Multivalent Glycoconjugates for Drug Delivery in Hepatocytes. *ChemBioChem* **17**, 590–594 (2016).
310. McKee, T., DeRome, M., Wu, G. & Findeis, M. Preparation of asialoorosomucoid-polylysine conjugates. *Bioconjug. Chem.* **5**, 306–311 (1994).
311. Arangoa, M. A., Düzgüneş, N. & Tros de Ilarduya, C. Increased receptor-mediated gene delivery to the liver by protamine-enhanced-asialofetuin-lipoplexes. *Gene Ther.* **10**, 5–14 (2003).
312. Nair, J. K. *et al.* Multivalent *N* -Acetylgalactosamine-Conjugated siRNA Localizes in Hepatocytes and Elicits Robust RNAi-Mediated Gene Silencing. *J. Am. Chem. Soc.* **136**, 16958–16961 (2014).
313. Korin, E., Bejerano, T. & Cohen, S. GalNAc bio-functionalization of nanoparticles assembled by electrostatic interactions improves siRNA targeting to the liver. *J. Control. Release* **266**, 310–320 (2017).
314. Saunier, B. *et al.* Role of the asialoglycoprotein receptor in binding and entry of hepatitis C virus structural proteins in cultured human hepatocytes. *J. Virol.* **77**, 546–59 (2003).
315. McAbee, D. D. & Jiang, X. Copper and Zinc Ions Differentially Block Asialoglycoprotein Receptor-mediated Endocytosis in Isolated Rat Hepatocytes. *J. Biol. Chem.* **274**, 14750–14758 (1999).
316. Geffen, I. & Spiess, M. Phorbol ester-induced redistribution of the ASGP receptor is independent of receptor phosphorylation. *FEBS Lett.* **305**, 209–212 (1992).
317. Cavallaro, G. *et al.* Galactosylated polyaspartamide copolymers for siRNA targeted delivery to hepatocellular carcinoma cells. *Int. J. Pharm.* **525**, 397–406 (2017).
318. Li, Y., Huang, G., Diakur, J. & Wiebe, L. I. Targeted delivery of macromolecular drugs: asialoglycoprotein receptor (ASGPR) expression by selected hepatoma cell lines used in antiviral drug development. *Curr. Drug Deliv.* **5**, 299–302 (2008).
319. Hyodo, I., Mizuno, M., Yamada, G. & Tsuji, T. Distribution of asialoglycoprotein receptor in human hepatocellular carcinoma. *Liver* **13**, 80–5 (1993).
320. Litwack, G. Protein Biosynthesis. in *Human Biochemistry* 319–336 (Elsevier, 2018). doi:10.1016/B978-0-12-383864-3.00011-9
321. Dever, T. E. & Green, R. The elongation, termination, and recycling phases of translation in eukaryotes. *Cold Spring Harb. Perspect. Biol.* **4**, a013706 (2012).
322. Andersen, G. R. *et al.* Structural basis for nucleotide exchange and competition with tRNA in the yeast elongation factor complex eEF1A:eEF1Balpha. *Mol. Cell* **6**, 1261–6 (2000).
323. Scaggiante, B. *et al.* Translation Elongation. in *Translation and Its Regulation in Cancer Biology and Medicine* 241–265 (Springer Netherlands, 2014). doi:10.1007/978-94-017-9078-9_12
324. Sasikumar, A. N., Perez, W. B. & Kinzy, T. G. The Many Roles of the Eukaryotic Elongation Factor 1 Complex. *Wiley Interdiscip. Rev. RNA* **3**, 543 (2012).
325. Khacho, M. *et al.* eEF1A is a novel component of the mammalian nuclear protein export machinery. *Mol. Biol. Cell* **19**, 5296–308 (2008).
326. Lund, A., Knudsen, S. M., Vissing, H., Clark, B. & Tommerup, N. Assignment of Human Elongation Factor 1α Genes:EEF1AMaps to Chromosome 6q14 andEEF1A2to 20q13.3. *Genomics* **36**, 359–361 (1996).
327. Liu, T. *et al.* Human eukaryotic elongation factor 1A forms oligomers through specific

cysteine residues. (2015). doi:10.1093/abbs/gmv113
328. Timchenko, A. A. *et al.* Different Oligomeric Properties and Stability of Highly Homologous A1 and Proto-Oncogenic A2 Variants of Mammalian Translation Elongation Factor eEF1. *Biochemistry* **52**, 5345–5353 (2013).
329. Knudsen, S. M., Frydenberg, J., Clark, B. F. & Leffers, H. Tissue-dependent variation in the expression of elongation factor-1 alpha isoforms: isolation and characterisation of a cDNA encoding a novel variant of human elongation-factor 1 alpha. *Eur. J. Biochem.* **215**, 549–54 (1993).
330. Sanges, C. *et al.* Raf kinases mediate the phosphorylation of eukaryotic translation elongation factor 1A and regulate its stability in eukaryotic cells. *Cell Death Dis.* **3**, e276 (2012).
331. Lin, K. W., Yakymovych, I., Jia, M., Yakymovych, M. & Souchelnytskyi, S. Phosphorylation of eEF1A1 at Ser300 by TβR-I Results in Inhibition of mRNA Translation. *Curr. Biol.* **20**, 1615–1625 (2010).
332. Negrutskii, B., Vlasenko, D. & El'skaya, A. From global phosphoproteomics to individual proteins: the case of translation elongation factor eEF1A. *Expert Rev. Proteomics* **9**, 71–83 (2012).
333. Lee, M.-H. *et al.* Tumor suppressor p16(INK4a) inhibits cancer cell growth by downregulating eEF1A2 through a direct interaction. *J. Cell Sci.* **126**, 1744–52 (2013).
334. Vislovukh, A. *et al.* Proto-oncogenic isoform A2 of eukaryotic translation elongation factor eEF1 is a target of miR-663 and miR-744. *Br. J. Cancer* **108**, 2304–2311 (2013).
335. Jakobsson, M. E. *et al.* Methylation of human eukaryotic elongation factor alpha (eEF1A) by a member of a novel protein lysine methyltransferase family modulates mRNA translation. *Nucleic Acids Res.* **45**, 8239–8254 (2017).
336. Jakobsson, M. E., Małecki, J. & Falnes, P. Ø. Regulation of eukaryotic elongation factor 1 alpha (eEF1A) by dynamic lysine methylation. *RNA Biol.* **15**, 314–319 (2018).
337. Abbas, W., Kumar, A. & Herbein, G. The eEF1A Proteins: At the Crossroads of Oncogenesis, Apoptosis, and Viral Infections. *Front. Oncol.* **5**, 75 (2015).
338. Ruest, L.-B., Marcotte, R. & Wang, E. Peptide Elongation Factor eEF1A-2/S1 Expression in Cultured Differentiated Myotubes and Its Protective Effect against Caspase- 3-mediated Apoptosis. *J. Biol. Chem.* **277**, 5418–5425 (2002).
339. Jeganathan, S., Morrow, A., Amiri, A. & Lee, J. M. Eukaryotic Elongation Factor 1A2 Cooperates with Phosphatidylinositol-4 Kinase III To Stimulate Production of Filopodia through Increased Phosphatidylinositol-4,5 Bisphosphate Generation. *Mol. Cell. Biol.* **28**, 4549–4561 (2008).
340. Lamberti, A. *et al.* The translation elongation factor 1A in tumorigenesis, signal transduction and apoptosis: Review article. *Amino Acids* **26**, 443–8 (2004).
341. Lee, M.-H. & Surh, Y.-J. eEF1A2 as a Putative Oncogene. *Ann. N. Y. Acad. Sci.* **1171**, 87–93 (2009).
342. Grassi, G. *et al.* The expression levels of the translational factors eEF1A 1/2 correlate with cell growth but not apoptosis in hepatocellular carcinoma cell lines with different differentiation grade. *Biochimie* **89**, 1544–1552 (2007).
343. Tomlinson, V. A. L. *et al.* Expression of eEF1A2 is associated with clear cell histology in ovarian carcinomas: overexpression of the gene is not dependent on modifications at the EEF1A2 locus. *Br. J. Cancer* **96**, 1613–20 (2007).
344. Pellegrino, R. *et al.* EEF1A2 inactivates p53 by way of PI3K/AKT/mTOR-dependent stabilization of MDM4 in hepatocellular carcinoma. *Hepatology* **59**, 1886–1899 (2014).
345. Elgohary, N. *et al.* Protumorigenic role of Timeless in hepatocellular carcinoma. *Int. J. Oncol.* **46**, 597–606 (2014).
346. Losada, A. *et al.* Binding of eEF1A2 to the RNA-dependent protein kinase PKR modulates its activity and promotes tumour cell survival. *Br. J. Cancer* **119**, 1410–1420 (2018).

347. Lee, C. G. *et al.* Expression of the FAT10 gene is highly upregulated in hepatocellular carcinoma and other gastrointestinal and gynecological cancers. *Oncogene* **22**, 2592–2603 (2003).
348. Yu, X. *et al.* Identification of a Novel Binding Protein of FAT10: Eukaryotic Translation Elongation Factor 1A1. *Dig. Dis. Sci.* **57**, 2347–2354 (2012).
349. Blanch, A., Robinson, F., Watson, I. R., Cheng, L. S. & Irwin, M. S. Eukaryotic Translation Elongation Factor 1-Alpha 1 Inhibits p53 and p73 Dependent Apoptosis and Chemotherapy Sensitivity. *PLoS One* **8**, e66436 (2013).
350. Huang, J. *et al.* Overexpression of eEF1A1 regulates G1-phase progression to promote HCC proliferation through the STAT1-cyclin D1 pathway. *Biochem. Biophys. Res. Commun.* **494**, 542–549 (2017).
351. Scaggiante, B. *et al.* Aptamer targeting of the elongation factor 1A impairs hepatocarcinoma cells viability and potentiates bortezomib and idarubicin effects. *Int. J. Pharm.* **506**, 268–279 (2016).
352. Rhind, N. & Russell, P. Signaling pathways that regulate cell division. *Cold Spring Harb. Perspect. Biol.* **4**, (2012).
353. Chen, H.-Z., Tsai, S.-Y. & Leone, G. Emerging roles of E2Fs in cancer: an exit from cell cycle control. *Nat. Rev. Cancer* **9**, 785–797 (2009).
354. Rowland, B. D. & Bernards, R. Re-Evaluating Cell-Cycle Regulation by E2Fs. *Cell* **127**, 871–874 (2006).
355. Degregori, J., Kowalik, T. & Nevins, J. R. *Cellular Targets for Activation by the E2F1 Transcription Factor Include DNA Synthesis-and G 1 /S-Regulatory Genes*. *MOLECULAR AND CELLULAR BIOLOGY* **15**, (1995).
356. Dubrez, L. Regulation of E2F1 Transcription Factor by Ubiquitin Conjugation. *Int. J. Mol. Sci.* **18**, (2017).
357. Slansky, J. E. & Farnham, P. J. Introduction to the E2F Family: Protein Structure and Gene Regulation. in 1–30 (Springer, Berlin, Heidelberg, 1996). doi:10.1007/978-3-642-79910-5_1
358. Polager, S. & Ginsberg, D. E2F – at the crossroads of life and death. *Trends Cell Biol.* **18**, 528–535 (2008).
359. Bertoli, C., Skotheim, J. M. & de Bruin, R. A. M. Control of cell cycle transcription during G1 and S phases. *Nat. Rev. Mol. Cell Biol.* **14**, 518–28 (2013).
360. Poppy Roworth, A., Ghari, F. & La Thangue, N. B. To live or let die – complexity within the E2F1 pathway. *Mol. Cell. Oncol.* **2**, e970480 (2015).
361. Westendorp, B. *et al.* E2F7 represses a network of oscillating cell cycle genes to control S-phase progression. *Nucleic Acids Res.* **40**, 3511–3523 (2012).
362. Christensen, J. *et al.* Characterization of E2F8, a novel E2F-like cell-cycle regulated repressor of E2F-activated transcription. *Nucleic Acids Res.* **33**, 5458–5470 (2005).
363. Malumbres, M. & Carnero, A. Cell cycle deregulation: a common motif in cancer. *Prog. Cell Cycle Res.* **5**, 5–18 (2003).
364. huang, Y. *et al.* Cancer Management and Research Dovepress Promising diagnostic and prognostic value of e2Fs in human hepatocellular carcinoma. *Cancer Manag. Res.* 11–1725 (2019). doi:10.2147/CMAR.S182001
365. Malz, M., Pinna, F., Schirmacher, P. & Breuhahn, K. Transcriptional regulators in hepatocarcinogenesis – Key integrators of malignant transformation. *J. Hepatol.* **57**, 186–195 (2012).
366. Farra, R. *et al.* Effects of E2F1–cyclin E1–E2 circuit down regulation in hepatocellular carcinoma cells. *Dig. Liver Dis.* **43**, 1006–1014 (2011).
367. Calvisi, D. F. *et al.* SKP2 and CKS1 Promote Degradation of Cell Cycle Regulators and Are Associated With Hepatocellular Carcinoma Prognosis. *Gastroenterology* **137**, 1816-1826.e10 (2009).

368. Li, L. *et al.* Epigenetic modification of MiR-429 promotes liver tumour-initiating cell properties by targeting Rb binding protein 4. *Gut* **64**, 156–167 (2015).
369. Wang, S.-N. *et al.* Intestine-specific homeobox (ISX) upregulates E2F1 expression and related oncogenic activities in HCC. *Oncotarget* **7**, 36924–36939 (2016).
370. Wang, B. *et al.* POH1 deubiquitylates and stabilizes E2F1 to promote tumour formation. *Nat. Commun.* **6**, 8704 (2015).
371. Gu, Y. *et al.* SET7/9 promotes hepatocellular carcinoma progression through regulation of E2F1. *Oncol. Rep.* **40**, 1863–1874 (2018).
372. Ericsson, A. C., Crim, M. J. & Franklin, C. L. A brief history of animal modeling. *Mo. Med.* **110**, 201–5 (2013).
373. Brown, Z. J., Heinrich, B. & Greten, T. F. Mouse models of hepatocellular carcinoma: an overview and highlights for immunotherapy research. *Nat. Rev. Gastroenterol. Hepatol.* **15**, 536–554 (2018).
374. Santos, N. P., Colaço, A. A. & Oliveira, P. A. Animal models as a tool in hepatocellular carcinoma research: A Review. *Tumor Biol.* **39**, 101042831769592 (2017).
375. De Minicis, S. *et al.* Liver carcinogenesis: rodent models of hepatocarcinoma and cholangiocarcinoma. *Dig. Liver Dis.* **45**, 450–9 (2013).
376. Sheweita, S. A., Abd El-Gabar, M. & Bastawy, M. Carbon tetrachloride-induced changes in the activity of phase II drug-metabolizing enzyme in the liver of male rats: role of antioxidants. *Toxicology* **165**, 217–24 (2001).
377. Yanguas, S. C. *et al.* Experimental models of liver fibrosis. *Arch. Toxicol.* **90**, 1025–1048 (2016).
378. Heindryckx, F., Colle, I. & Van Vlierberghe, H. Experimental mouse models for hepatocellular carcinoma research. *Int. J. Exp. Pathol.* **90**, 367–86 (2009).
379. Kim, C.-M., Koike, K., Saito, I., Miyamura, T. & Jay, G. HBx gene of hepatitis B virus induces liver cancer in transgenic mice. *Nature* **351**, 317–320 (1991).
380. Martínez-Chantar, M. L. *et al.* Loss of the glycine N-methyltransferase gene leads to steatosis and hepatocellular carcinoma in mice. *Hepatology* **47**, 1191–1199 (2007).
381. Kramer, M. G., Hernandez-Alcoceba, R., Qian, C. & Prieto, J. Evaluation of hepatocellular carcinoma models for preclinical studies. *Drug Discov. Today Dis. Model.* **2**, 41–49 (2005).
382. Kerbel, R. S. Human tumor xenografts as predictive preclinical models for anticancer drug activity in humans: better than commonly perceived-but they can be improved. *Cancer Biol. Ther.* **2**, S134-9
383. Jung, J. Human tumor xenograft models for preclinical assessment of anticancer drug development. *Toxicol. Res.* **30**, 1–5 (2014).
384. Newell, P., Villanueva, A., Friedman, S. L., Koike, K. & Llovet, J. M. Experimental models of hepatocellular carcinoma q. doi:10.1016/j.jhep.2008.01.008
385. Bosma, M. J. & Carroll, A. M. The SCID Mouse Mutant: Definition, Characterization, and Potential Uses. *Annu. Rev. Immunol.* **9**, 323–350 (1991).
386. Morton, C. L. & Houghton, P. J. Establishment of human tumor xenografts in immunodeficient mice. *Nat. Protoc.* **2**, 247–250 (2007).
387. Yan, M. *et al.* Establishment of NOD/SCID mouse models of human hepatocellular carcinoma via subcutaneous transplantation of histologically intact tumor tissue. *Chin. J. Cancer Res.* **25**, 289–98 (2013).
388. Zhou, Q., Facciponte, J., Jin, M., Shen, Q. & Lin, Q. Humanized NOD-SCID IL2rg –/– mice as a preclinical model for cancer research and its potential use for individualized cancer therapies. *Cancer Lett.* **344**, 13–19 (2014).
389. Gonzalez, L., Strbo, N. & Podack, E. R. Humanized mice: novel model for studying mechanisms of human immune-based therapies. *Immunol. Res.* **57**, 326–34 (2013).
390. Notta, F., Doulatov, S. & Dick, J. E. Engraftment of human hematopoietic stem cells is more efficient in female NOD/SCID/IL-2Rgc-null recipients. *Blood* **115**, 3704–3707

(2010).
391. Wilson, E. M. *et al.* Extensive double humanization of both liver and hematopoiesis in FRGN mice. *Stem Cell Res.* **13**, 404–412 (2014).
392. Walsh, N. C. *et al.* Humanized Mouse Models of Clinical Disease. *Annu. Rev. Pathol.* **12**, 187–215 (2017).
393. Gerolami, R. *et al.* Gene transfer to hepatocellular carcinoma: Transduction efficacy and transgene expression kinetics by using retroviral and lentiviral vectors.
394. Merten, O.-W., Hebben, M. & Bovolenta, C. Production of lentiviral vectors. *Mol. Ther. Methods Clin. Dev.* **3**, 16017 (2016).
395. Farra, R. *et al.* Dissecting the role of the elongation factor 1A isoforms in hepatocellular carcinoma cells by liposome-mediated delivery of siRNAs. *Int. J. Pharm.* **525**, 367–376 (2017).
396. Dapas, B. *et al.* Role of E2F1-Cyclin E1-Cyclin E2 Circuit in Human Coronary Smooth Muscle Cell Proliferation and Therapeutic Potential of Its Downregulation by siRNAs. *Mol. Med.* **15**, 297–306 (2009).
397. Lamberti, A. *et al.* C-Raf antagonizes apoptosis induced by IFN-α in human lung cancer cells by phosphorylation and increase of the intracellular content of elongation factor 1A. *Cell Death Differ.* **14**, 952–962 (2007).
398. D'Souza, A. A. & Devarajan, P. V. Asialoglycoprotein receptor mediated hepatocyte targeting — Strategies and applications. *J. Control. Release* **203**, 126–139 (2015).
399. Campeau, E. *et al.* A Versatile Viral System for Expression and Depletion of Proteins in Mammalian Cells. *PLoS One* **4**, e6529 (2009).
400. Dull, T. *et al.* A third-generation lentivirus vector with a conditional packaging system. *J. Virol.* **72**, 8463–71 (1998).
401. Strober, W. Trypan Blue Exclusion Test of Cell Viability. in *Current Protocols in Immunology* (John Wiley & Sons, Inc., 2001). doi:10.1002/0471142735.ima03bs21
402. Patravale, V., Dandekar, P. & Jain, R. Nanotoxicology: evaluating toxicity potential of drug-nanoparticles. in *Nanoparticulate Drug Delivery* 123–155 (Elsevier, 2012). doi:10.1533/9781908818195.123
403. Kumar, P., Nagarajan, A. & Uchil, P. D. Analysis of Cell Viability by the Lactate Dehydrogenase Assay. *Cold Spring Harb. Protoc.* **2018**, pdb.prot095497 (2018).
404. He, F. BCA (Bicinchoninic Acid) Protein Assay. *BIO-PROTOCOL* **1**, (2011).
405. Yang, P.-C. & Mahmood, T. Western blot: Technique, theory, and trouble shooting. *N. Am. J. Med. Sci.* **4**, 429 (2012).
406. LAEMMLI, U. K. Cleavage of Structural Proteins during the Assembly of the Head of Bacteriophage T4. *Nature* **227**, 680–685 (1970).
407. Bosutti, A. *et al.* A rapid and specific method to simultaneously quantify eukaryotic elongation factor 1A1 and A2 protein levels in cancer cells. *J. Pharm. Biomed. Anal.* **176**, 112814 (2019).
408. Deepak, S. *et al.* Real-Time PCR: Revolutionizing Detection and Expression Analysis of Genes. *Curr. Genomics* **8**, 234–51 (2007).
409. Quan, P. L., Sauzade, M. & Brouzes, E. DPCR: A technology review. *Sensors (Switzerland)* **18**, (2018).
410. Laschke, M. W., Vollmar, B. & Menger, M. D. The dorsal skinfold chamber: window into the dynamic interaction of biomaterials with their surrounding host tissue. *Eur. Cell. Mater.* **22**, 147–64; discussion 164-7 (2011).
411. Palmer, G. M., Fontanella, A. N., Shan, S. & Dewhirst, M. W. High-resolution in vivo imaging of fluorescent proteins using window chamber models. *Methods Mol. Biol.* **872**, 31–50 (2012).
412. Bochicchio, S., Dalmoro, A., Barba, A., Grassi, G. & Lamberti, G. Liposomes as siRNA Delivery Vectors. *Curr. Drug Metab.* **15**, 882–892 (2015).

413. Krivitsky, A. *et al.* Structure–Function Correlation of Aminated Poly(α)glutamate as siRNA Nanocarriers. *Biomacromolecules* **17**, 2787–2800 (2016).
414. Posocco, B. *et al.* Polysaccharides for the delivery of antitumor drugs. *Materials* **8**, 2569–2615 (2015).
415. Cavallaro, G. *et al.* Synthesis and characterization of polyaspartamide copolymers obtained by ATRP for nucleic acid delivery. *Int. J. Pharm.* **466**, 246–257 (2014).
416. Sardo, C. *et al.* Development of a simple, biocompatible and cost-effective Inulin-Diethylenetriamine based siRNA delivery system. *Eur. J. Pharm. Sci.* **75**, 60–71 (2015).
417. Poelstra, K., Prakash, J. & Beljaars, L. Drug targeting to the diseased liver. *Journal of Controlled Release* **161**, 188–197 (2012).
418. Baenziger, J. U. & Maynard, Y. Human hepatic lectin. Physiochemical properties and specificity. *J. Biol. Chem.* **255**, 4607–4613 (1980).
419. Craparo, E. F. *et al.* Galactosylated polymeric carriers for liver targeting of sorafenib. *Int. J. Pharm.* **466**, 172–180 (2014).
420. Mu, H. *et al.* Identification of biomarkers for hepatocellular carcinoma by semiquantitative immunocytochemistry. *World J. Gastroenterol.* **20**, 5826–5838 (2014).
421. Tanida, I., Ueno, T. & Kominami, E. LC3 and Autophagy. in 77–88 (Humana Press, 2008). doi:10.1007/978-1-59745-157-4_4
422. Morales, J. *et al.* Review of poly (ADP-ribose) polymerase (PARP) mechanisms of action and rationale for targeting in cancer and other diseases. *Crit. Rev. Eukaryot. Gene Expr.* **24**, 15–28 (2014).
423. Colonies, A. *SCID Beige Mouse Hematology CB17.Cg-Prkdc scid Lyst bg-J /Crl WBC NEUT LYMPH MONO EOS BASO NEUT LYMPH MONO EOS (K/μL) (K/μL) (K/μL) (K/μL) (K/μL) (K/μL) (%) (%) (%) (%)*. (2011).
424. Goodman, Z. D. Neoplasms of the liver. *Mod. Pathol.* **20**, 49–60 (2007).
425. Knox, J. J., Cleary, S. P. & Dawson, L. A. Localized and systemic approaches to treating hepatocellular carcinoma. *Journal of Clinical Oncology* **33**, 1835–1844 (2015).
426. Gabrielson, A. *et al.* Phase II study of temozolomide and veliparib combination therapy for sorafenib-refractory advanced hepatocellular carcinoma. *Cancer Chemother. Pharmacol.* **76**, 1073–1079 (2015).
427. Lencioni, R., Marrero, J., Venook, A., Ye, S. L. & Kudo, M. Design and rationale for the non-interventional Global Investigation of therapeutic DEcisions in hepatocellular carcinoma and of its treatment with sorafeNib (GIDEON) study. *Int. J. Clin. Pract.* **64**, 1034–1041 (2010).
428. Bruix, J. & Sherman, M. Management of hepatocellular carcinoma: An update. *Hepatology* **53**, 1020–1022 (2011).
429. Ryder, S. D. Guidelines for the diagnosis and treatment of hepatocellular carcinoma (HCC) in adults. *Gut* **52**, (2003).
430. Llovet, J. M. *et al.* Sorafenib in advanced hepatocellular carcinoma. *N. Engl. J. Med.* **359**, 378–390 (2008).
431. Forner, A., Llovet, J. M. & Bruix, J. Hepatocellular carcinoma. in *The Lancet* **379**, 1245–1255 (2012).
432. Qiu, F. N. *et al.* Eukaryotic elongation factor-1α 2 knockdown inhibits hepatocarcinogenesis by suppressing PI3K/Akt/NF-κB signaling. *World J. Gastroenterol.* **22**, 4226–4237 (2016).
433. Schlaeger, C. *et al.* Etiology-dependent molecular mechanisms in human hepatocarcinogenesis. *Hepatology* **47**, 511–520 (2008).
434. Evangelou, K., Havaki, S. & Kotsinas, A. E2F transcription factors and digestive system malignancies: How much do we know? *World J. Gastroenterol.* 10212–10216 (2014). doi:10.3748/wjg.v20.i29.10212
435. Zhan, L. *et al.* Promising roles of mammalian E2Fs in hepatocellular carcinoma. *Cellular*

Signalling **26**, 1075–1081 (2014).
436. Conner, E. A. *et al.* Dual functions of E2F-1 in a transgenic mouse model of liver carcinogenesis. *Oncogene* **19**, 5054–5062 (2000).
437. Farra, R. *et al.* Effects of E2F1–cyclin E1–E2 circuit down regulation in hepatocellular carcinoma cells. *Dig. Liver Dis.* **43**, 1006–1014 (2011).
438. Liu, J., Xu, Y., Stoleru, D. & Salic, a. Imaging protein synthesis in cells and tissues with an alkyne analog of puromycin. *Proc. Natl. Acad. Sci.* **109**, 413–418 (2012).
439. Levy, J. M. M., Towers, C. G. & Thorburn, A. Targeting autophagy in cancer. *Nature Reviews Cancer* **17**, 528–542 (2017).
440. Novosylna, O. *et al.* Comparison of the ability of mammalian eEF1A1 and its oncogenic variant eEF1A2 to interact with actin and calmodulin. *Biol. Chem.* **398**, 113–124 (2017).
441. Wojnacki, J. & Galli, T. A new actin-binding domain glues autophagy together. *Journal of Biological Chemistry* **293**, 4575–4576 (2018).
442. Khan, A. A., Alanazi, A. M., Jabeen, M., Chauhan, A. & Ansari, M. A. Therapeutic potential of functionalized siRNA nanoparticles on regression of liver cancer in experimental mice. *Sci. Rep.* **9**, (2019).
443. Han, L., Tang, C. & Yin, C. Enhanced antitumor efficacies of multifunctional nanocomplexes through knocking down the barriers for siRNA delivery. *Biomaterials* **44**, 111–121 (2015).
444. Huang, K. W. *et al.* Galactose Derivative-Modified Nanoparticles for Efficient siRNA Delivery to Hepatocellular Carcinoma. *Biomacromolecules* **19**, 2330–2339 (2018).
445. Liver | anatomy | Britannica.com. Available at: https://www.britannica.com/science/liver. (Accessed: 30th August 2019)
446. Stenvall, A., Larsson, E., Strand, S.-E. & Jönsson, B.-A. A small-scale anatomical dosimetry model of the liver. *Phys. Med. Biol.* **59**, 3353–3371 (2014).
447. El–Serag, H. B. & Rudolph, K. L. Hepatocellular Carcinoma: Epidemiology and Molecular Carcinogenesis. *Gastroenterology* **132**, 2557–2576 (2007).
448. Liaw, Y.-F., Sheen, I.-S., Chen, T.-J., Chu, C.-M. & Pao, C.-C. Incidence, determinants and significance of delayed clearance of serum HBsAg in chronic hepatitis B virus infection: A prospective study. *Hepatology* **13**, 627–631 (1991).
449. Fako, V. & Wang, X. W. Molecular Carcinogenesis of HBV-Related HCC. in *Hepatitis B Virus and Liver Disease* 143–162 (Springer Singapore, 2018). doi:10.1007/978-981-10-4843-2_8
450. Morozov, V. A. & Lagaye, S. Hepatitis C virus: Morphogenesis, infection and therapy. *World J. Hepatol.* **10**, 186–212 (2018).
451. Axley, P., Ahmed, Z., Ravi, S. & Singal, A. K. Hepatitis C Virus and Hepatocellular Carcinoma: A Narrative Review. *J. Clin. Transl. Hepatol.* **6**, 79–84 (2018).
452. Li, D., Wei, T., Abbott, C. M. & Harrich, D. The unexpected roles of eukaryotic translation elongation factors in RNA virus replication and pathogenesis. *Microbiol. Mol. Biol. Rev.* **77**, 253–66 (2013).